

Nuclear Science
NEA/NSC/DOC(2005)16

ISBN 92-64-01069-6

Benchmark on Deterministic Transport Calculations Without Spatial Homogenisation

MOX Fuel Assembly 3-D Extension Case

© OECD 2005
NEA No. 5420

NUCLEAR ENERGY AGENCY
ORGANISATION FOR ECONOMIC CO-OPERATION AND DEVELOPMENT

ORGANISATION FOR ECONOMIC COOPERATION AND DEVELOPMENT

The OECD is a unique forum where the governments of 30 democracies work together to address the economic, social and environmental challenges of globalisation. The OECD is also at the forefront of efforts to understand and to help governments respond to new developments and concerns, such as corporate governance, the information economy and the challenges of an ageing population. The Organisation provides a setting where governments can compare policy experiences, seek answers to common problems, identify good practice and work to co-ordinate domestic and international policies.

The OECD member countries are: Australia, Austria, Belgium, Canada, the Czech Republic, Denmark, Finland, France, Germany, Greece, Hungary, Iceland, Ireland, Italy, Japan, Korea, Luxembourg, Mexico, the Netherlands, New Zealand, Norway, Poland, Portugal, the Slovak Republic, Spain, Sweden, Switzerland, Turkey, the United Kingdom and the United States. The Commission of the European Communities takes part in the work of the OECD.

OECD Publishing disseminates widely the results of the Organisation's statistics gathering and research on economic, social and environmental issues, as well as the conventions, guidelines and standards agreed by its members.

* * *

This work is published on the responsibility of the Secretary-General of the OECD. The opinions expressed and arguments employed herein do not necessarily reflect the official views of the Organisation or of the governments of its member countries.

NUCLEAR ENERGY AGENCY

The OECD Nuclear Energy Agency (NEA) was established on 1st February 1958 under the name of the OEEC European Nuclear Energy Agency. It received its present designation on 20th April 1972, when Japan became its first non-European full member. NEA membership today consists of 28 OECD member countries: Australia, Austria, Belgium, Canada, the Czech Republic, Denmark, Finland, France, Germany, Greece, Hungary, Iceland, Ireland, Italy, Japan, Luxembourg, Mexico, the Netherlands, Norway, Portugal, Republic of Korea, the Slovak Republic, Spain, Sweden, Switzerland, Turkey, the United Kingdom and the United States. The Commission of the European Communities also takes part in the work of the Agency.

The mission of the NEA is:

- to assist its member countries in maintaining and further developing, through international co-operation, the scientific, technological and legal bases required for a safe, environmentally friendly and economical use of nuclear energy for peaceful purposes, as well as
- to provide authoritative assessments and to forge common understandings on key issues, as input to government decisions on nuclear energy policy and to broader OECD policy analyses in areas such as energy and sustainable development.

Specific areas of competence of the NEA include safety and regulation of nuclear activities, radioactive waste management, radiological protection, nuclear science, economic and technical analyses of the nuclear fuel cycle, nuclear law and liability, and public information. The NEA Data Bank provides nuclear data and computer program services for participating countries.

In these and related tasks, the NEA works in close collaboration with the International Atomic Energy Agency in Vienna, with which it has a Cooperation Agreement, as well as with other international organisations in the nuclear field.

© OECD 2005

No reproduction, copy, transmission or translation of this publication may be made without written permission. Applications should be sent to OECD Publishing: rights@oecd.org or by fax (+33-1) 45 24 13 91. Permission to photocopy a portion of this work should be addressed to the Centre Français d'exploitation du droit de Copie, 20 rue des Grands Augustins, 75006 Paris, France (contact@cfcopies.com).

FOREWORD

Within the framework of the OECD/NEA Expert Group on 3-D Radiation Transport Benchmarks, an international benchmark exercise for testing the ability of modern deterministic transport methods and codes to treat reactor problems without spatial homogenisation was proposed in March 2001. That benchmark was completed in 2003 and the OECD report is available. As a follow-up to that benchmark, an extension of the 3-D calculations was proposed in May 2003 to provide a more challenging test of present day three-dimensional methods' ability to handle spatial homogeneities. The reactor core size was decreased to allow the calculations to be carried out within the limitations of present-day computers. Control rods were introduced, adding to the heterogeneity of the problems.

Fourteen solutions were submitted for the new benchmark by twelve participants. All of the participant solutions were compared to a reference multigroup Monte Carlo solution. The analysis of results shows modern deterministic transport codes and methods can calculate the flux distribution reasonably well without relying upon spatial homogenisation techniques, provided the domain size is small enough that the problem can be performed on available computing equipment.

Acknowledgements

The Secretariat expresses its sincere gratitude to the participants who willingly devoted their time and effort to this benchmark exercise.

Dedication

The authors of the report wish to dedicate this report to the memory of Mrs Diana Broderick Smith.

TABLE OF CONTENTS

Foreword	3
Executive summary	13
Chapter 1. Introduction	15
Chapter 2. Description of the benchmark	17
Chapter 3. Participants and codes used	23
Chapter 4. Method of results analysis	25
Chapter 5. Comparisons of the reference Monte Carlo solutions	27
Chapter 6. <i>Unrodded</i> configuration benchmark results	37
Chapter 7. <i>Rodded A</i> configuration benchmark results	57
Chapter 8. <i>Rodded B</i> configuration benchmark results	75
Chapter 9. Conclusions	93
References	95
Appendix A. Benchmark specification for deterministic MOX fuel assembly transport calculations without spatial homogenisation (3-D Extension C5G7 MOX)	97
Appendix B. Calculation details provided by the participants	111
Appendix C. Clarification of the AVG, RMS, and MRE error measures	147
Appendix D. Reference multigroup Monte Carlo solution (electronic appendix)	153
Appendix E. All contributed results and descriptions (electronic appendix)	153
Appendix F. Benchmark result analysis (electronic appendix)	153
Appendix G. Additional continuous energy Monte Carlo solutions (electronic appendix)	153
List of Contributors	155

List of Tables

Table 1. Participant information for the reference solutions29
Table 2. Estimated number of histories (in millions) used for the Monte Carlo solutions of the benchmark29
Table 3. Eigenvalue solutions for the <i>Unrodded</i> configuration29
Table 4. Eigenvalue solutions for the <i>Rodded A</i> configuration30
Table 5. Eigenvalue solutions for the <i>Rodded B</i> configuration30
Table 6. Per cent error results for specific pin powers in the <i>Unrodded</i> configuration30
Table 7. Per cent error results for specific pin powers in the <i>Rodded A</i> configuration31
Table 8. Per cent error results for specific pin powers in the <i>Rodded B</i> configuration31
Table 9. Assembly power per cent error for the <i>Unrodded</i> configuration of the benchmark31
Table 10. Assembly power per cent error for the <i>Rodded A</i> configuration of the benchmark32
Table 11. Assembly power per cent error for the <i>Rodded B</i> configuration of the benchmark32
Table 12. Pin power distribution error measures for the <i>Unrodded</i> configuration of the benchmark32
Table 13. Pin power distribution error measures for the <i>Rodded A</i> configuration of the benchmark33
Table 14. Pin power distribution error measures for the <i>Rodded B</i> configuration of the benchmark33
Table 15. Percentage of fuel pins within the reference confidence intervals for the <i>Unrodded</i> configuration of the benchmark33
Table 16. Percentage of fuel pins within the reference confidence intervals for the <i>Rodded A</i> configuration of the benchmark34
Table 17. Percentage of fuel pins within the reference confidence intervals for the <i>Rodded B</i> configuration of the benchmark34
Table 18. Per cent error results for specific pin powers in slice #3 of the <i>Rodded B</i> configuration34
Table 19. Assembly power per cent error for slice #3 of the <i>Rodded B</i> configuration35
Table 20. Pin power distribution error measures for slice #3 of the <i>Rodded B</i> configuration35

Table 21. Percentage of fuel pins within the reference confidence intervals for slice #3 of the <i>Rodded B</i> configuration35
Table 22. Participant information for the three-dimensional extension benchmark problem40
Table 23. Brief code description for each participant three-dimensional extension benchmark problem41
Table 24. Eigenvalue solutions for the <i>Unrodded</i> configuration41
Table 25. Participant results for specific pin powers in slice #1 of the <i>Unrodded</i> configuration ..	.43
Table 26. Participant results for specific pin powers in slice #2 of the <i>Unrodded</i> configuration ..	.43
Table 27. Participant results for specific pin powers in slice #3 of the <i>Unrodded</i> configuration ..	.44
Table 28. Participant results for specific pin powers in the <i>Unrodded</i> configuration44
Table 29. Assembly power per cent errors for slice #1 of the <i>Unrodded</i> configuration46
Table 30. Assembly power per cent errors for slice #2 of the <i>Unrodded</i> configuration46
Table 31. Assembly power per cent errors for slice #3 of the <i>Unrodded</i> configuration47
Table 32. Assembly power per cent errors for the <i>Unrodded</i> configuration47
Table 33. Pin power distribution error measures for slice #1 of the <i>Unrodded</i> configuration50
Table 34. Pin power distribution error measures for slice #2 of the <i>Unrodded</i> configuration50
Table 35. Pin power distribution error measures for slice #3 of the <i>Unrodded</i> configuration51
Table 36. Pin power distribution error measures for the <i>Unrodded</i> configuration51
Table 37. Number of fuel pins within the reference confidence intervals for slice #1 of the <i>Unrodded</i> configuration54
Table 38. Percentage of fuel pins within the reference confidence intervals for slice #1 of the <i>Unrodded</i> configuration54
Table 39. Number of fuel pins within the reference confidence intervals for slice #2 of the <i>Unrodded</i> configuration54
Table 40. Percentage of fuel pins within the reference confidence intervals for slice #2 of the <i>Unrodded</i> configuration54
Table 41. Number of fuel pins within the reference confidence intervals for slice #3 of the <i>Unrodded</i> configuration55

Table 42. Percentage of fuel pins within the reference confidence intervals for slice #3 of the <i>Unrodded</i> configuration55
Table 43. Number of fuel pins within the reference confidence intervals for the <i>Unrodded</i> configuration55
Table 44. Percentage of fuel pins within the reference confidence intervals for the <i>Unrodded</i> configuration55
Table 45. Estimated CPU time for the <i>Unrodded</i> configuration56
Table 46. Eigenvalue solutions for the <i>Rodded A</i> configuration59
Table 47. Participant results for specific pin powers in slice #1 of the <i>Rodded A</i> configuration61
Table 48. Participant results for specific pin powers in slice #2 of the <i>Rodded A</i> configuration61
Table 49. Participant results for specific pin powers in slice #3 of the <i>Rodded A</i> configuration62
Table 50. Participant results for specific pin powers in the <i>Rodded A</i> configuration62
Table 51. Assembly power per cent errors for slice #1 of the <i>Rodded A</i> configuration64
Table 52. Assembly power per cent errors for slice #2 of the <i>Rodded A</i> configuration64
Table 53. Assembly power per cent errors for slice #3 of the <i>Rodded A</i> configuration65
Table 54. Assembly power per cent errors for the <i>Rodded A</i> configuration65
Table 55. Pin power distribution error measures for slice #1 of the <i>Rodded A</i> configuration68
Table 56. Pin power distribution error measures for slice #2 of the <i>Rodded A</i> configuration68
Table 57. Pin power distribution error measures for slice #3 of the <i>Rodded A</i> configuration69
Table 58. Pin power distribution error measures for the <i>Rodded A</i> configuration69
Table 59. Number of fuel pins within the reference confidence intervals for slice #1 of the <i>Rodded A</i> configuration72
Table 60. Percentage of fuel pins within the reference confidence intervals for slice #1 of the <i>Rodded A</i> configuration72
Table 61. Number of fuel pins within the reference confidence intervals for slice #2 of the <i>Rodded A</i> configuration72

Table 62. Percentage of fuel pins within the reference confidence intervals for slice #2 of the <i>Rodded A</i> configuration	72
Table 63. Number of fuel pins within the reference confidence intervals for slice #3 of the <i>Rodded A</i> configuration	73
Table 64. Percentage of fuel pins within the reference confidence intervals for slice #3 of the <i>Rodded A</i> configuration	73
Table 65. Number of fuel pins within the reference confidence intervals for the <i>Rodded A</i> configuration	73
Table 66. Percentage of fuel pins within the reference confidence intervals for the <i>Rodded A</i> configuration	73
Table 67. Estimated CPU time for the <i>Rodded A</i> configuration	74
Table 68. Eigenvalue solutions for the <i>Rodded B</i> configuration	77
Table 69. Participant results for specific pin powers in slice#1 of the <i>Rodded B</i> configuration	79
Table 70. Participant results for specific pin powers in slice#2 of the <i>Rodded B</i> configuration	79
Table 71. Participant results for specific pin powers in slice#3 of the <i>Rodded B</i> configuration	80
Table 72. Participant results for specific pin powers in the <i>Rodded B</i> configuration	80
Table 73. Assembly power per cent errors for slice#1 of the <i>Rodded B</i> configuration	82
Table 74. Assembly power per cent errors for slice#2 of the <i>Rodded B</i> configuration	82
Table 75. Assembly power per cent errors for slice#3 of the <i>Rodded B</i> configuration	83
Table 76. Assembly power per cent errors for the <i>Rodded B</i> configuration	83
Table 77. Pin power distribution error measures for slice#1 of the <i>Rodded B</i> configuration	86
Table 78. Pin power distribution error measures for slice#2 of the <i>Rodded B</i> configuration	86
Table 79. Pin power distribution error measures for slice#3 of the <i>Rodded B</i> configuration	87
Table 80. Pin power distribution error measures for the <i>Rodded B</i> configuration	87
Table 81. Number of fuel pins within the reference confidence intervals for slice#1 of the <i>Rodded B</i> configuration	90
Table 82. Percentage of fuel pins within the reference confidence intervals for slice#1 of the <i>Rodded B</i> configuration	90

Table 83. Number of fuel pins within the reference confidence intervals for slice#2 of the <i>Rodded B</i> configuration90
Table 84. Percentage of fuel pins within the reference confidence intervals for slice#2 of the <i>Rodded B</i> configuration90
Table 85. Number of fuel pins within the reference confidence intervals for slice#3 of the <i>Rodded B</i> configuration91
Table 86. Percentage of fuel pins within the reference confidence intervals for slice#3 of the <i>Rodded B</i> configuration91
Table 87. Number of fuel pins within the reference confidence intervals for the <i>Rodded B</i> configuration91
Table 88. Percentage of fuel pins within the reference confidence intervals for the <i>Rodded B</i> configuration91
Table 89. Estimated CPU time for the <i>Rodded B</i> configuration92

List of Figures

Figure 1. Modified three-dimensional configuration19
Figure 2. Fuel pin layout20
Figure 3. Benchmark fuel pin compositions and numbering scheme20
Figure 4. Three-dimensional geometry for the <i>Unrodded</i> configuration21
Figure 5. Geometry configuration for the upper axial water reflector21
Figure 6. Three-dimensional geometry for the <i>Rodded A</i> configuration22
Figure 7. Three-dimensional geometry for the <i>Rodded B</i> configuration22
Figure 8. Eigenvalue solutions for the <i>Unrodded</i> configuration42
Figure 9. Eigenvalue per cent errors for the <i>Unrodded</i> configuration42
Figure 10. Maximum pin power results for the <i>Unrodded</i> configuration45
Figure 11. Maximum per cent errors for the <i>Unrodded</i> configuration45
Figure 12. Inner UO ₂ assembly power per cent errors for the <i>Unrodded</i> configuration48
Figure 13. MOX assembly power per cent errors for the <i>Unrodded</i> configuration48
Figure 14. Outer UO ₂ assembly power results for the <i>Unrodded</i> configuration49
Figure 15. AVG per cent error for the <i>Unrodded</i> configuration52
Figure 16. RMS per cent error for the <i>Unrodded</i> configuration52

Figure 17. MRE per cent error for the <i>Unrodded</i> configuration	53
Figure 18. Percentage of fuel pins within the <i>Unrodded</i> configuration confidence intervals	56
Figure 19. Eigenvalue solutions for the <i>Rodded A</i> configuration	60
Figure 20. Eigenvalue per cent errors for the <i>Rodded A</i> configuration	60
Figure 21. Maximum pin power results for the <i>Rodded A</i> configuration	63
Figure 22. Maximum per cent errors for the <i>Rodded A</i> configuration	63
Figure 23. Inner UO ₂ assembly power per cent errors for the <i>Rodded A</i> configuration	66
Figure 24. MOX assembly power per cent errors for the <i>Rodded A</i> configuration	66
Figure 25. Outer UO ₂ assembly power per cent errors for the <i>Rodded A</i> configuration	67
Figure 26. AVG per cent error for the <i>Rodded A</i> configuration	70
Figure 27. RMS per cent error for the <i>Rodded A</i> configuration	70
Figure 28. MRE per cent error for the <i>Rodded A</i> configuration	71
Figure 29. Percentage of fuel pins within the <i>Rodded A</i> configuration confidence intervals	74
Figure 30. Eigenvalue solutions for the <i>Rodded B</i> configuration	78
Figure 31. Eigenvalue per cent errors for the <i>Rodded B</i> configuration	78
Figure 32. Maximum pin power results for the <i>Rodded B</i> configuration	81
Figure 33. Maximum per cent errors for the <i>Rodded B</i> configuration	81
Figure 34. Inner UO ₂ assembly power per cent errors for the <i>Rodded B</i> configuration	84
Figure 35. MOX assembly power per cent errors for the <i>Rodded B</i> configuration	84
Figure 36. Outer UO ₂ assembly power per cent errors for the <i>Rodded B</i> configuration	85
Figure 37. AVG per cent error for the <i>Rodded B</i> configuration	88
Figure 38. RMS per cent error for the <i>Rodded B</i> configuration	88
Figure 39. MRE per cent error for the <i>Rodded B</i> configuration	89
Figure 40. Percentage of fuel pins within the <i>Rodded B</i> configuration confidence intervals	92

EXECUTIVE SUMMARY

One of the important issues of deterministic transport methods for whole core reactor calculations concerns the accuracy of homogenisation techniques. A direct calculation for whole core heterogeneous geometries was not feasible in the past due to the limited capability of computers. One had to rely upon homogenisation techniques to collapse the spatial heterogeneities into a tractable homogenous description. These homogenisation techniques can introduce substantial error into the flux distribution and consequently reaction rates in the homogenised zone can be significantly in error. With modern computational abilities, direct whole core heterogeneous calculations are becoming ever increasingly more feasible. Given the trend in computational ability observed thus far, it is not unreasonable to assume that, with time, such whole core calculations will eventually become common place.

In this context, an OECD/NEA benchmark problem was created to test the ability of modern deterministic transport methods and codes to treat such reactor core problems without spatial homogenisation [1]. That benchmark was completed in 2003 and the OECD report is available [2]. In addition, detailed individual results of participants were published in a special issue of Progress in Nuclear Energy [3]. As a follow-up to that benchmark, an extension of the 3-D calculations was proposed in 2003 to provide a more challenging test of present day three-dimensional methods' ability to handle spatial homogeneities [4].

As for the benchmark model, three configurations were proposed with different levels of control rod insertion to focus more on the difficulties of a three-dimensional benchmark. However, the core height was reduced and a non-realistic symmetry was introduced to reduce the computational burden on all participants. When combined, these new features added to the difficulty of the benchmark by introducing steeper flux gradients across the core (both angular and spatial approximations became important). As in the previous benchmark, a seven group set of cross-sections was provided to the participants to describe the geometry.

Three configurations were devised: *Unrodded*, *Rodded A*, and *Rodded B*. As was the case with the original benchmark, very accurate multigroup Monte Carlo reference solutions were obtained for all three configurations. These reference Monte Carlo solutions were performed such that very precise estimates of the pin powers were obtained in three three-dimensional sections. This leads to four times as much data for the "extension" benchmark than that required for the original benchmark.

A total of twenty participants attempted the benchmark with only twelve completing and submitting a total of thirteen results. A fourteenth result utilising a homogenisation approach to the benchmark was performed by the authors of this benchmark and was included for comparison purposes. All of the participant solutions were compared to a reference Monte Carlo solution. Overall all the results submitted by the participants agree very well with the reference solutions. A majority of the participants obtained solutions that were more than acceptable for typical reactor calculations, showing that modern deterministic transport codes and methods can calculate the flux distribution reasonably well without relying upon spatial homogenisation techniques. As was the case with the original benchmark, the remaining errors in the participant solutions can be attributed to the high order space-angle approximation necessary to solve these particular benchmark problems, which may not be indicative of all heterogeneous problems.

Chapter 1

INTRODUCTION

The OECD/NEA Expert Group on 3-D Radiation Transport Benchmarks was formed to deal with scientific issues in the field of deterministic and stochastic methods and computer codes relative to three dimensional radiation transport. The main objectives of the Expert Group are to develop benchmarks and comparison exercises for 3-D radiation transport computer codes, to carry out validation of methods and identify their strengths, limitations, and accuracy, and to suggest needs for method development.

A recent benchmark, “3-D Radiation Transport Benchmarks for Simple Geometries with Void Regions,” considered geometries composed of highly absorbing medium with voided streaming paths. The analysis of the participant results was completed in 2000 and it was published as an OECD/NEA report [5]. Moreover, the detailed participant results can be found in a special issue of Progress of Nuclear Energy [6]. In a similar fashion, a more recent benchmark was proposed and contributions from participants were obtained. That benchmark, titled *Benchmark on Deterministic – A2-D/3-D MOX Fuel Assembly Benchmark Transport Calculations Without Spatial Homogenisation* was completed in 2003 and it was published as an OECD/NEA report [2]. In addition, detailed individual results of participants were published in a special issue of Progress in Nuclear Energy [3]. Using the lessons learned from the second benchmark, a third benchmark was proposed to increase the information gained from the analysis of the results.

The benchmark of this report focuses upon obviating homogenisation techniques. A direct calculation for whole core heterogeneous geometries was not feasible in the past due to the limited capability of computers. One had to rely upon homogenisation techniques to collapse the spatial heterogeneities into a tractable homogenous description. These homogenisation techniques can introduce substantial error in the flux distribution and thereby inaccurately predict the reaction rates in the homogenised zones. With modern computational abilities, direct whole core heterogeneous calculations have become more feasible although still very computationally expensive. However, it is not unreasonable to assume that with time, such calculations will eventually become common place with the advent of massively parallel computing platforms and vast memory and disk space capabilities.

With this premise, the previous benchmark investigated a two-dimensional and three-dimensional LWR type problem in which fuel-coolant homogenisation was not performed. In that work, participants found that the space-angle approximations needed were large and cumbersome. The results of that benchmark indicated good performance by modern transport codes, however, due to the large problem size, participants could not thoroughly investigate the accuracy of their codes because of computational limits. To reduce the computational burden, the core height was therefore shortened for the current 3-D extension case. To make the problem “more interesting,” control rods were introduced. These two changes put more focus on the accuracy of the three-dimensional capabilities of participant’s codes rather than on the ability to treat very large problems.

In the same manner as carried out for the previous benchmark, accurate multigroup Monte Carlo reference solutions were obtained for all configurations. Twelve participants submitted a total of fourteen results for the new benchmark. This report provides an analysis of all of the participant results compared to the reference Monte Carlo solutions.

Chapter 2

DESCRIPTION OF THE BENCHMARK

The benchmark geometry chosen is a three-dimensional representation of the sixteen assembly (quarter core symmetry) C5 MOX fuel assembly problem specified by Cavarec *et. al.* in reference [7]. The new geometry is similar to that used in the preceding OECD benchmark [2]. The modifications introduced to the geometry here are meant to provide a more challenging test of present day three-dimensional methods' abilities to handle spatial heterogeneities while still allowing participants to investigate sensitivities to spatial and angular approximations implemented in their codes.

There are three significant changes that have been made to the three-dimensional geometry. First, the height of the geometry is reduced from 192.78 cm to 64.26 cm to allow participants to put the entire problem domain into memory and reduce computational times without trivialising the problem. Second, the control rod guide tubes and fission chamber are defined in the upper axial reflector. Third, a control rod macroscopic cross-section definition is introduced and is used to replace the control rod guide composition, in certain parts of the reactor. Figure 1 gives the new dimensions of the three-dimensional geometry where the pin-cell (Figure 2) and assembly layout (Figure 3) of reference 2 have been maintained. In Figure 2, the side length of the fuel-pin cell is 1.26 cm and the radius of the cylinder is 0.54 cm. It is important to note that in Figure 1 the fuel assemblies have been split into three axial zones (lower, middle, upper slices are called slice #1, #2, #3 respectively in the analysis). The intent is to allow each participant to provide fission rates for each pin-cell in each zone and from these the fission rate for each fuel pin is obtained.

We have chosen to define three calculational problems named *Unrodded*, *Rodded A*, and *Rodded B*. We begin by defining the *Unrodded* configuration detailed by Figure 4. In this configuration control rod clusters (one cluster for each assembly) are inserted into the upper axial water reflector as indicated by the shading in Figure 4. Figure 5 shows a slice in the radial direction through the upper axial reflector and should more clearly show the layout of the control rod clusters and fission chamber in the axial reflector region. It is important to note that the fission chambers and control rods are present in the axial reflector region and thus should be modelled. It is important to note that this geometrical configuration is unrealistic given the lower symmetry boundary condition. In short, control rods are inserted from both the top and bottom of the proposed reactor if no axial symmetry conditions were applied.

The second configuration, *Rodded A*, takes the *Unrodded* configuration as its starting position. In this configuration a control rod cluster is inserted 1/3 of the way into the inner UO₂ assembly as indicated by the shading in Figure 6. Similarly, the *Rodded B* configuration also takes the *Unrodded* configuration as its starting point. In this configuration, however, control rod clusters are inserted 2/3 of the way into the inner UO₂ assembly and 1/3 of the way into both MOX assemblies as indicated by the shading in Figure 6.

To describe the geometry, a seven group set of cross-sections was obtained. The number densities and the dimensions of the fuel, cladding, and assemblies specified by S. Cathalau *et al.* in reference [8] were inputted into the collision probability code DRAGON (G. Marleau *et al.*) which made use of the WIMS-AECL 69 group library [9]. The seven group, transport corrected, isotropic scattering cross-sections for UO₂, the three enrichments of MOX, the guide tubes and fission chambers, and the moderator described in the problem specification are provided in Appendix A. The participants are meant to use all of the provided cross-section as specified but substitute the transport corrected total cross-section for the total cross-section in their solutions.

In DRAGON, each fuel type was represented as a single pin-cell in an infinite-lattice fine-mesh collision probability calculation. A full anisotropic collision probability calculation was performed and standard flux weighting was used to collapse to seven energy groups and to homogenize fuel, gap, and cladding materials into homogenised fuel compositions. The seven-group moderator, homogenised guide tube, control rod, and fission chamber cross-sections were obtained using a UO₂ fuel spectrum. It is very important to note that all of the pin-cells in Figure 3 have the geometry shown in Figure 2, where for the fission chamber and guide tube, the “Fuel-Clad Mix” in Figure 2 is to be replaced with Fission chamber or guide tube compositions as necessary.

It is acknowledged that the individual pin-cell lattice representation, the spatial homogenisation, the group collapse, and the use of a single set of water cross-sections introduced error into the multigroup solution compared to a continuous energy solution of the same problem. However, the object of this benchmark is not to examine the validity of the multigroup approximation with respect to the continuous energy approach, but instead to provide a reasonable set of multigroup cross-sections in which there is no fuel-coolant homogenisation. In an attempt to assess the errors incurred by the multigroup cross-section methodology, some of the participants solved the continuous energy specification of the benchmark as supplementary contributions. However, these additional continuous energy solutions were not taken into account in the analysis of results for the consistency of result comparison against the multigroup reference solutions.

With the errors in cross-sections neglected, the geometry defined by Figures 1-7 combined with the seven-group cross-sections of Appendix A, provide an adequate basis for determining the accuracy of deterministic transport codes. For each configuration, the participants were requested to report the eigenvalue and the fission rates in each pin over each axial slice, and a reference multigroup Monte Carlo solution was obtained using the MCNP code [10]. These reference solutions provided very precise eigenvalue solutions in addition to pin power predictions for all of the fuel pin-cell slices. Similar to the previous benchmark, auxiliary multigroup Monte Carlo reference solutions were obtained by some of the participants. A comparison of the reference solutions obtained by the participants is provided in Chapter 5 of this report.

Figure 1. Modified three-dimensional configuration

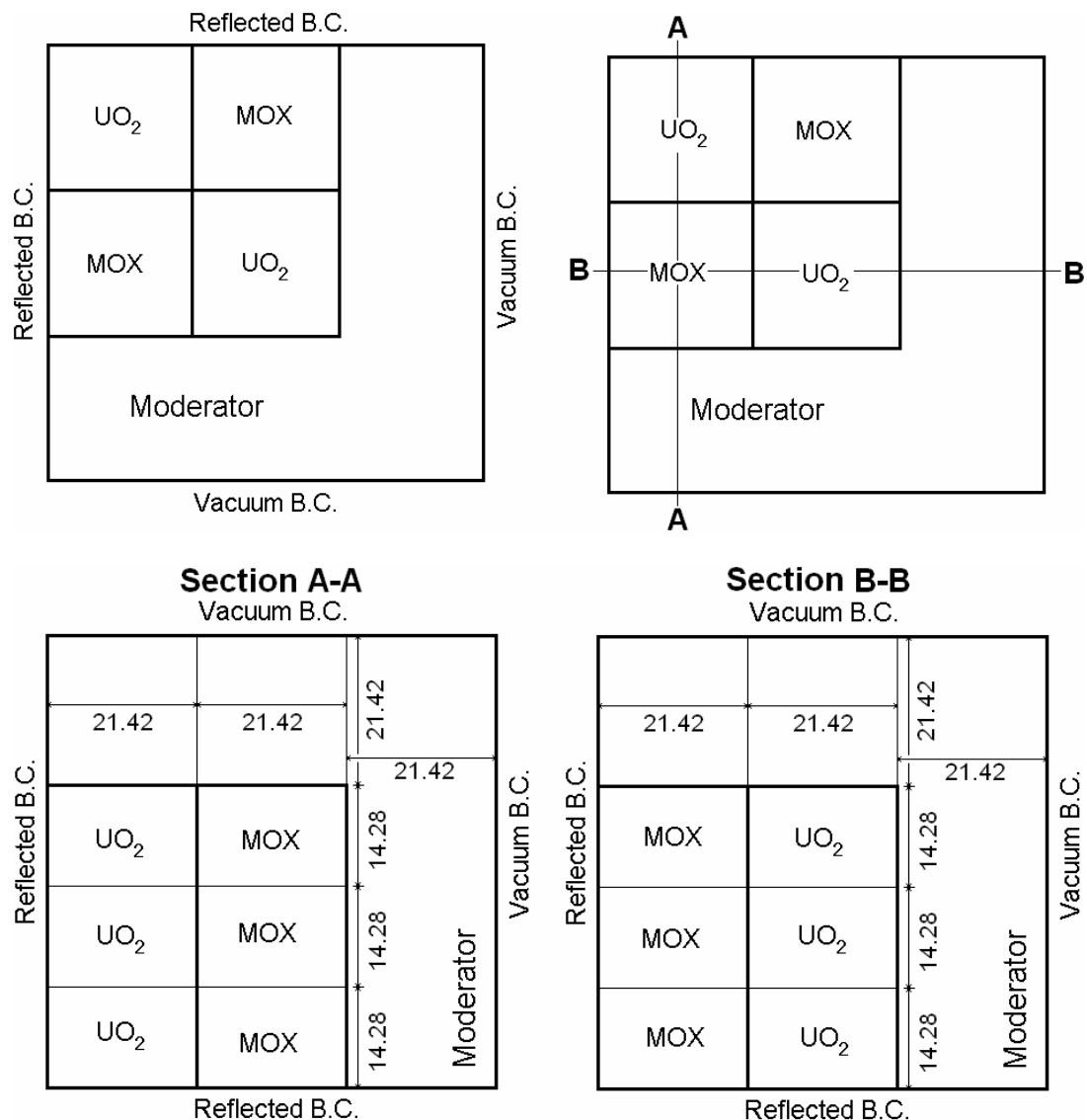


Figure 2. Fuel pin layout

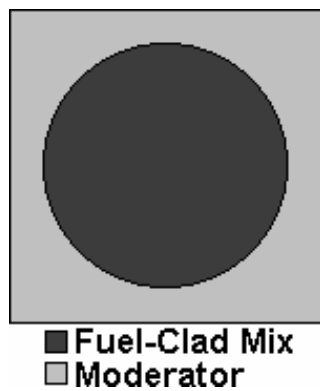


Figure 3. Benchmark fuel pin compositions and numbering scheme

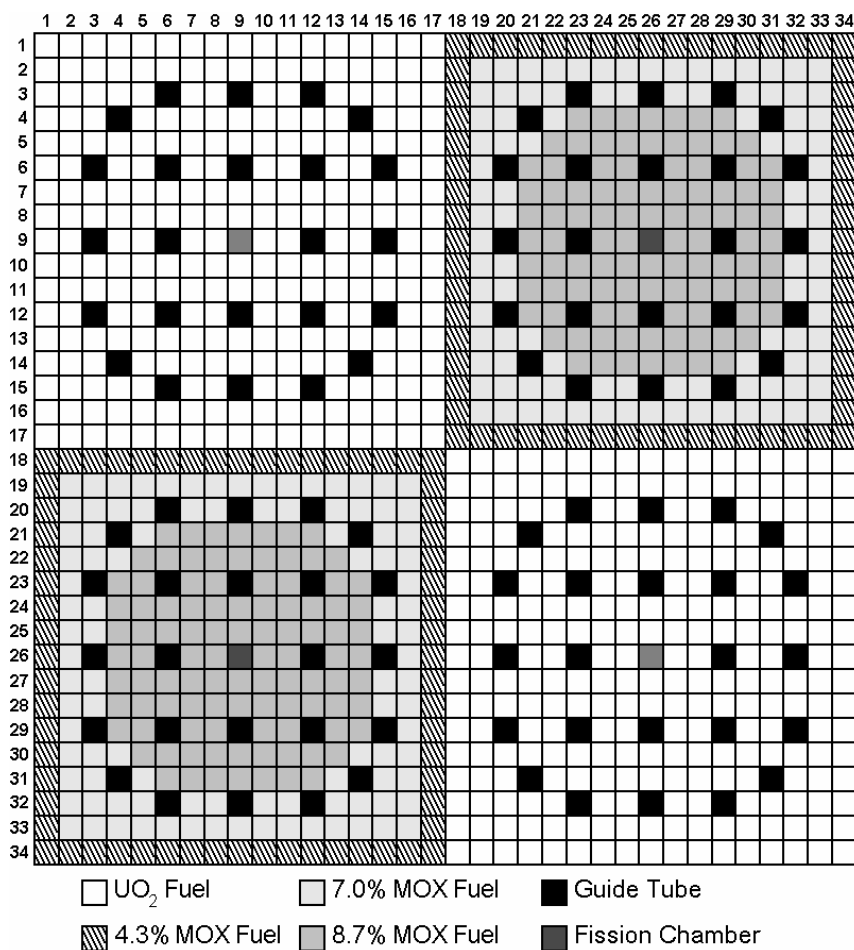


Figure 4. Three-dimensional geometry for the *Unrodded* configuration

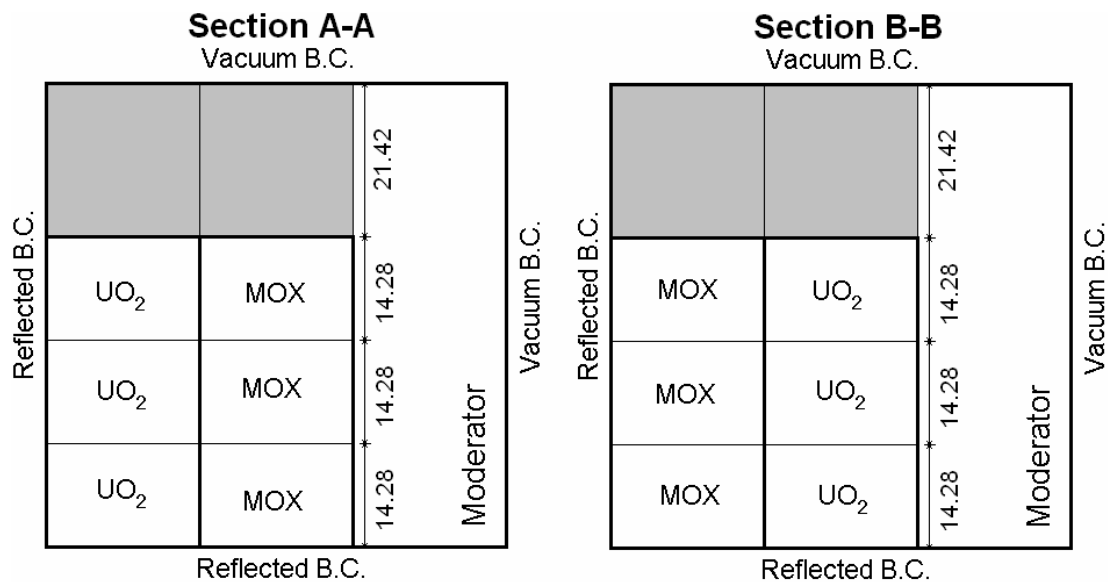


Figure 5. Geometry configuration for the upper axial water reflector

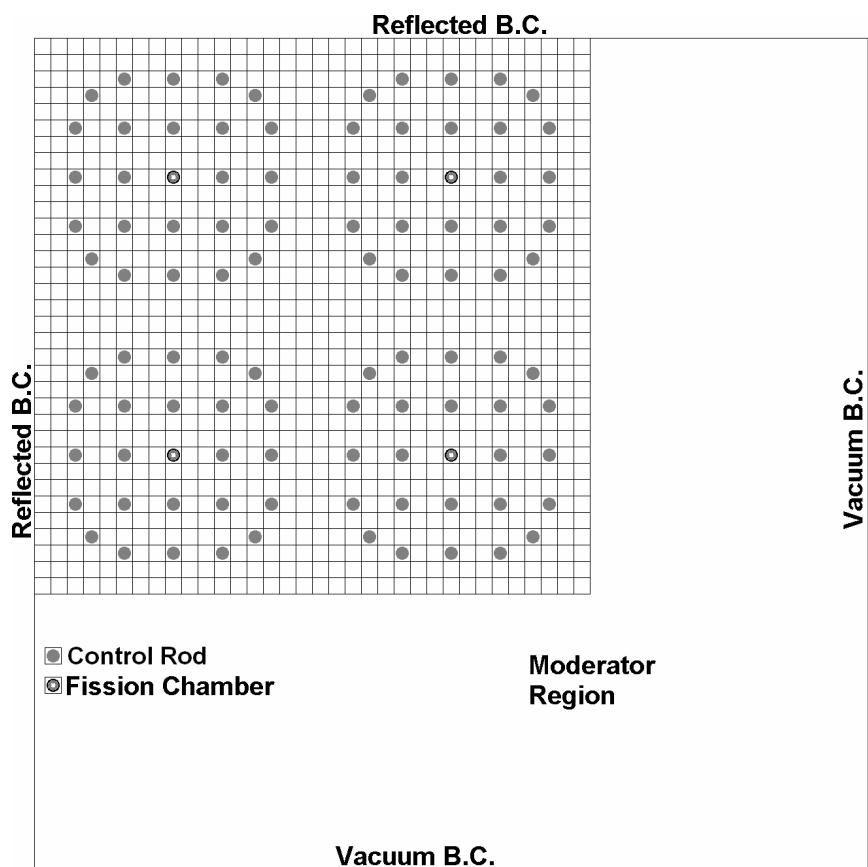


Figure 6. Three-dimensional geometry for the *Rodded A* configuration

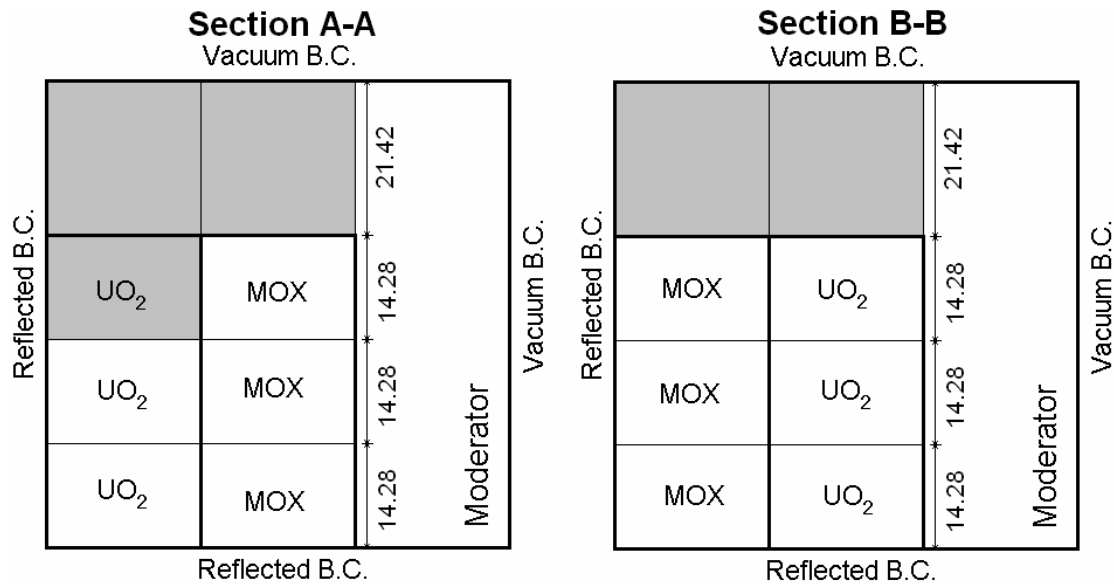
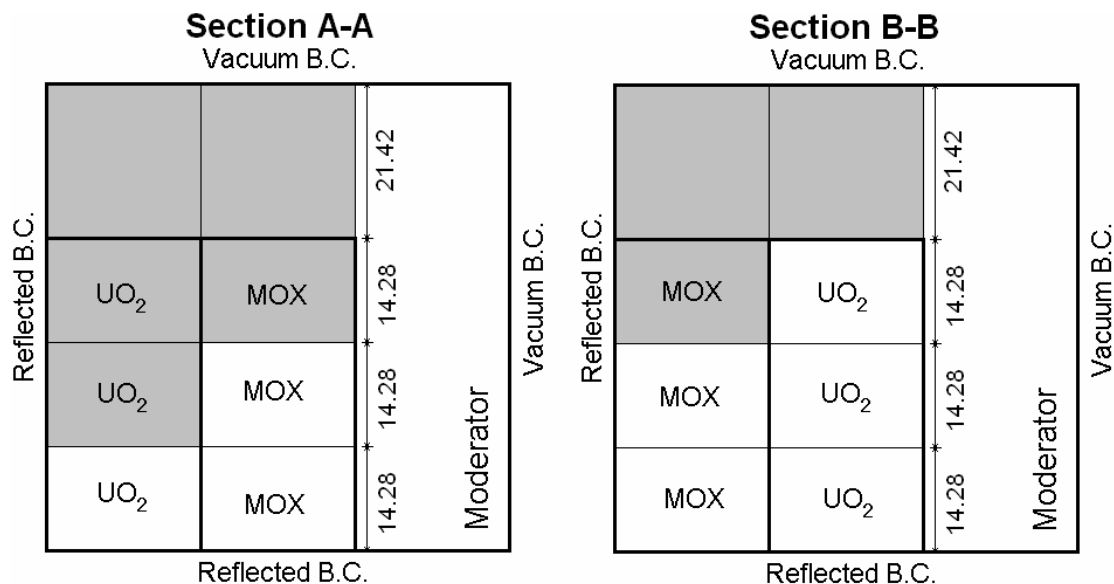


Figure 7. Three-dimensional geometry for the *Rodded B* configuration



Chapter 3

PARTICIPANTS AND CODES USED

Apart from the Monte Carlo multigroup reference solution (ANL solution) used for the final comparison of contributed results, a few additional Monte Carlo reference solutions were provided by participants and a comparison of those reference solutions obtained by the participants is made in Chapter 5. The following describe those contributors who provided the additional reference solutions.

1. Argonne National Laboratory (ANL), USA

Participants: M.A. Smith, N. Tsoulfanidis, R.N. Blomquist and E.E. Lewis
Code used: MCNP and VIM

2. Russian Research Center Kurchatov Institute (RRC KI), Russian Federation

Participants: V.D. Davidenko and V.F. Tsibulsky
Code used: UNKMK

A total of 12 participants contributed 13 results for the three-dimensional configuration. An additional solution based upon a homogenisation approach was also included for comparison purposes. The complete list of participants is presented below. Calculation details provided by participants can be found in Appendix B.

1. Gesellschaft fuer Anlagen- und Reaktorsicherheit (GRS) mbH, Germany

Participants: A. Seubert, S. Langenbuch, and W. Zwermann
Code used: TORT (S_N)

2. Hanyang University (HU), Korea

Participants: Hong-Chul Kim, J.K. Kim, and C.Y. Han
Code used: THREEANT (S_N)

3. Korea Advanced Institute of Science and Technology (KAIST), Korea

Participants: N.Z. Cho and G.S. Lee
Code used: CRX (method of characteristics 2-D/ S_N 1-D)

4. Institute of Physics and Power Engineering (IPPE), Russian Federation

Participants: I.R. Suslov
Code used: MCCG3-D (method of characteristics)

5. Russian Research Center Kurchatov Institute (RRC KI), Russian Federation

Participants: V.D. Davidenko and V.F. Tsibulsky
Code used: UNKGRO (method of characteristics with stochastic rays)

6. Argonne National Laboratory (ANL), USA

Participants: M.A. Smith, N. Tsoulfanidis, E.E. Lewis, G. Palmiotti, T. Taiwo and R. Blomquist

Code used: VARIANT-ISE (nodal spherical harmonics with integral transport),
VARIANT-SE (nodal spherical harmonics), and
VARIANT-Homog (nodal P_N with homogenised cross-sections)

7. Los Alamos National Laboratory (LANL), USA

Participants: J.A. Dahl, R.E. Alcouffe and R.S. Baker

Code used: PARTISN (S_N)

8. Radion Technologies, USA

Participants: T. Wareing

Code used: ATTILA (3-D) (S_N)

9. Penn State University (PSU), USA

Participants: J. Klingensmith, Y. Azmy, J. Gehin and R. Orsi (ENEA-Italy)

Code used: TORT (S_N)

10. TEPCO Systems Corporation (TEPSYS), Japan

Participants: S. Kosaka

Code used: CHAPLET (method of characteristics)

11. Commissariat à l'Energie Atomique (CEA), France

Participants: P. Humbert

Code used: PANDA (S_N)

12. University of Florida (UF), USA

Participants: Alireza Haghishat, Ce Yi, Glenn E. Sjoden, and G. Longoni

Code used: PENTRAN- SS_N (S_N)

Chapter 4

METHOD OF RESULTS ANALYSIS

The goal set forth to each participant was to provide an eigenvalue and normalised pin power solution (total power = number of fuel pins) for the benchmark problem. The comparison of the eigenvalue result is straightforward since it is a unique number for which a very precise estimate can be obtained using the Monte Carlo code. The comparison of the pin power distribution is not so straightforward since there are 1 056 total fuel pins or 540 unique fuel pins by symmetry reduction in Figure 3. For each configuration, 1 620 fuel pin powers were requested from each participant leading to a total of 4 860 data points for the entire problem. A direct comparison of all 4 860 pin powers on an individual basis, like that done with the eigenvalue, would result in an overwhelming amount of information and is not very instructive.

To reduce the amount of information, the following unique pin power per cent error measures were selected: per cent error on maximum pin power (peaking), maximum per cent error in the distribution, and the per cent errors of the individual assembly powers. The importance of these per cent error measures is clear since they represent individual estimates of unique quantities.

To assess the overall pin power distribution, the following collective per cent error measures were selected: average pin power per cent error (AVG), root mean square (RMS) of the pin power per cent error distribution, and mean relative pin power per cent error (MRE). Equation 1 defines the AVG error, where N is the number of fuel pins and e_n is the calculated per cent error for the n th pin power, p_n .

$$AVG = \frac{\sum_{n=1}^N |e_n|}{N} \quad (1)$$

Using similar notation, Eq. 2 defines the RMS per cent error (note this equation was defined improperly in the previous benchmark, but the correct definition was used in the results analysis), and Eq. 3 defines the MRE error (p_{avg} is the average pin power).

$$RMS = \sqrt{\frac{\sum_{n=1}^N e_n^2}{N}} \quad (2)$$

$$MRE = \frac{\sum_{n=1}^N |e_n| \cdot p_n}{N \cdot p_{avg}} \quad (3)$$

From Eq.1, one can see that the AVG error measure will give a simple average of the pin power per cent error. This is a very useful quantity since it is a straightforward number that gives an overall idea of the pin power distribution accuracy. However the simple average does not indicate the way in which the error is distributed. Thus the RMS and MRE error measures are also used. The RMS error measure weights the largest per cent errors more than the smallest ones. Consequently, it gives a better assessment of the distribution of the per cent errors than the AVG error measure can give. The MRE error measure weights the per cent error with the reference pin power, thereby linking the per cent error distribution to the power distribution. Consequently, the MRE error measure gives an estimate of the total amount of error in the pin power distribution where the RMS error is not linked to the actual power distribution. In effect, the MRE error measure diminishes the importance of error in the low power region in favour of error in the high power region. An instructional example is included in Appendix C for clarity of the three measures of the error distribution.

The last information gathered from the participant solutions was a tally of the number of fuel pin power predictions that made it within the 68%, 90%, 98%, and 99.8% confidence intervals of the reference solution pin power prediction. This error measure indicates the per centage of the fuel pins that the participant's code predicts within the levels of precision of the Monte Carlo reference solution.

A comparison of the participant computational times was not carried out for this benchmark. With present day computational abilities, comparison of computational efficiency between different codes is almost impossible without first performing a series of identical timing benchmarks on all of the various participant platforms. Additionally, some methods are penalised by the computational resources available to them, such as core memory size, available scratch disk space, limited parallel computing capabilities, etc. Such complications quite simply cannot be accounted for in timing benchmarks and would inevitably result in an inadequate estimation of the methods involved. We have therefore chosen to forego a rigorous comparison of computational efficiency and simply report a crude estimate of the CPU time that each participant reported. This result is representative of the time required for the participant to obtain their submitted solution on a regular basis and should not be construed as a figure of merit for computational efficiency.

Chapter 5

COMPARISONS OF THE REFERENCE MONTE CARLO SOLUTIONS

With the error measures selected, we now compare the various Monte Carlo multigroup reference solutions submitted by the participants. Table 1 gives the information about the participants while Table 2 gives the estimated number of histories for all of the Monte Carlo solutions. As can be seen in Table 2, the reference MCNP solution used for this work does not implement the largest number of histories and therefore does not necessarily constitute the best solution. However, it was felt for this benchmark that it would be sufficient. The three different MCNP solutions provided by ANL were carried out using different starting random number seeds and different particle management (number of particles per batch and the number of batches). No uncertainty data was provided for UNKMK, therefore, the error results were estimated using the reference solution uncertainties and the relative number of particles used in the calculations.

Tables 3, 4, and 5 give the eigenvalue solutions for the *Unrodded*, *Rodded A*, and *Rodded B* configurations, respectively. In Tables 3-5, the per cent error with respect to the reference MCNP solution, and the 68%, 98%, and 99.8% confidence intervals associated with all of the Monte Carlo solutions is given. As can be seen, several of the solutions are within the 68% confidence interval of the reference with most being within a 99.8% confidence interval. It is important to note that the statistical error associated with both the reference MCNP solution and the participant Monte Carlo solution must be combined to give the overall confidence interval.

Tables 6, 7, and 8 summarise the information for several specific pin powers selected as error measures in Chapter 4 for the *Unrodded*, *Rodded A*, and *Rodded B* configurations, respectively. These results represent the overall pin power results rather than a selected slice. Later in this section we will look at the worst case result for a single slice of results. In Tables 6-8, the per cent error information for the reference MCNP solution represents the 98% confidence intervals associated with the various pin powers. Similarly, the associated reference statistical errors provided with the participant maximum per cent error are the reference MCNP 98% confidence intervals for the fuel pin that had the maximum error. For the maximum pin power most of the participant Monte Carlo solutions agree with the reference Monte Carlo solution within the 98% confidence interval, but not a 68% confidence interval. For the maximum per cent error, none of the participant Monte Carlo solutions are within the reference 98% confidence interval. However, similar to the eigenvalue, the confidence interval of both solutions must be merged to obtain the true confidence interval.

Tables 9, 10, and 11 give the assembly powers for the participant reference solutions along with the reference MCNP solution for the *Unrodded*, *Rodded A*, and *Rodded B* configurations, respectively. As can be seen, all of the assembly powers come well within or very close to the 98% confidence intervals of the reference MCNP solution.

Tables 12, 13, and 14 give the pin power distribution error measures for the Monte Carlo reference solutions for the *Unrodded*, *Rodded A*, and *Rodded B* configurations, respectively. As can be seen, none of the participant Monte Carlo solutions are outside of the 98% confidence interval of the reference MCNP solution for any of the pin power distribution error measures.

The final error measure to compare is the per centage of fuel pins within the reference MCNP 68%, 90%, 98% and 99.8% confidence intervals tabulated in Tables 15, 16, and 17, for the *Unrodded*, *Rodded A*, and *Rodded B* configurations, respectively. Given that we are comparing Monte Carlo solutions to Monte Carlo solutions we should expect the per centage of fuel pins within the confidence interval to agree with the confidence interval of the reference MCNP solution (68% within the 68% confidence interval). As can be seen, with the exception of the UNKMK code, the participant solutions tend to agree with the reference Monte Carlo solutions. A possible reason for the discrepancy in the UNKMK solution is the lack of accurate uncertainty data (it was estimated for this report).

Continuing, the Monte Carlo results for slice #3 of the *Rodded B* configuration are inspected. The maximum pin power and the maximum per cent error are tabulated in Table 18 along with the per cent errors from the reference MCNP. As was the case for the overall pin power results, the reference MCNP information represents the 98% confidence intervals associated with the error measures. For the maximum pin power, all of the participant Monte Carlo solutions agree well with the reference MCNP solution with only one outside of the 98% confidence interval. For the maximum per cent error, none of the participant reference solutions are within the reference 98% confidence interval, the confidence interval of both solutions have been merged to obtain the true confidence interval.

Table 19 gives the assembly powers for the participant reference solutions and the reference MCNP for slice #3 of the *Rodded B* Configuration. As was the case for the overall pin power results, all of the assembly powers are well within the 98% confidence intervals of the reference MCNP solution. The same is found to be true for the pin power distribution error measures which are given in Table 20.

Table 21 gives the per centage of fuel pins that fall within the reference MCNP confidence 68%, 90%, 98% and 99.8% confidence intervals. These results are similar to those seen in Tables 15-16.

We can conclude from the analysis of the above Monte Carlo solutions that they all agree well using a 98% confidence interval. Although some of the error measures such as the eigenvalue and assembly powers agreed well using a 68% or 90% confidence interval, only a 98% confidence interval guaranteed that all of the error measures were satisfied. In general, the maximum per cent error was the limiting error measure making the 98% confidence interval essential. Thus, 98% reference MCNP confidence intervals are used throughout the rest of this document to determine whether deterministic calculations are “in agreement” with the Monte Carlo reference solution.

The reference MCNP solution is provided electronically in Appendix D and both the pin power and statistical error tables for the two- and three-dimensional geometries can be printed out using the preformatted worksheets in the EXCEL workbooks. Similarly, all of the analysis tools and information used to compare the various Monte Carlo solutions are provided electronically in Appendix D. All of the Monte Carlo pin power solutions and error calculations with respect to the reference MCNP solution can also be printed or viewed if desired.

Table 1. Participant information for the reference solutions

Code names	Institution	Abbreviation	Country	Participants
Reference MCNP	Argonne National Laboratory	ANL	United States	M.A. Smith, N. Tsoulfanidis, R. N. Blomquist, E. E. Lewis
MCNP	Argonne National Laboratory	ANL	United States	M.A. Smith, N. Tsoulfanidis, R. N. Blomquist, E. E. Lewis
MCNP	Argonne National Laboratory	ANL	United States	M.A. Smith, N. Tsoulfanidis, R. N. Blomquist, E. E. Lewis
VIM	Argonne National Laboratory	ANL	United States	M.A. Smith, N. Tsoulfanidis, R. N. Blomquist, E. E. Lewis
UNKMK	Russian Research Center Kurchatov Institute	RRC KI	Russia	V. D. Davidenko V. F. Tsibulsky

Table 2. Estimated number of histories (in millions) used for the Monte Carlo solutions of the benchmark

Code names	<i>Unrodded</i>	<i>Rodded A</i>	<i>Rodded B</i>
Reference MCNP	500	500	500
MCNP	300	300	300
MCNP	500	500	500
VIM	513	513	513
UNKMK	2700	2800	2900

Table 3. Eigenvalue solutions for the *Unrodded* configuration

Code names	Eigenvalue	Per cent error	68%	98%	99.8%
Reference MCNP	1.14308		0.003	0.006	0.008
MCNP	1.14290	-0.016	0.004	0.010	0.014
MCNP	1.14309	0.001	0.003	0.006	0.008
VIM	1.14301	-0.006	0.003	0.007	0.010
UNKMK	1.14303	-0.004	0.002	0.003	0.005

Table 4. Eigenvalue solutions for the *Rodded A* configuration

Code names	Eigenvalue	Per cent error	68%	98%	99.8%
Reference MCNP	1.12806		0.003	0.006	0.008
MCNP	1.12808	0.002	0.004	0.010	0.014
MCNP	1.12807	0.001	0.003	0.006	0.008
VIM	1.12811	0.004	0.003	0.007	0.010
UNKMK	1.12806	0.000	0.002	0.003	0.005

Table 5. Eigenvalue solutions for the *Rodded B* configuration

Code names	Eigenvalue	Per cent error	68%	98%	99.8%
Reference MCNP	1.07777		0.003	0.006	0.008
MCNP	1.07779	0.002	0.004	0.010	0.014
MCNP	1.07775	-0.002	0.003	0.006	0.008
VIM	1.07771	-0.005	0.003	0.007	0.010
UNKMK	1.07772	-0.005	0.002	0.003	0.005

Table 6. Per cent error results for specific pin powers in the *Unrodded* configuration

Code names	Maximum pin power	Per cent error	Maximum per cent error	Associated reference MCNP statistical error
Reference MCNP	2.481	± 0.14		
MCNP	2.477	-0.18	0.67	± 0.38
MCNP	2.484	0.10	0.75	± 0.63
VIM	2.478	-0.15	0.76	± 0.56
UNKMK	2.482	0.03	0.65	± 0.19

Table 7. Per cent error results for specific pin powers in the *Rodded A* configuration

Code names	Maximum pin power	Per cent error	Maximum per cent error	Associated reference MCNP statistical error
Reference MCNP	2.253	± 0.14		
MCNP	2.255	0.06	0.87	± 0.55
MCNP	2.252	-0.05	0.73	± 0.43
VIM	2.253	-0.02	0.74	± 0.65
UNKMK	2.250	-0.15	0.51	± 0.36

Table 8. Per cent error results for specific pin powers in the *Rodded B* configuration

Code names	Maximum pin power	Per cent error	Maximum per cent error	Associated reference MCNP statistical error
Reference MCNP	1.835	± 0.19		
MCNP	1.839	0.21	0.77	± 0.54
MCNP	1.835	0.01	0.63	± 0.48
VIM	1.835	0.00	0.79	± 0.52
UNKMK	1.835	-0.01	0.44	± 0.26

Table 9. Assembly power per cent error for the *Unrodded* configuration of the benchmark

Code names	Inner UO ₂	Per cent error	MOX	Per cent error	Outer UO ₂	Per cent error
Reference MCNP	491.2	± 0.29	212.7	± 0.21	139.4	± 0.15
MCNP	491.1	-0.03	212.7	0.02	139.4	0.03
MCNP	491.2	-0.01	212.7	-0.01	139.5	0.05
VIM	491.0	-0.04	212.8	0.03	139.4	0.04
UNKMK	491.1	-0.02	212.7	0.02	139.4	0.01

Table 10. Assembly power per cent error for the *Rodded A* configuration of the benchmark

Code names	Inner UO ₂	Per cent error	MOX	Per cent error	Outer UO ₂	Per cent error
Reference MCNP	461.2	±0.28	221.7	±0.22	151.4	±0.16
MCNP	461.2	0.01	221.8	0.03	151.2	-0.12
MCNP	461.1	-0.01	221.7	0.01	151.4	0.01
VIM	461.3	0.02	221.7	-0.02	151.4	0.02
UNKMK	461.1	-0.03	221.8	0.02	151.4	0.02

Table 11. Assembly power per cent error for the *Rodded B* configuration of the benchmark

Code names	Inner UO ₂	Per cent error	MOX	Per cent error	Outer UO ₂	Per cent error
Reference MCNP	395.4	±0.26	236.6	±0.23	187.3	±0.18
MCNP	395.8	0.09	236.6	-0.02	187.1	-0.15
MCNP	395.6	0.04	236.6	-0.02	187.3	-0.03
VIM	395.4	0.00	236.7	0.02	187.3	-0.03
UNKMK	395.5	0.03	236.6	-0.01	187.3	-0.04

Table 12. Pin power distribution error measures for the *Unrodded* configuration of the benchmark

Code names	AVG	RMS	MRE
Reference MCNP	0.25	0.26	0.22
MCNP	0.15	0.19	0.13
MCNP	0.13	0.17	0.11
VIM	0.15	0.20	0.13
UNKMK	0.12	0.16	0.10

Table 13. Pin power distribution error measures for the *Rodded A* configuration of the benchmark

Code names	AVG	RMS	MRE
Reference MCNP	0.25	0.26	0.22
MCNP	0.15	0.20	0.12
MCNP	0.13	0.17	0.11
VIM	0.15	0.19	0.13
UNKMK	0.12	0.15	0.10

Table 14. Pin power distribution error measures for the *Rodded B* configuration of the benchmark

Code names	AVG	RMS	MRE
Reference MCNP	0.24	0.25	0.23
MCNP	0.16	0.21	0.15
MCNP	0.12	0.15	0.11
VIM	0.15	0.18	0.13
UNKMK	0.10	0.13	0.10

Table 15. Percentage of fuel pins within the reference confidence intervals for the *Unrodded* configuration of the benchmark

Code names	68%	90%	98%	99.8%
MCNP	64.8	93.3	98.7	99.8
MCNP	65.7	91.3	97.6	99.8
VIM	65.7	92.6	98.0	99.8
UNKMK	55.2	84.6	91.7	95.6

Table 16. Percentage of fuel pins within the reference confidence intervals for the *Rodded A* configuration of the benchmark

Code names	68%	90%	98%	99.8%
MCNP	65.9	92.8	97.8	99.8
MCNP	62.8	93.1	97.4	99.6
VIM	64.4	94.1	98.0	99.8
UNKMK	51.7	83.7	92.6	96.7

Table 17. Percentage of fuel pins within the reference confidence intervals for the *Rodded B* configuration of the benchmark

Code names	68%	90%	98%	99.8%
MCNP	59.1	90.0	96.3	99.3
MCNP	65.7	94.1	98.7	99.6
VIM	63.9	93.5	98.3	99.6
UNKMK	55.7	85.2	94.1	97.0

Table 18. Per cent error results for specific pin powers in slice #3 of the *Rodded B* configuration

Code names	Maximum pin power	Per cent error	Maximum per cent error	Associated reference MCNP statistical error
Reference MCNP	0.554	± 0.15		
MCNP	0.555	0.31	1.06	± 0.64
MCNP	0.555	0.18	1.01	± 0.56
VIM	0.553	-0.22	0.98	± 0.88
UNKMK	0.552	-0.36	0.86	± 0.51

Table 19. Assembly power per cent error for slice #3 of the *Rodded B* configuration

Code names	Inner UO ₂	Per cent error	MOX	Per cent error	Outer UO ₂	Per cent error
Reference MCNP	106.6	±0.13	81.4	±0.14	65.0	±0.11
MCNP	106.6	0.04	81.4	-0.02	64.9	-0.15
MCNP	106.6	0.00	81.3	-0.08	65.0	-0.06
VIM	106.6	0.00	81.4	-0.03	65.0	-0.01
UNKMK	106.6	0.01	81.4	-0.02	65.0	-0.04

Table 20. Pin power distribution error measures for slice #3 of the *Rodded B* configuration

Code names	AVG	RMS	MRE
Reference MCNP	0.42	0.43	0.13
MCNP	0.23	0.30	0.07
MCNP	0.21	0.27	0.06
VIM	0.25	0.32	0.08
UNKMK	0.18	0.23	0.05

Table 21. Percentage of fuel pins within the reference confidence intervals for slice #3 of the *Rodded B* configuration

Code names	68%	90%	98%	99.8%
MCNP	69.1	94.4	98.7	99.6
MCNP	66.1	94.1	98.7	99.4
VIM	64.4	93.9	98.3	99.8
UNKMK	60.7	91.5	98.5	99.3

Chapter 6

UNRODDED CONFIGURATION BENCHMARK RESULTS

There were 12 participants who submitted a total of 14 solutions for the three-dimensional extension benchmark. Table 22 gives the names of the participants along with their institution, the country that they are from, and the name of the code that produced the results they submitted. A brief description of the spatial and angular approximations implemented in each participant's code is given in Table 23. To view a complete summary of the participants' code and method used, refer to the original documentation submitted by each participant in Appendix B.

The purpose of the following analysis is not to point out the weaknesses or successes of any individual participant's code or method. Especially when considering that minor changes in the spatial and angular approximations implemented in any individual participant's code can substantially change the results shown here. The point of this analysis is to simply provide the participants with an objective comparison of the results they submitted with a reference MCNP solution and solutions submitted by their peers.

For this benchmark, the solutions from eleven first order codes and three second order codes were submitted. Four of the first order codes implement the method of characteristics with the remaining seven implementing a form of discrete ordinates. Six of discrete ordinates approaches implemented a fine mesh approach and one used a finite element approach. For the second order codes, two implement a finite element approach combined with a nodal spherical harmonics approximation. The last second order code implemented a nodal spherical harmonics method using homogenised pin-cell cross-sections (no explicit fuel pin representation).

As discussed in Chapter 2, the three-dimensional extension benchmark contains three configurations: *Unrodded*, *Rodded A*, and *Rodded B*. The results for the *Unrodded* configuration will be inspected in this chapter with the other configurations inspected in each consecutive chapter. To minimise the content of this report, plots of the data will only be provided for the core pin power solutions.

Table 24 tabulates the participant eigenvalue solutions and the per cent errors with respect to the reference MCNP solution. Again, the statistical errors for the reference MCNP solution are the 98% confidence intervals. Figure 8 displays the eigenvalue solutions ordered with respect to decreasing eigenvalue accuracy where the dashed line represents the reference MCNP solution and the confidence intervals are too small to view. Figure 9 displays the eigenvalue per cent error with respect to decreasing eigenvalue accuracy where the reference MCNP statistical error again is too small to be distinguished on this plot. As can be seen in Figures 8 and 9 and Table 24, a wide range of solutions were obtained but a majority of the solutions are reasonably close to the reference MCNP solution. While none of the participants' codes are within the 98% confidence interval of the MCNP eigenvalue, the average error for all the participant solutions is only about 0.12%, with only six of the solutions having large errors greater than 0.1% or 100 pcm.

The specific pin power error measures for each slice are tabulated in Tables 25-27 with the results for the core distribution given in Table 28. Figure 10 displays the maximum pin power results and Figure 11 the maximum per cent errors found in each participant solution. For each participant solution, the pin location of the maximum error was determined and the statistical error associated with that pin obtained. This statistical error has been tabulated for each participant in Tables 25-28 in the column titled “associated reference MCNP statistical error” and included in Figure 11 as “associated statistical error.” All of the participant solutions in Figures 10-11 are ordered with respect to decreasing solution accuracy.

Starting with slice #1 in Table 25, three participants obtained a maximum pin power within the 98% confidence interval with the remainder of participants significantly greater than 98%. This pattern is not continued for slices #2 and #3 where five participants succeed in slice #2 and eight succeed in slice #3 as seen in Tables 26 and 27. The core pin power results are different from slices #1-3 in Table 28 with three participants within the 98% confidence interval.

The maximum per cent error results in Tables 25-28 and Figure 11 show that none of the participants’ codes succeed in coming within the 98% MCNP confidence intervals. Only three of the participant codes have maximum errors less than 1% but eleven achieved maximum errors less than 5%. Not surprisingly, the maximum per cent error proved to be the most difficult measure for deterministic methods to satisfy. It also represented the largest deviations between Monte Carlo calculations.

The assembly power error measures are considered next, the results of which are tabulated in Tables 29-32. Figure 12 displays the participant results for the inner UO₂ assembly power, Figure 13 the results for the MOX assembly power, and Figure 14 the results of the outer UO₂ assembly power. For the slice #1 inner UO₂ assembly power four participant solutions are within the 98% confidence interval. For slice #2, six are within the 98% confidence intervals while there are only three for slice #3. It is important to note that only two participants are within the 98% confidence interval for all three slices. For the core assembly power distribution, three participants are within the 98% confidence interval, only two of which met this goal for all three slices. A different trend is seen for the outer UO₂ assembly. Seven participants are within the 98% confidence interval for slice #1 with six succeeding for slice #2 and none for slice #3. For the core pin power results in Table 30, seven succeeded in meeting the 98% confidence interval. For the MOX assembly, six meet the 98% interval for slice #1 with only two in slice #2 and only one in slice #3. For the core result in Table 30, eight participant solutions are within the 98% confidence interval.

Tables 33-36 give the pin power distribution error measures. Figure 15 displays the AVG error measure results, Figure 16 the RMS error measure results, and Figure 17 the MRE error measure results. Six of the participants are within the 98% confidence interval for the AVG error measure in slice #1. In both slices #2 and #3 there are seven participants within the 98% confidence interval. For the core wide results, six participants agree with the reference MCNP solution with twelve less than 1% in error. The results of the RMS error measure are consistent with the AVG measure. Six of the participants are within the 98% confidence interval in slice #1 with six in slice #2 and six in slice #3. The core wide results are not as good with only three of the participants within the 98% confidence interval and eleven less than 1% in error. For the MRE error measure, six of the participants are within the 98% confidence interval for slice #1 with six for slice #2 and seven for slice #3. For the core wide results, six participants are within the 98% confidence interval with twelve less than 1% in error. The conclusion that can be drawn from these results is that, on the whole, a majority of the error in the participants results is small (as indicated by the AVG error measure), but there are a substantial number of small errors (as indicated by

the decrease in accuracy of the RMS error measure) with most of this lying in the low power region of the core (as indicated by the consistent accuracy of AVG and MRE).

The last information gathered from the participant results is the number of fuel pins that lay within the 68%, 90%, 98%, and 99.8% confidence intervals of the reference MCNP solution. Tables 37, 39, 41, and 43 tabulate the number of fuel pins within the various confidence intervals while Tables 38, 40, 42, and 44 tabulate the percentage of fuel pins that are within the confidence intervals. Figure 18 plots the participant results, ordered with respect to the 98% confidence interval results. As can be seen, none of the participants match the 98% confidence interval for any individual slice and relatively few are close. This error measure represents by far the strictest measure of accuracy that can be applied to the pin power distribution; however, it is subject to significant uncertainty from the normalization procedure applied as discussed in the original benchmark. For this reason, this error measure should not be assumed essential to guarantee the accuracy of any given solution.

Overall the inaccuracies in the *Unrodded* configuration can be attributed, in part, to insufficient space-angle approximations implemented by the participants in their codes. In some cases the participants submitted multiple results using coarser mesh or coarser angular approximations than those used in the above analysis. In almost all of those cases the coarser solutions were significantly less accurate than those shown in this chapter. Since relatively few participants turned in multiple solutions, a complete analysis of the refinement of the participant solution was not possible and therefore it is not included here. For cross referencing, the details of the spatial and angular refinements can be found in the participants' original submittal results and documentation provided in Appendix E (see also Appendix B). Also, for completeness, an estimate of each participant CPU time is provided in Table 45.

It is suggested that as a first approach to improving the accuracy of a solution, that additional simultaneous refinement of the angular and spatial variables be investigated by the participants. The analysis tools used for the *Unrodded* configuration of this benchmark are provided electronically in Appendix F and can be used by the participants for future comparisons if desired.

Table 22. Participant information for the three-dimensional extension benchmark problem

Code names	Institution	Abbreviation	Country	Participants
CHAPLET-3D	TEPCO Systems Corporation	TEPSYS	Japan	Shinya Kosaka
CRX	Korea Advanced Institute of Science and Technology	KAIST	Korea	Nam Zin Cho and Gil Soo Lee
MCCG3D	Institute of Physics and Power Engineering	IPPE	Russia	Igor R. Suslov
PANDA	Commissariat à l'Energie Atomique	CEA	France	Philippe Humbert
PARTISN	Los Alamos National Laboratory	LANL	United States	Jon A. Dahl, Raymond E. Alcouffe, and Randal S. Baker
ATTILA	Radion Technologies	RADION	United States	Todd A. Wareing
THREEDANT-HU	Hanyang University, Dept. Nuclear Engineering	HU-Korea	Korea	Hong-Chul Kim, Chi Young Han, and Jong Kyung Kim
TORT-GRS	Gesellschaft fuer Anlagen- und Reaktorsicherheit (GRS) mbH	GRS	Germany	Armin Seubert, Winfried Zwermann, and Siegfried Langenbuch
TORT-PSU	Pennsylvania State University, Dept. Nuclear Engineering	PSU-USA	United States	J. Klingensmith, Y. Azmy, J. Gehin, and R. Orsi (ENEA, Italy)
UNKGRO	Russian Research Centre "Kurchatov Institute"	RRC KI	Russia	Vladimir D.Davidenko, Viktor F. Tsibulsky
PENTRAN	Florida University, Nuclear and Radiological Eng. Dept.	UF-USA	United States	Alireza Haghishat
VARIANT-ISE	Argonne National Laboratory	ANL	United States	Micheal Smith, Elmer E. Lewis, and Nicholas Tsoufanidis
VARIANT-SE	Argonne National Laboratory	ANL	United States	Micheal Smith, Elmer E. Lewis, and Nicholas Tsoufanidis
VARIANT-Homog	Argonne National Laboratory	ANL	United States	Micheal Smith, Elmer E. Lewis, and Nicholas Tsoufanidis

Table 23. Brief code description for each participant three-dimensional extension benchmark problem

Code names	Method description
CHAPLET-3D	3-D finite difference calculation with the corrections of internal 1-D / 2-D MOC solutions
CRX	Fusion method (2-D method of characteristics and 1-D SN)
MCCG3D	Method of characteristics
PANDA	Finite difference discrete ordinates
PARTISN	Discrete ordinates
ATTILA	Discrete ordinates using a unstructured mesh of discontinuous finite elements with linear basis functions
THREEDANT-HU	Finite difference discrete ordinates
TORT-GRS	Finite difference discrete ordinates
TORT-PSU	Finite difference discrete ordinates
UNKGRO	Method of characteristics with stochastic rays and non-linear correction of scattering cross section
PENTRAN	Discrete ordinates
VARIANT-ISE	Nodal integral spherical harmonics; finite element substructure
VARIANT-SE	Nodal spherical harmonics; finite element substructure
VARIANT-Homog	Nodal spherical harmonics with homogenised cross-sections (no pin structure, homogenised pin-cells)

Table 24. Eigenvalue solutions for the *Unrodded* configuration

Code names	Eigenvalue	Per cent error
Reference MCNP	1.14308	±0.006
ATTILA	1.14285	-0.020
CHAPLET-3D	1.14223	-0.074
CRX	1.14335	0.024
MCCG3D	1.14322	0.012
PANDA	1.14204	-0.091
PARTISN	1.14295	-0.011
PENTRAN	1.14477	0.148
THREEDANT-HU	1.14290	-0.016
TORT-GRS	1.13989	-0.279
TORT-PSU	1.14177	-0.115
UNKGRO	1.14317	0.007
VARIANT-ISE	1.14501	0.169
VARIANT-SE	1.13934	-0.327
VARIANT-Homog	1.146979	0.341

Figure 8. Eigenvalue solutions for the *Unrodded* configuration

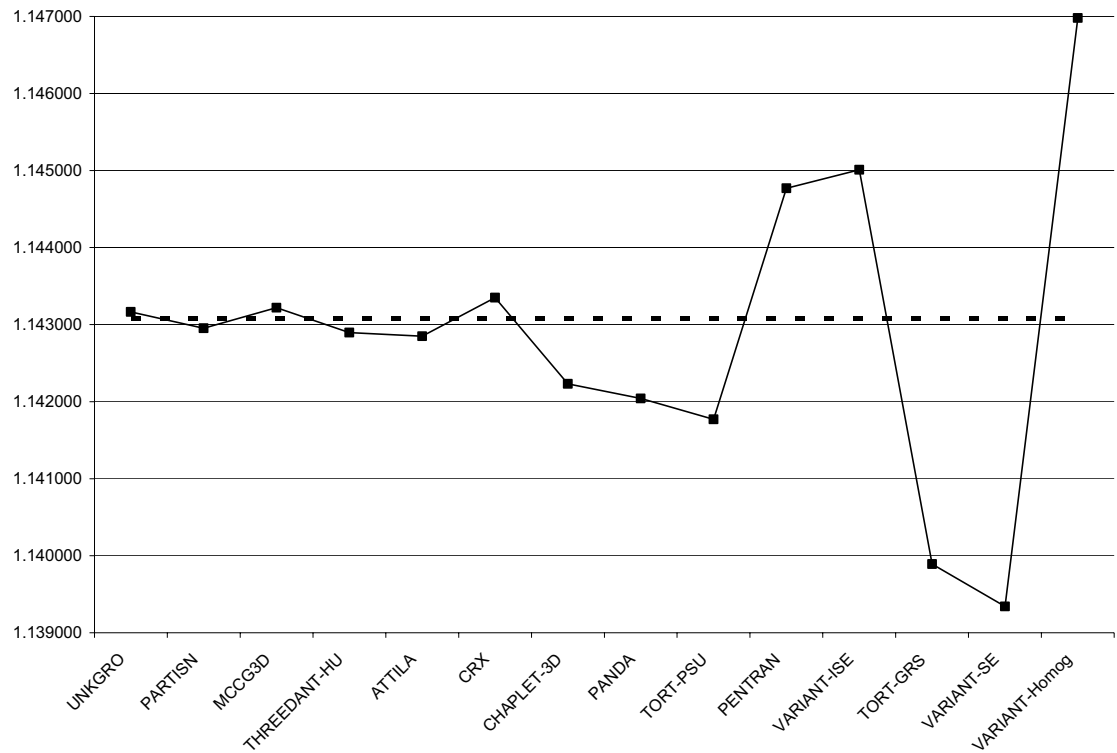


Figure 9. Eigenvalue per cent errors for the *Unrodded* configuration

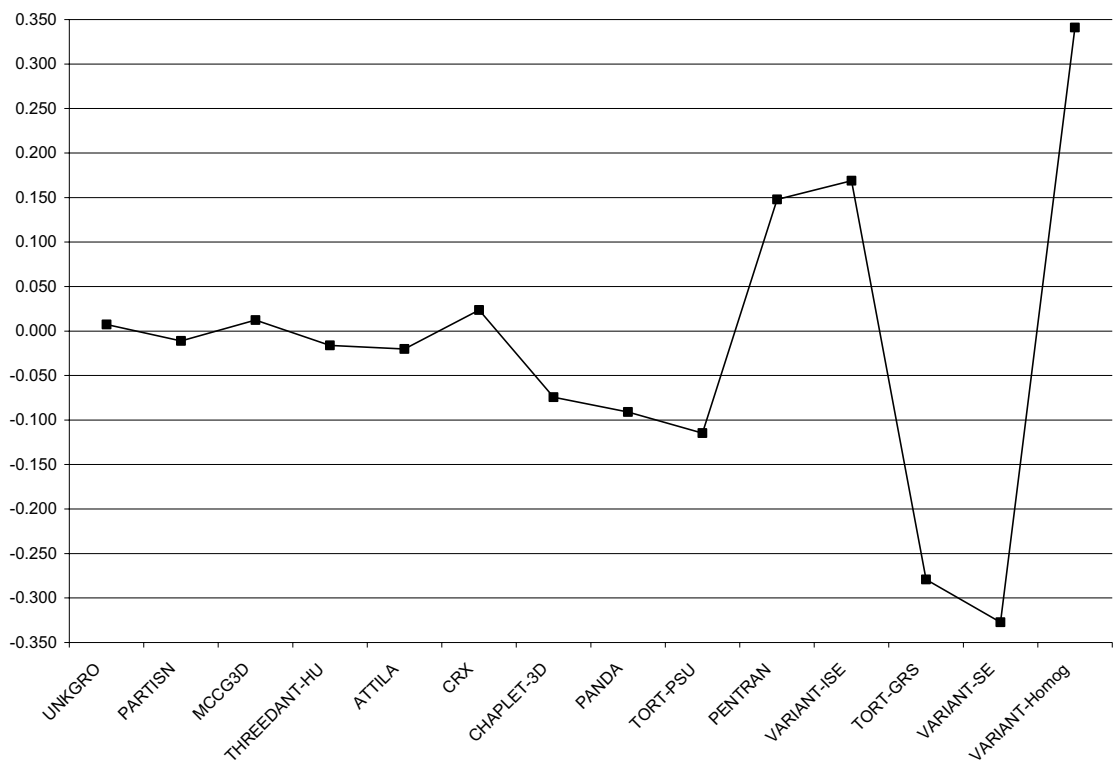


Table 25. Participant results for specific pin powers in slice #1 of the *Unrodded* configuration

Code names	Maximum pin power	Per cent error	Maximum per cent error	Associated reference MCNP statistical error
Reference MCNP	1.108	± 0.21		
ATTILA	1.110	0.15	0.98	± 0.51
CHAPLET-3D	1.107	-0.11	1.37	± 0.67
CRX	1.109	0.11	1.15	± 0.47
MCCG3D	1.115	0.65	1.47	± 0.67
PANDA	1.130	1.97	9.84	± 0.47
PARTISN	1.112	0.36	0.83	± 0.51
PENTRAN	1.041	-6.06	10.88	± 0.67
THREEDANT-HU	1.121	1.15	2.02	± 0.51
TORT-GRS	1.119	1.02	1.29	± 0.51
TORT-PSU	1.113	0.46	0.96	± 0.47
UNKGRO	1.088	-1.80	5.22	± 0.67
VARIANT-ISE	1.104	-0.37	1.32	± 0.47
VARIANT-SE	1.121	1.13	3.07	± 0.51
VARIANT-Homog	1.120	1.07	2.85	± 0.67

Table 26. Participant results for specific pin powers in slice #2 of the *Unrodded* configuration

Code names	Maximum pin power	Per cent error	Maximum per cent error	Associated reference MCNP statistical error
Reference MCNP	0.882	± 0.23		
ATTILA	0.884	0.15	1.12	± 0.74
CHAPLET-3D	0.880	-0.21	1.42	± 0.74
CRX	0.882	-0.08	1.36	± 0.58
MCCG3D	0.886	0.40	1.58	± 0.74
PANDA	0.894	1.33	9.98	± 0.53
PARTISN	0.884	0.22	1.08	± 0.74
PENTRAN	0.854	-3.15	8.03	± 0.74
THREEDANT-HU	0.891	1.02	1.72	± 0.63
TORT-GRS	0.887	0.53	1.53	± 0.63
TORT-PSU	0.884	0.18	0.90	± 0.51
UNKGRO	0.871	-1.31	5.41	± 0.51
VARIANT-ISE	0.879	-0.34	1.44	± 0.74
VARIANT-SE	0.893	1.19	2.60	± 0.49
VARIANT-Homog	0.890	0.88	2.88	± 0.74

Table 27. Participant results for specific pin powers in slice #3 of the *Unrodded* configuration

Code names	Maximum pin power	Per cent error	Maximum per cent error	Associated reference MCNP statistical error
Reference MCNP	0.491	± 0.30		
ATTILA	0.491	0.08	1.21	± 0.56
CHAPLET-3D	0.488	-0.49	1.31	± 1.00
CRX	0.490	-0.22	1.33	± 0.70
MCCG3D	0.490	-0.17	1.94	± 0.70
PANDA	0.493	0.45	9.48	± 0.72
PARTISN	0.490	-0.14	1.44	± 0.79
PENTRAN	0.497	1.22	9.84	± 0.67
THREEDANT-HU	0.494	0.64	2.08	± 0.79
TORT-GRS	0.490	-0.11	2.08	± 0.79
TORT-PSU	0.488	-0.66	1.21	± 0.67
UNKGRO	0.490	-0.23	5.82	± 1.00
VARIANT-ISE	0.491	0.04	2.48	± 0.70
VARIANT-SE	0.499	1.63	2.51	± 0.30
VARIANT-Homog	0.491	0.13	2.29	± 0.70

Table 28. Participant results for specific pin powers in the *Unrodded* configuration

Code names	Maximum pin power	Per cent error	Maximum per cent error	Associated reference MCNP statistical error
Reference MCNP	2.481	± 0.14		
ATTILA	2.485	0.14	0.63	± 0.36
CHAPLET-3D	2.476	-0.22	1.27	± 0.45
CRX	2.481	-0.02	1.14	± 0.31
MCCG3D	2.491	0.40	1.28	± 0.45
PANDA	2.517	1.44	9.82	± 0.32
PARTISN	2.486	0.21	0.65	± 0.36
PENTRAN	2.392	-3.58	8.81	± 0.45
THREEDANT-HU	2.506	1.00	1.67	± 0.35
TORT-GRS	2.497	0.62	1.19	± 0.36
TORT-PSU	2.485	0.14	0.61	± 0.31
UNKGRO	2.449	-1.31	5.19	± 0.31
VARIANT-ISE	2.474	-0.27	1.44	± 0.45
VARIANT-SE	2.512	1.25	2.25	± 0.34
VARIANT-Homog	2.501	0.81	2.74	± 0.45

Figure 10. Maximum pin power results for the *Unrodded* configuration

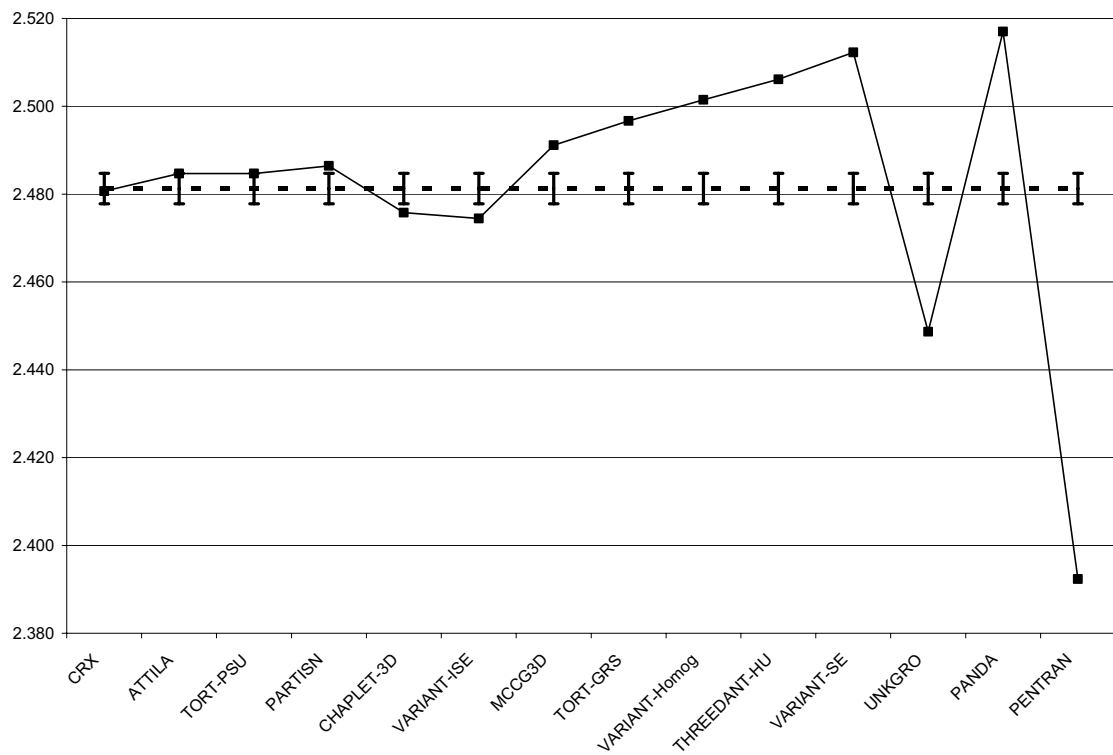


Figure 11. Maximum per cent errors for the *Unrodded* configuration

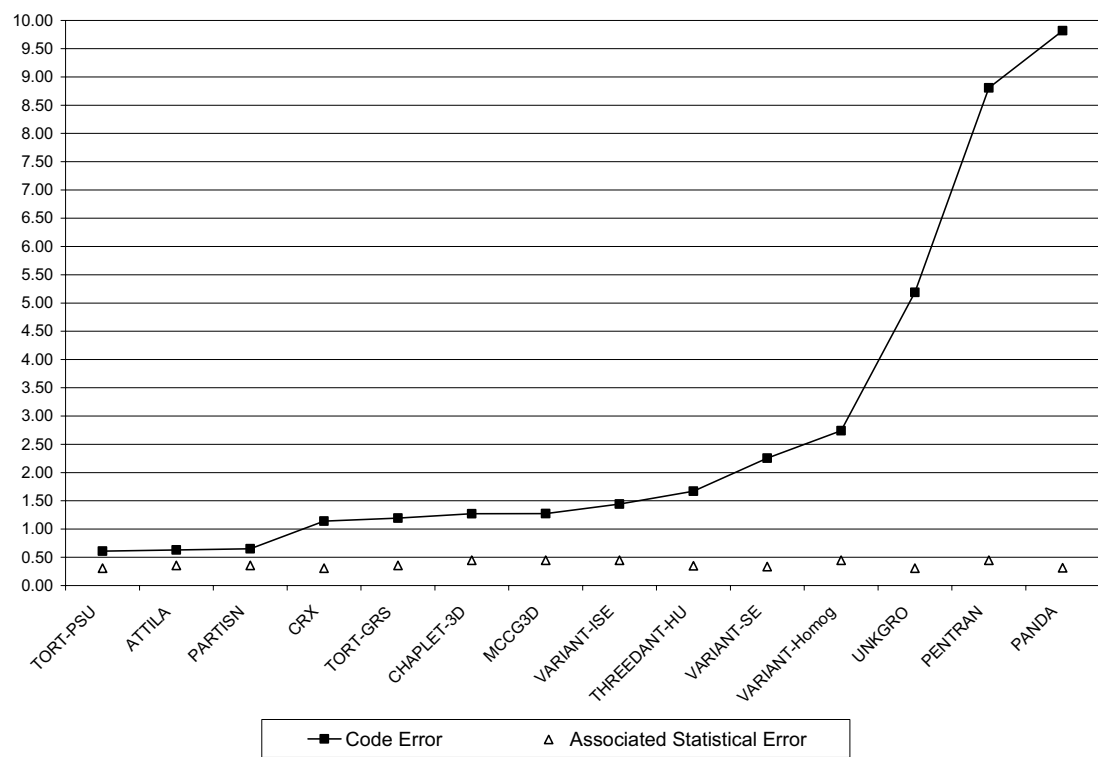


Table 29. Assembly power per cent errors for slice #1 of the *Unrodded* configuration

Code names	Inner UO ₂	Per cent error	MOX	Per cent error	Outer UO ₂	Per cent error
Reference MCNP	219.0	± 0.19	94.5	± 0.14	62.1	± 0.10
ATTILA	219.0	-0.02	94.3	-0.23	62.1	-0.10
CHAPLET-3D	218.7	-0.17	94.6	0.09	62.3	0.31
CRX	219.0	-0.01	94.6	0.06	62.1	-0.04
MCCG3D	219.8	0.33	94.5	-0.01	62.2	0.16
PANDA	221.1	0.92	94.0	-0.58	62.1	-0.02
PARTISN	219.4	0.16	94.5	-0.09	62.1	0.02
PENTRAN	208.9	-4.64	93.9	-0.69	60.8	-2.09
THREEDANT-HU	220.6	0.73	93.8	-0.81	62.1	0.03
TORT-GRS	220.5	0.67	94.3	-0.20	62.2	0.06
TORT-PSU	219.6	0.25	94.4	-0.09	62.2	0.09
UNKGRO	217.1	-0.89	94.5	-0.02	62.4	0.41
VARIANT-ISE	218.4	-0.31	94.1	-0.42	62.4	0.48
VARIANT-SE	220.6	0.71	93.1	-1.56	62.2	0.11
VARIANT-Homog	219.6	0.27	94.4	-0.15	62.2	0.05

Table 30. Assembly power per cent errors for slice #2 of the *Unrodded* configuration

Code names	Inner UO ₂	Per cent error	MOX	Per cent error	Outer UO ₂	Per cent error
Reference MCNP	174.2	± 0.17	75.2	± 0.13	49.5	± 0.09
ATTILA	174.3	0.04	75.1	-0.20	49.4	-0.08
CHAPLET-3D	173.9	-0.17	75.3	0.08	49.6	0.27
CRX	174.1	-0.09	75.3	0.00	49.4	-0.15
MCCG3D	174.5	0.13	75.1	-0.22	49.4	-0.09
PANDA	175.5	0.71	74.7	-0.78	49.3	-0.24
PARTISN	174.5	0.12	75.1	-0.14	49.4	-0.04
PENTRAN	171.6	-1.53	77.2	2.61	50.0	1.15
THREEDANT-HU	175.5	0.71	74.6	-0.83	49.5	0.02
TORT-GRS	174.7	0.29	74.8	-0.55	49.3	-0.31
TORT-PSU	174.4	0.09	75.1	-0.22	49.4	-0.05
UNKGRO	173.1	-0.68	75.7	0.66	49.9	0.92
VARIANT-ISE	173.9	-0.18	75.0	-0.28	49.7	0.60
VARIANT-SE	175.8	0.87	74.2	-1.40	49.6	0.26
VARIANT-Homog	174.6	0.20	75.1	-0.21	49.4	-0.03

Table 31. Assembly power per cent errors for slice #3 of the *Unrodded* configuration

Code names	Inner UO ₂	Per cent error	MOX	Per cent error	Outer UO ₂	Per cent error
Reference MCNP	97.9	±0.13	42.9	±0.10	27.8	±0.07
ATTILA	98.3	0.42	43.1	0.40	27.9	0.23
CHAPLET-3D	97.8	-0.15	43.0	0.21	27.8	0.08
CRX	98.0	0.02	43.0	0.17	27.8	-0.10
MCCG3D	97.8	-0.14	42.7	-0.44	27.7	-0.47
PANDA	98.2	0.29	42.5	-1.09	27.6	-0.76
PARTISN	98.0	0.05	42.8	-0.21	27.8	-0.23
PENTRAN	101.0	3.13	46.1	7.32	29.4	5.71
THREEDANT-HU	98.6	0.64	42.6	-0.77	27.8	-0.11
TORT-GRS	97.9	0.01	42.7	-0.54	27.6	-0.64
TORT-PSU	97.7	-0.20	42.9	0.07	27.7	-0.33
UNKGRO	97.7	-0.20	43.6	1.55	28.1	1.18
VARIANT-ISE	98.6	0.68	43.2	0.66	28.2	1.38
VARIANT-SE	99.7	1.81	42.8	-0.36	28.1	1.11
VARIANT-Homog	97.8	-0.14	42.9	-0.13	27.7	-0.42

Table 32. Assembly power per cent errors for the *Unrodded* configuration

Code names	Inner UO ₂	Per cent error	MOX	Per cent error	Outer UO ₂	Per cent error
Reference MCNP	491.2	±0.29	212.7	±0.21	139.4	±0.15
ATTILA	491.6	0.09	212.5	-0.09	139.3	-0.03
CHAPLET-3D	490.4	-0.17	212.9	0.11	139.7	0.25
CRX	491.1	-0.03	212.8	0.06	139.3	-0.09
MCCG3D	492.0	0.16	212.3	-0.17	139.3	-0.05
PANDA	494.8	0.72	211.1	-0.75	139.0	-0.24
PARTISN	491.8	0.13	212.4	-0.13	139.3	-0.05
PENTRAN	481.5	-1.99	217.2	2.09	140.2	0.62
THREEDANT-HU	494.7	0.70	211.0	-0.81	139.4	0.00
TORT-GRS	493.2	0.40	211.9	-0.39	139.1	-0.21
TORT-PSU	491.7	0.10	212.5	-0.10	139.3	-0.05
UNKGRO	487.9	-0.68	213.8	0.54	140.4	0.74
VARIANT-ISE	490.9	-0.07	212.4	-0.15	140.4	0.70
VARIANT-SE	496.1	0.99	210.0	-1.26	139.9	0.36
VARIANT-Homog	492.0	0.16	212.4	-0.17	139.3	-0.07

Figure 12. Inner UO₂ assembly power per cent errors for the *Unrodded* configuration

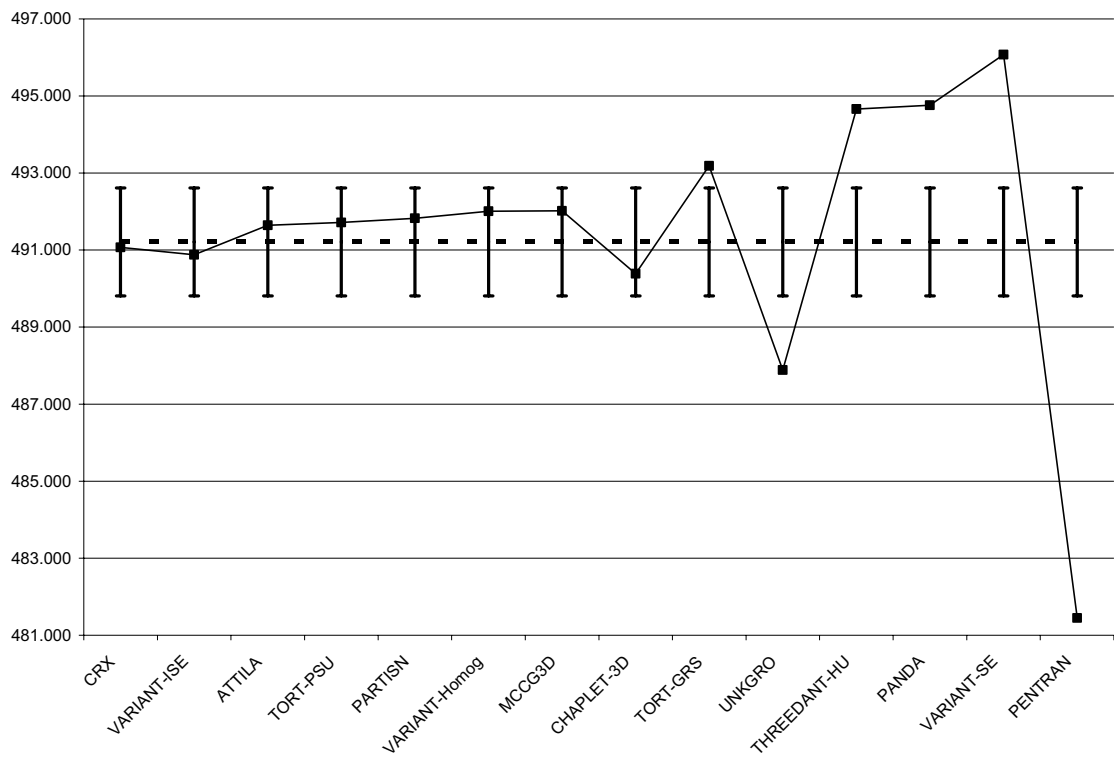


Figure 13. MOX assembly power per cent errors for the *Unrodded* configuration

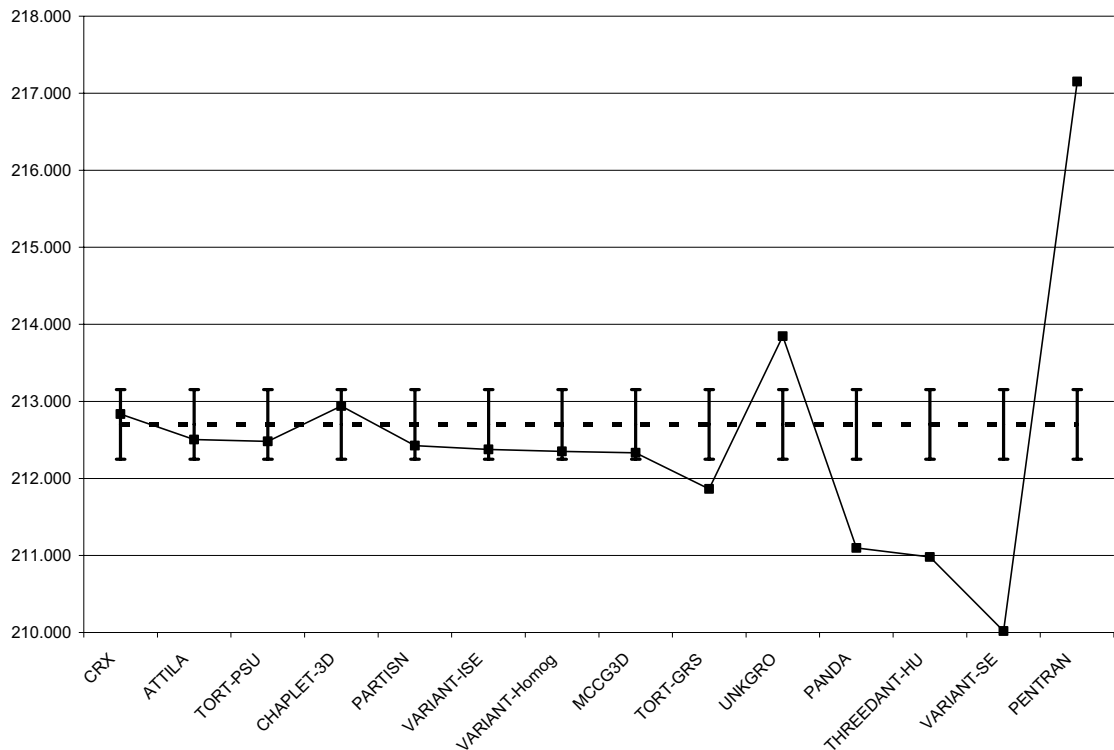
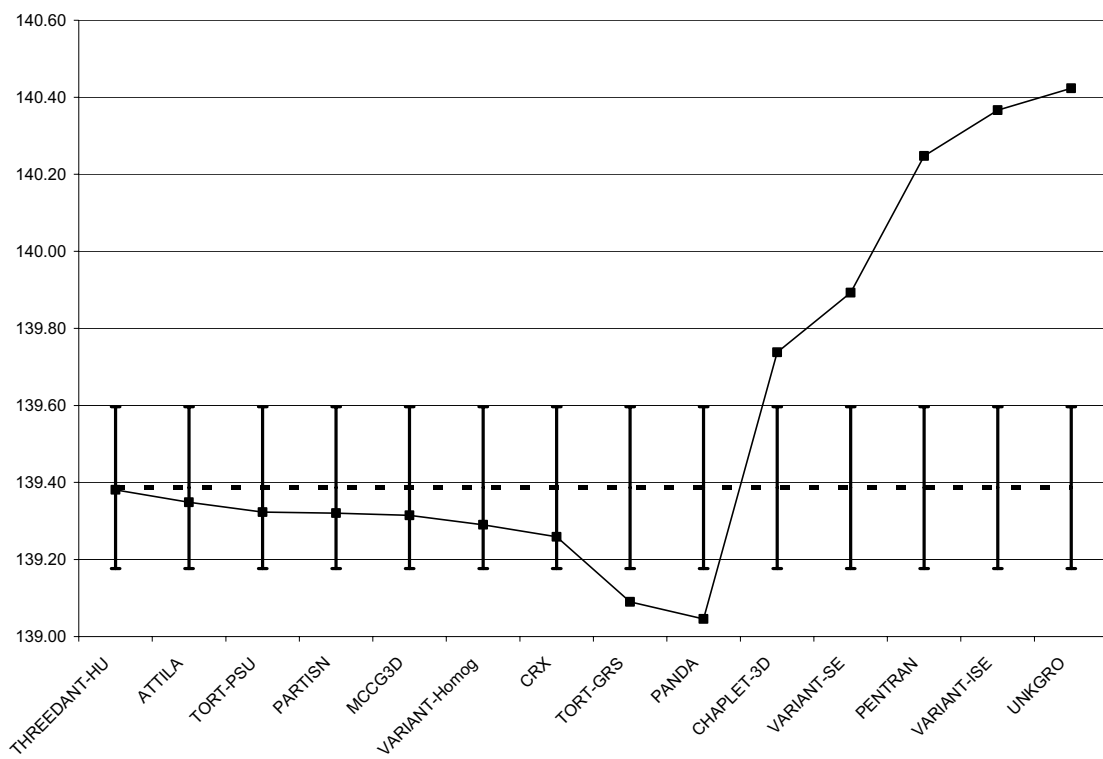


Figure 14. Outer UO₂ assembly power results for the *Unrodded* configuration



**Table 33. Pin power distribution error measures
for slice #1 of the *Unrodded* configuration**

Code names	Avg	RMS	MRE
Reference MCNP	0.38	0.40	0.14
ATTILA	0.21	0.27	0.07
CHAPLET-3D	0.25	0.34	0.09
CRX	0.24	0.32	0.09
MCCG3D	0.26	0.33	0.12
PANDA	0.70	0.93	0.34
PARTISN	0.18	0.23	0.08
PENTRAN	2.33	3.20	1.28
THREEDANT-HU	0.68	0.81	0.31
TORT-GRS	0.39	0.48	0.21
TORT-PSU	0.21	0.26	0.10
UNKGRO	0.96	1.29	0.40
VARIANT-ISE	0.43	0.49	0.19
VARIANT-SE	1.07	1.31	0.44
VARIANT-Homog	0.62	0.80	0.24

**Table 34. Pin power distribution error measures
for slice #2 of the *Unrodded* configuration**

Code names	Avg	RMS	MRE
Reference MCNP	0.43	0.44	0.13
ATTILA	0.20	0.26	0.06
CHAPLET-3D	0.27	0.36	0.08
CRX	0.26	0.35	0.07
MCCG3D	0.28	0.35	0.09
PANDA	0.75	0.97	0.27
PARTISN	0.19	0.24	0.06
PENTRAN	2.51	2.80	0.82
THREEDANT-HU	0.68	0.79	0.25
TORT-GRS	0.47	0.55	0.15
TORT-PSU	0.22	0.27	0.07
UNKGRO	1.06	1.53	0.30
VARIANT-ISE	0.43	0.52	0.14
VARIANT-SE	1.04	1.22	0.36
VARIANT-Homog	0.62	0.81	0.19

**Table 35. Pin power distribution error measures
for slice #3 of the *Unrodded* configuration**

Code names	AVG	RMS	MRE
Reference MCNP	0.57	0.59	0.10
ATTILA	0.40	0.46	0.08
CHAPLET-3D	0.28	0.36	0.05
CRX	0.28	0.37	0.05
MCCG3D	0.44	0.56	0.07
PANDA	0.93	1.15	0.16
PARTISN	0.27	0.36	0.04
PENTRAN	5.86	6.42	1.05
THREEDANT-HU	0.66	0.78	0.13
TORT-GRS	0.52	0.65	0.08
TORT-PSU	0.30	0.38	0.05
UNKGRO	1.40	1.86	0.20
VARIANT-ISE	0.91	1.04	0.15
VARIANT-SE	1.07	1.22	0.25
VARIANT-Homog	0.65	0.80	0.11

**Table 36. Pin power distribution error measures
for the *Unrodded* configuration**

Code names	AVG	RMS	MRE
Reference MCNP	0.25	0.26	0.22
ATTILA	0.13	0.16	0.11
CHAPLET-3D	0.23	0.30	0.18
CRX	0.22	0.29	0.17
MCCG3D	0.22	0.27	0.21
PANDA	0.73	0.95	0.73
PARTISN	0.15	0.19	0.14
PENTRAN	2.32	2.63	2.24
THREEDANT-HU	0.66	0.78	0.68
TORT-GRS	0.40	0.47	0.39
TORT-PSU	0.14	0.18	0.12
UNKGRO	0.94	1.36	0.76
VARIANT-ISE	0.39	0.49	0.32
VARIANT-SE	1.01	1.17	1.02
VARIANT-Homog	0.60	0.78	0.51

Figure 15. AVG per cent error for the *Unrodded* configuration

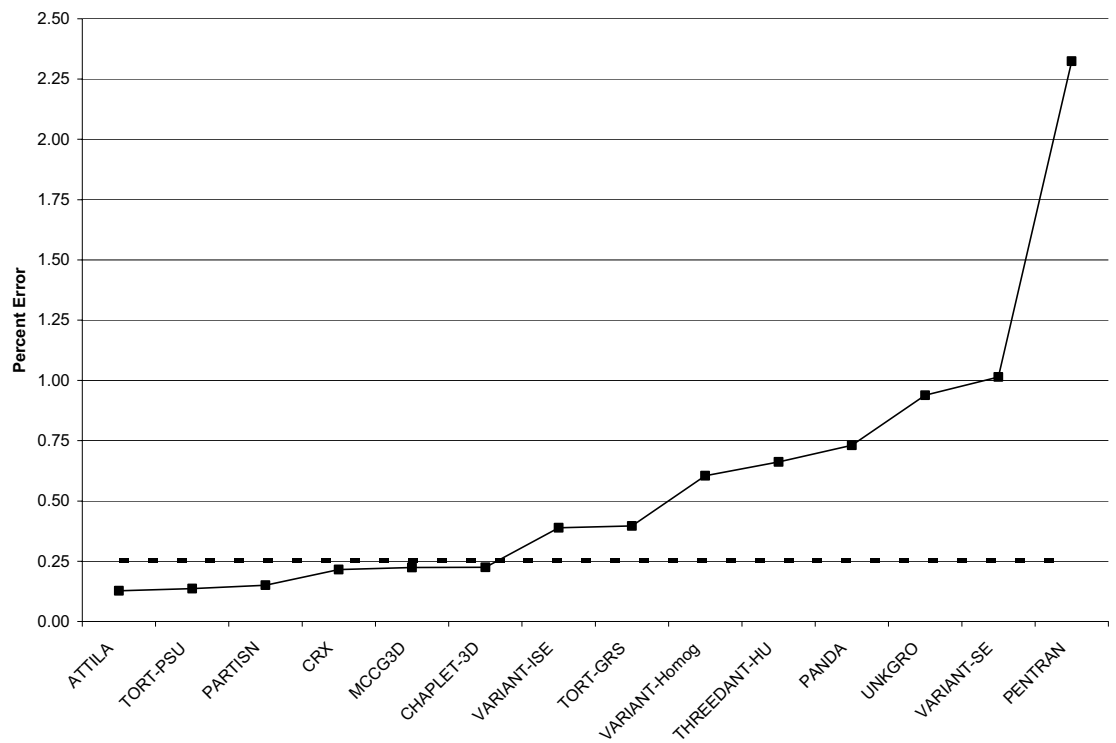


Figure 16. RMS per cent error for the *Unrodded* configuration

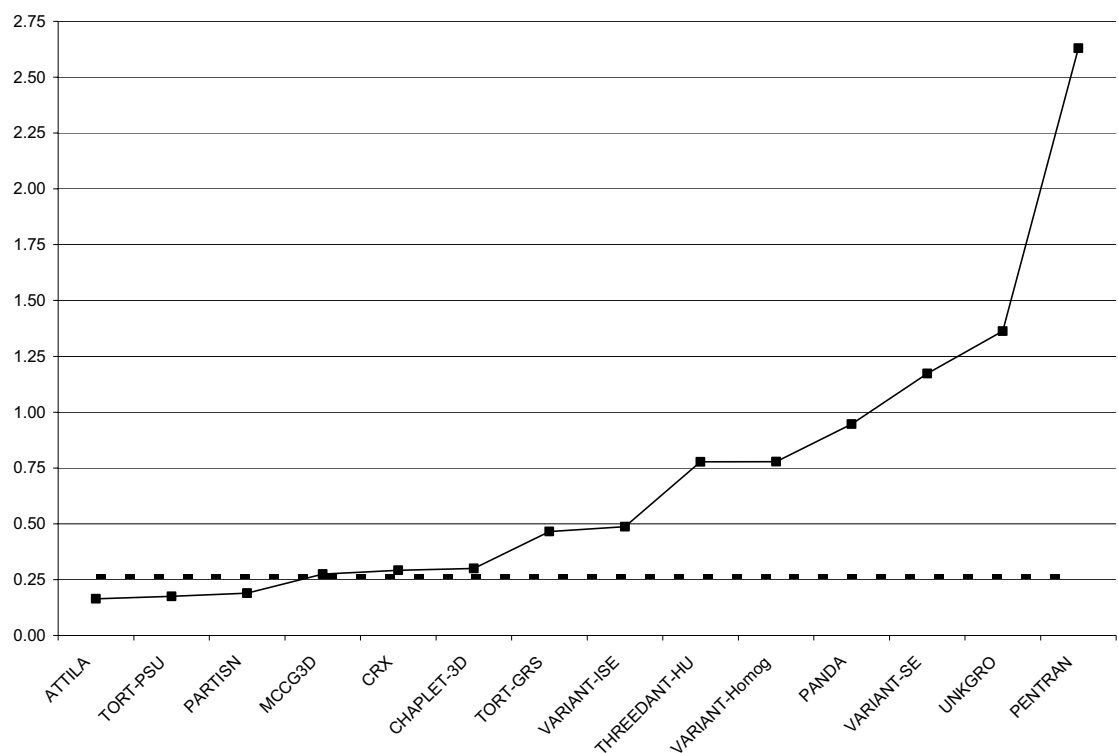


Figure 17. MRE per cent error for the *Unrodded* configuration

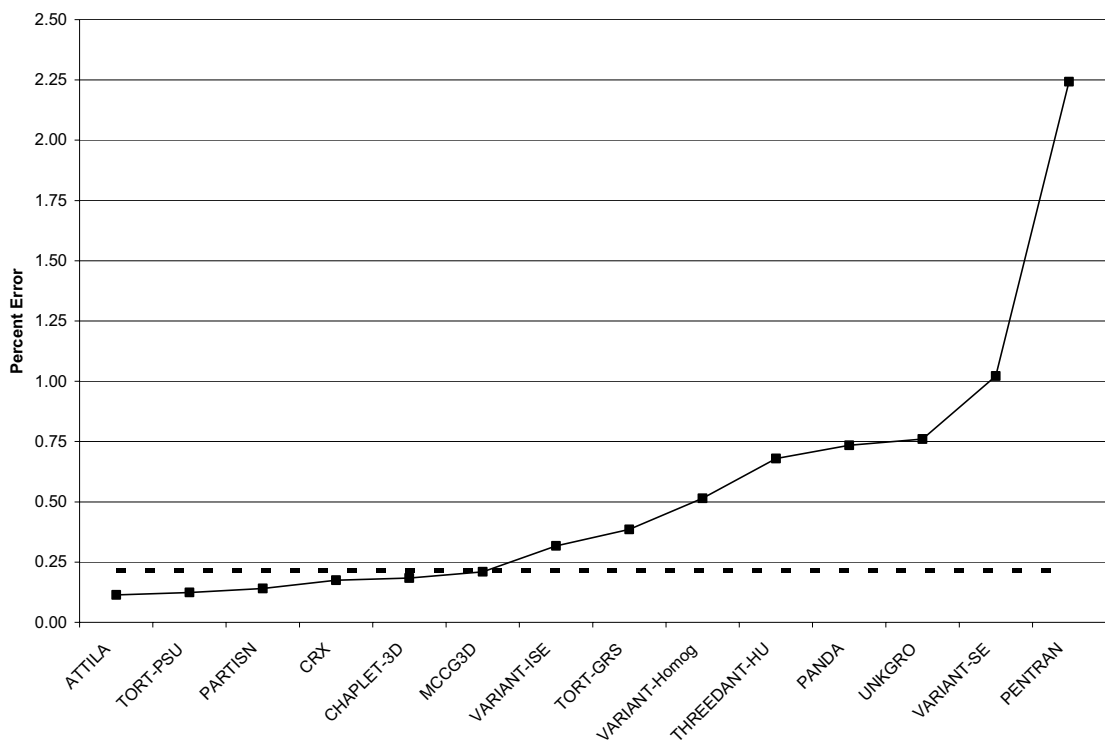


Table 37. Number of fuel pins within the reference confidence intervals for slice #1 of the *Unrodded* configuration

Code names	68%	90%	98%	99.8%
ATTILA	260	431	491	530
CHAPLET-3D	212	380	447	496
CRX	225	387	461	508
MCCG3D	204	347	407	451
PANDA	85	158	195	237
PARTISN	278	447	494	527
PENTRAN	50	90	119	141
THREEDANT-HU	87	149	174	207
TORT-GRS	162	284	325	376
TORT-PSU	252	389	456	499
UNKGRO	57	120	153	188
VARIANT-ISE	87	201	272	347
VARIANT-SE	60	115	143	169
VARIANT-Homog	109	174	231	287

Table 38. Percentage of fuel pins within the reference confidence intervals for slice #1 of the *Unrodded* configuration

Code names	68%	90%	98%	99.8%
ATTILA	48.1	79.8	90.9	98.1
CHAPLET-3D	39.3	70.4	82.8	91.9
CRX	41.7	71.7	85.4	94.1
MCCG3D	37.8	64.3	75.4	83.5
PANDA	15.7	29.3	36.1	43.9
PARTISN	51.5	82.8	91.5	97.6
PENTRAN	9.3	16.7	22.0	26.1
THREEDANT-HU	16.1	27.6	32.2	38.3
TORT-GRS	30.0	52.6	60.2	69.6
TORT-PSU	46.7	72.0	84.4	92.4
UNKGRO	10.6	22.2	28.3	34.8
VARIANT-ISE	16.1	37.2	50.4	64.3
VARIANT-SE	11.1	21.3	26.5	31.3
VARIANT-Homog	20.2	32.2	42.8	53.1

Table 39. Number of fuel pins within the reference confidence intervals for slice #2 of the *Unrodded* configuration

Code names	68%	90%	98%	99.8%
ATTILA	277	469	520	535
CHAPLET-3D	238	393	465	506
CRX	240	403	471	506
MCCG3D	201	366	444	498
PANDA	76	126	169	214
PARTISN	272	466	519	538
PENTRAN	11	26	34	45
THREEDANT-HU	82	149	174	214
TORT-GRS	85	194	276	363
TORT-PSU	261	437	510	534
UNKGRO	75	130	176	223
VARIANT-ISE	113	239	316	386
VARIANT-SE	49	108	143	176
VARIANT-Homog	108	197	243	301

Table 40. Percentage of fuel pins within the reference confidence intervals for slice #2 of the *Unrodded* configuration

Code names	68%	90%	98%	99.8%
ATTILA	51.3	86.9	96.3	99.1
CHAPLET-3D	44.1	72.8	86.1	93.7
CRX	44.4	74.6	87.2	93.7
MCCG3D	37.2	67.8	82.2	92.2
PANDA	14.1	23.3	31.3	39.6
PARTISN	50.4	86.3	96.1	99.6
PENTRAN	2.0	4.8	6.3	8.3
THREEDANT-HU	15.2	27.6	32.2	39.6
TORT-GRS	15.7	35.9	51.1	67.2
TORT-PSU	48.3	80.9	94.4	98.9
UNKGRO	13.9	24.1	32.6	41.3
VARIANT-ISE	20.9	44.3	58.5	71.5
VARIANT-SE	9.1	20.0	26.5	32.6
VARIANT-Homog	20.0	36.5	45.0	55.7

Table 41. Number of fuel pins within the reference confidence intervals for slice #3 of the *Unrodded* configuration

Code names	68%	90%	98%	99.8%
ATTILA	164	313	394	468
CHAPLET-3D	279	459	509	532
CRX	276	447	503	531
MCCG3D	180	328	412	473
PANDA	48	109	155	231
PARTISN	288	466	511	534
PENTRAN	9	15	21	26
THREEDANT-HU	106	198	260	334
TORT-GRS	132	289	378	457
TORT-PSU	260	432	480	516
UNKGRO	60	110	157	201
VARIANT-ISE	45	94	145	227
VARIANT-SE	56	102	155	218
VARIANT-Homog	94	218	278	355

Table 42. Percentage of fuel pins within the reference confidence intervals for slice #3 of the *Unrodded* configuration

Code names	68%	90%	98%	99.8%
ATTILA	30.4	58.0	73.0	86.7
CHAPLET-3D	51.7	85.0	94.3	98.5
CRX	51.1	82.8	93.1	98.3
MCCG3D	33.3	60.7	76.3	87.6
PANDA	8.9	20.2	28.7	42.8
PARTISN	53.3	86.3	94.6	98.9
PENTRAN	1.7	2.8	3.9	4.8
THREEDANT-HU	19.6	36.7	48.1	61.9
TORT-GRS	24.4	53.5	70.0	84.6
TORT-PSU	48.1	80.0	88.9	95.6
UNKGRO	11.1	20.4	29.1	37.2
VARIANT-ISE	8.3	17.4	26.9	42.0
VARIANT-SE	10.4	18.9	28.7	40.4
VARIANT-Homog	17.4	40.4	51.5	65.7

Table 43. Number of fuel pins within the reference confidence intervals for the *Unrodded* configuration

Code names	68%	90%	98%	99.8%
ATTILA	257	433	489	532
CHAPLET-3D	159	305	368	434
CRX	168	311	393	464
MCCG3D	147	275	359	420
PANDA	44	89	112	144
PARTISN	213	387	454	507
PENTRAN	14	26	31	35
THREEDANT-HU	62	113	137	162
TORT-GRS	74	146	187	245
TORT-PSU	244	418	484	517
UNKGRO	41	86	123	145
VARIANT-ISE	83	162	216	263
VARIANT-SE	31	49	66	93
VARIANT-Homog	62	119	150	196

Table 44. Percentage of fuel pins within the reference confidence intervals for the *Unrodded* configuration

Code names	68%	90%	98%	99.8%
ATTILA	47.6	80.2	90.6	98.5
CHAPLET-3D	29.4	56.5	68.1	80.4
CRX	31.1	57.6	72.8	85.9
MCCG3D	27.2	50.9	66.5	77.8
PANDA	8.1	16.5	20.7	26.7
PARTISN	39.4	71.7	84.1	93.9
PENTRAN	2.6	4.8	5.7	6.5
THREEDANT-HU	11.5	20.9	25.4	30.0
TORT-GRS	13.7	27.0	34.6	45.4
TORT-PSU	45.2	77.4	89.6	95.7
UNKGRO	7.6	15.9	22.8	26.9
VARIANT-ISE	15.4	30.0	40.0	48.7
VARIANT-SE	5.7	9.1	12.2	17.2
VARIANT-Homog	11.5	22.0	27.8	36.3

Figure 18. Percentage of fuel pins within the *Unrodded* configuration confidence intervals

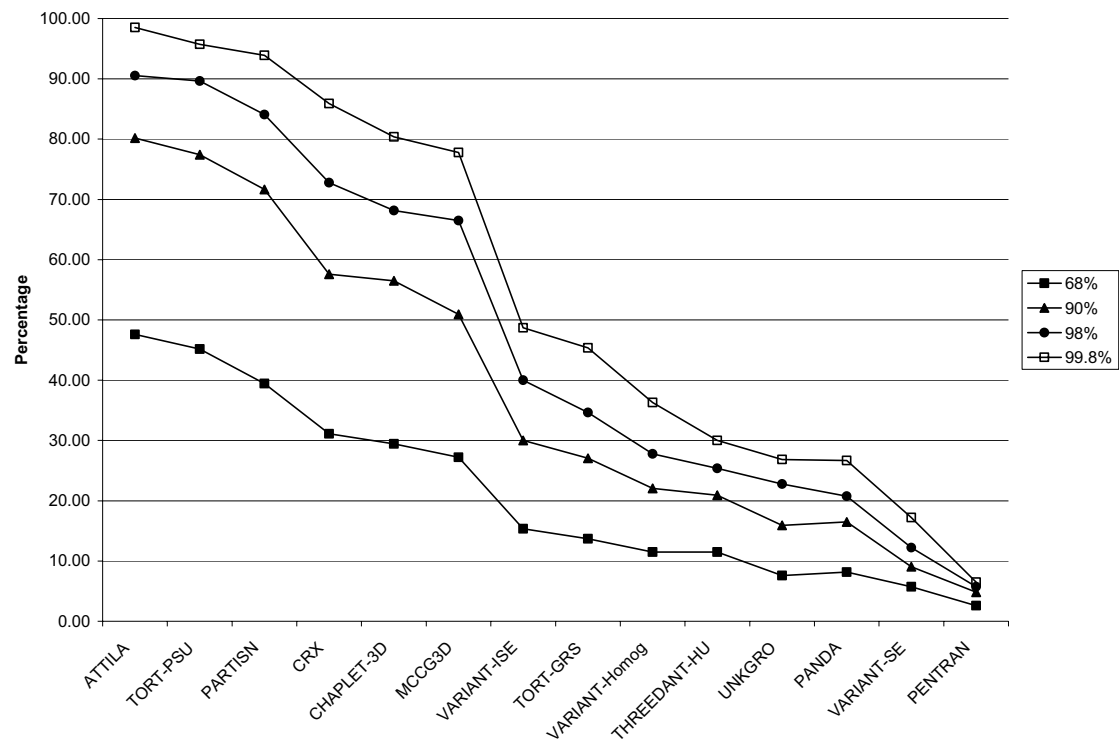


Table 45. Estimated CPU time for the *Unrodded* configuration

Code names	Estimated CPU Time
ATTILA	hours
CHAPLET-3D	days
CRX	Not Given
MCCG3D	weeks
PANDA	hours
PARTISN	hours
PENTRAN	hours
THREEDANT-HU	days
TORT-GRS	days
TORT-PSU	days
UNKGRO	days
VARIANT-ISE	days
VARIANT-SE	days
VARIANT-Homog	minutes

Chapter 7

RODDED A CONFIGURATION BENCHMARK RESULTS

As discussed in Chapter 2, the three-dimensional extension benchmark contains three configurations: *Unrodded*, *Rodded A*, and *Rodded B*. The results for the *Rodded A* configuration will be inspected in this chapter. To minimise the content of this report, plots of the data will only be provided for the core pin power solutions.

Table 46 tabulates the participant eigenvalue solutions and the per cent errors with respect to the reference MCNP solution. Figure 19 displays the eigenvalue solutions ordered with respect to decreasing eigenvalue accuracy where the dashed line represents the reference MCNP solution and the confidence intervals are too small to view. Figure 20 displays the eigenvalue per cent error with respect to decreasing eigenvalue accuracy where the reference MCNP statistical error again is too small to be distinguished on this plot. As can be seen in Figures 19 and 20 and Table 46, a majority of the solutions are reasonably close to the reference MCNP solution. Unlike the *Unrodded* configuration, two of the participants' codes are within the 98% confidence interval of the MCNP eigenvalue, but the average error for all the participant solutions has not changed from 0.12%. The number of participants greater than 0.1% or 100 pcm in error from the reference solution has increased from 5 to 6.

The specific pin power error measures for each slice are tabulated in Tables 47-49 with the results for the core distribution given in Table 50. Figure 21 displays the maximum pin power results and Figure 22 the maximum per cent errors found in each participant solution. For each participant solution, the pin location of the maximum error was determined and the statistical error associated with that pin obtained. This statistical error has been tabulated for each participant in Tables 25-28 in the column titled "associated reference MCNP statistical error" and included in Figure 22 as "associated statistical error." All of the participant solutions in Figures 21 and 22 are ordered with respect to decreasing solution accuracy.

In slice #1, Table 47, two participants obtained a maximum pin power within the 98% confidence interval with the remainder of participants significantly greater than the 98% confidence interval. This pattern is not continued for slices #2 and #3 where five participants succeed in slice #2 and four succeed in slice #3 as seen in Tables 48 and 49. The core pin power results in Table 50 show that four participants are within the 98% confidence interval.

The maximum per cent error results in Tables 47-50 and Figure 22 show that none of the participants' codes succeed in coming within the 98% MCNP confidence intervals. For the core pin power results, only four of the participant codes have maximum errors less than 1% but eleven achieved maximum errors less than 5%. Not surprisingly, the maximum per cent error proved to be the most difficult measure for deterministic methods to satisfy. It also represented the largest deviations between Monte Carlo calculations.

The assembly power error measures results are tabulated in Tables 51-54. Figure 23 displays the participant results for the inner UO₂ assembly power, Figure 24 the results for the MOX assembly power, and Figure 25 the results of the outer UO₂ assembly power. For the slice #1 inner UO₂ assembly power two participant solutions are within the 98% confidence interval. For slice #2, six are within the 98% confidence intervals while there are only two for slice #3. For the core assembly power distribution, eight participants are within the 98% confidence interval. A similar trend is seen for the outer UO₂ assembly. Three participants are within the 98% confidence interval for slice #1 with five succeeding for slice #2 and none for slice #3. For the core pin power results in Table 54, eight succeeded in meeting the 98% confidence interval. For the MOX assembly, three meet the 98% interval for slice #1 with only five in slice #2 and only two in slice #3. For the core result in Table 54, eight participant solutions are within the 98% confidence interval.

Tables 55-58 give the pin power distribution error measures. Figure 26 displays the AVG error measure results, Figure 27 the RMS error measure results, and Figure 28 the MRE error measure results. Seven of the participants are within the 98% confidence interval for the AVG error measure in slice #1. In slice #2 there are seven participants within the 98% confidence interval while for slice #3 there are only five. For the core wide results, six participants agree with the reference MCNP solution with thirteen less than 1% in error. For the RMS error measure, three of the participants are within the 98% confidence interval in slice #1 with seven in slice #2 and three in slice #3. The core wide results are not as good as the AVG results with only two of the participants within the 98% confidence interval and eleven less than 1% in error. For the MRE error measure, four of the participants are within the 98% confidence interval for slice #1 with seven for slice #2 and four for slice #3. For the core wide results, six participants are within the 98% confidence interval with thirteen less than 1% in error. Compared to the *Unrodded* configuration, the AVG, RMS, and MRE participant error has increased noticeably. However, as was the case in the *Unrodded* configuration, a majority of the error in the participants results is small as indicated by the AVG error measure. The lower accuracy of the RMS error measure relative to the AVG error measure indicates that there are a substantial number of small errors in the participant power distribution. In the *Unrodded* configuration most of this error appeared to lie in the low power region of the core since the accuracy of the MRE and AVG error measures were similar. Although control rods were introduced into the inner assembly, it appears as though the radial distribution of error was only slightly changed. The axial error, as would be expected, noticeably increased when compared to the *Unrodded* configuration.

Tables 59, 61, 63, and 65 tabulate the number of fuel pins within the various confidence intervals while Tables 60, 62, 64, and 66 tabulate the percentage of fuel pins that are within the confidence intervals. Figure 29 plots the participant results, ordered with respect to the 98% confidence interval results. As can be seen, none of the participants match the 98% confidence interval for any individual slice and relatively few are close. This error measure represents by far the strictest measure of accuracy that can be applied to the pin power distribution; however, it is subject to significant uncertainty from the normalization procedure applied as discussed in the original benchmark. For this reason, this error measure should not be assumed essential to guarantee the accuracy of any given solution.

Overall, the *Rodded A* configuration results are significantly worse than those seen in the *Unrodded* configuration. This is probably a result of the steeper flux gradients caused by the introduction of control rods. Once again, the inaccuracies in this benchmark can be attributed to insufficient space-angle approximations implemented by the participants in their codes. For completeness, an estimate of each participant CPU time is provided in Table 67 which are effectively the same as those seen for the *Unrodded* configuration (Table 45). The analysis tools used for the *Rodded A* configuration are provided electronically in Appendix F.

Table 46. Eigenvalue solutions for the *Rodded A* configuration

Code names	Eigenvalue	Per cent error
Reference MCNP	1.12806	0.006
ATTILA	1.12781	-0.022
CHAPLET-3D	1.12720	-0.076
CRX	1.12810	0.004
MCCG3D	1.12836	0.027
PANDA	1.12672	-0.119
PARTISN	1.12754	-0.046
PENTRAN	1.12890	0.074
THREEDANT-HU	1.12778	-0.024
TORT-GRS	1.12481	-0.288
TORT-PSU	1.12680	-0.112
UNKGRO	1.12801	-0.004
VARIANT-ISE	1.12970	0.145
VARIANT-SE	1.12343	-0.410
VARIANT-Homog	1.131346	0.291

Figure 19. Eigenvalue solutions for the *Rodded A* configuration

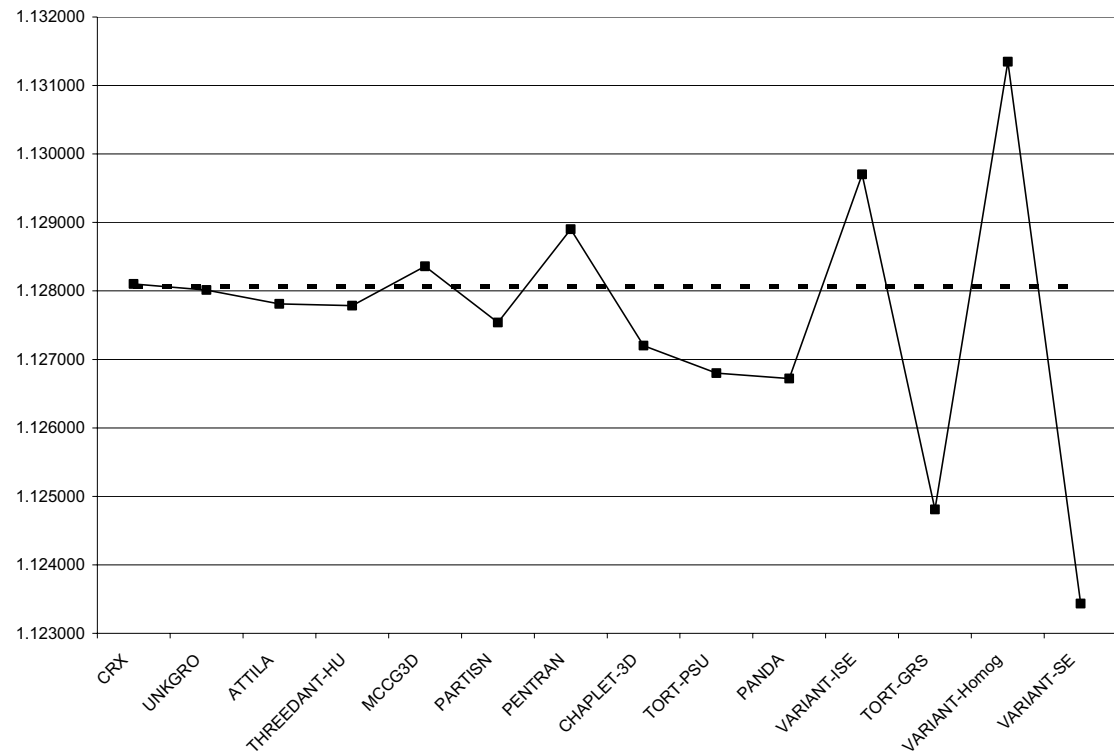


Figure 20. Eigenvalue per cent errors for the *Rodded A* configuration

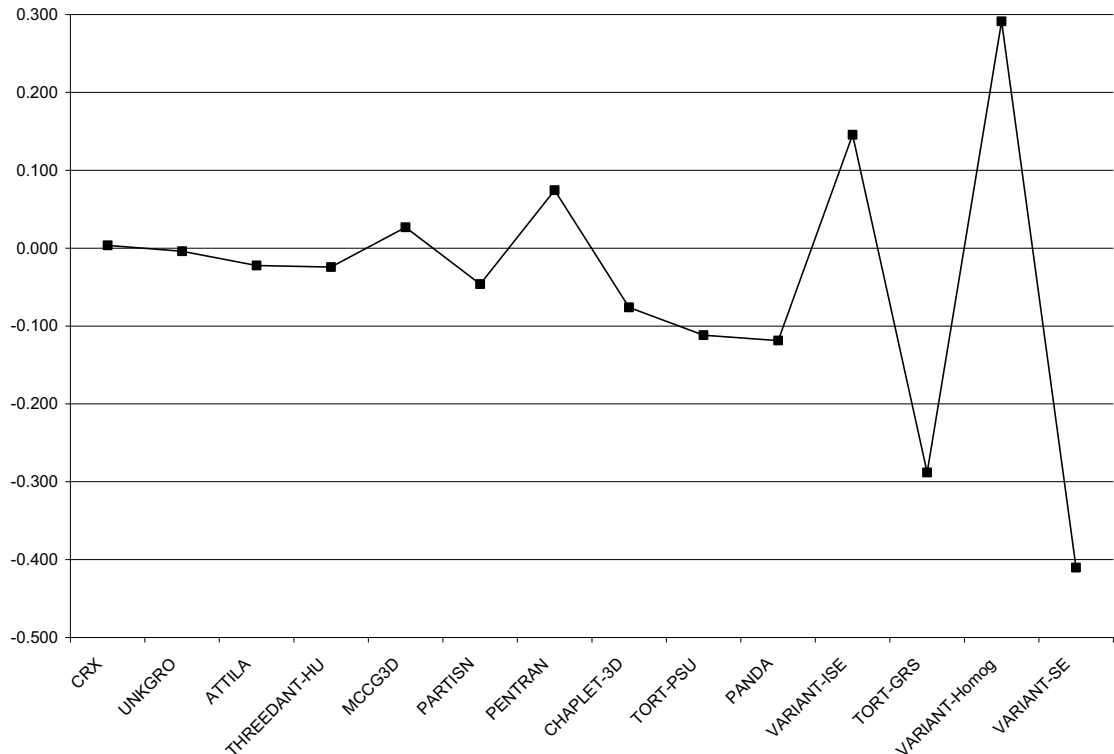


Table 47. Participant results for specific pin powers in slice #1 of the *Rodded A* configuration

Code names	Maximum pin power	Per cent error	Maximum Per cent error	Associated Reference MCNP Statistical Error
Reference MCNP	1.197	± 0.19		
ATTILA	1.198	0.12	0.82	± 0.51
CHAPLET-3D	1.192	-0.41	1.28	± 0.49
CRX	1.191	-0.49	1.04	± 0.51
MCCG3D	1.199	0.18	1.45	± 0.49
PANDA	1.220	1.93	10.55	± 0.47
PARTISN	1.202	0.39	0.85	± 0.44
PENTRAN	1.089	-9.02	12.87	± 0.63
THREEDANT-HU	1.211	1.15	1.84	± 0.51
TORT-GRS	1.205	0.71	1.32	± 0.51
TORT-PSU	1.200	0.28	0.83	± 0.51
UNKGRO	1.172	-2.08	4.79	± 0.44
VARIANT-ISE	1.191	-0.52	1.27	± 0.44
VARIANT-SE	1.213	1.30	2.16	± 0.47
VARIANT-Homog	1.212	1.27	3.10	± 0.49

Table 48. Participant results for specific pin powers in slice #2 of the *Rodded A* configuration

Code names	Maximum pin power	Per cent error	Maximum per cent error	Associated reference MCNP statistical error
Reference MCNP	0.832	± 0.23		
ATTILA	0.831	-0.01	0.86	± 0.58
CHAPLET-3D	0.830	-0.17	1.33	± 0.58
CRX	0.829	-0.35	1.65	± 0.56
MCCG3D	0.832	0.01	1.73	± 0.72
PANDA	0.842	1.27	9.95	± 0.51
PARTISN	0.831	0.00	0.96	± 0.58
PENTRAN	0.795	-4.38	9.55	± 0.72
THREEDANT-HU	0.840	1.07	1.86	± 0.49
TORT-GRS	0.835	0.47	1.19	± 0.49
TORT-PSU	0.830	-0.14	0.87	± 0.51
UNKGRO	0.820	-1.32	5.57	± 0.51
VARIANT-ISE	0.824	-0.92	1.69	± 0.56
VARIANT-SE	0.834	0.36	2.51	± 0.49
VARIANT-Homog	0.836	0.59	3.07	± 0.58

Table 49. Participant results for specific pin powers in slice #3 of the *Rodded A* configuration

Code names	Maximum pin power	Per cent error	Maximum per cent error	Associated reference MCNP statistical error
Reference MCNP	0.304	± 0.47		
ATTILA	0.307	0.83	0.94	± 0.44
CHAPLET-3D	0.305	0.28	0.95	± 0.51
CRX	0.309	1.58	2.91	± 0.77
MCCG3D	0.303	-0.39	1.99	± 0.98
PANDA	0.304	0.00	9.07	± 0.72
PARTISN	0.300	-1.27	2.45	± 0.42
PENTRAN	0.352	15.95	20.14	± 0.47
THREEDANT-HU	0.306	0.61	2.33	± 0.70
TORT-GRS	0.306	0.72	1.74	± 0.77
TORT-PSU	0.305	0.43	1.23	± 0.65
UNKGRO	0.298	-2.07	5.83	± 0.70
VARIANT-ISE	0.307	0.87	2.70	± 0.70
VARIANT-SE	0.308	1.16	2.66	± 0.98
VARIANT-Homog	0.298	-2.05	6.52	± 0.42

Table 50. Participant results for specific pin powers in the *Rodded A* configuration

Code names	Maximum pin power	Per cent error	Maximum Per cent error	Associated reference MCNP statistical error
Reference MCNP	2.253	± 0.14		
ATTILA	2.255	0.06	0.60	± 0.38
CHAPLET-3D	2.247	-0.30	0.99	± 0.43
CRX	2.246	-0.33	1.29	± 0.33
MCCG3D	2.253	-0.04	1.54	± 0.43
PANDA	2.282	1.27	10.07	± 0.31
PARTISN	2.253	-0.03	0.55	± 0.35
PENTRAN	2.151	-4.55	10.37	± 0.43
THREEDANT-HU	2.275	0.95	1.78	± 0.35
TORT-GRS	2.265	0.49	1.21	± 0.35
TORT-PSU	2.256	0.10	0.67	± 0.38
UNKGRO	2.215	-1.72	5.16	± 0.30
VARIANT-ISE	2.241	-0.56	1.48	± 0.30
VARIANT-SE	2.271	0.76	2.00	± 0.29
VARIANT-Homog	2.259	0.24	2.80	± 0.30

Figure 21. Maximum pin power results for the *Rodded A* configuration

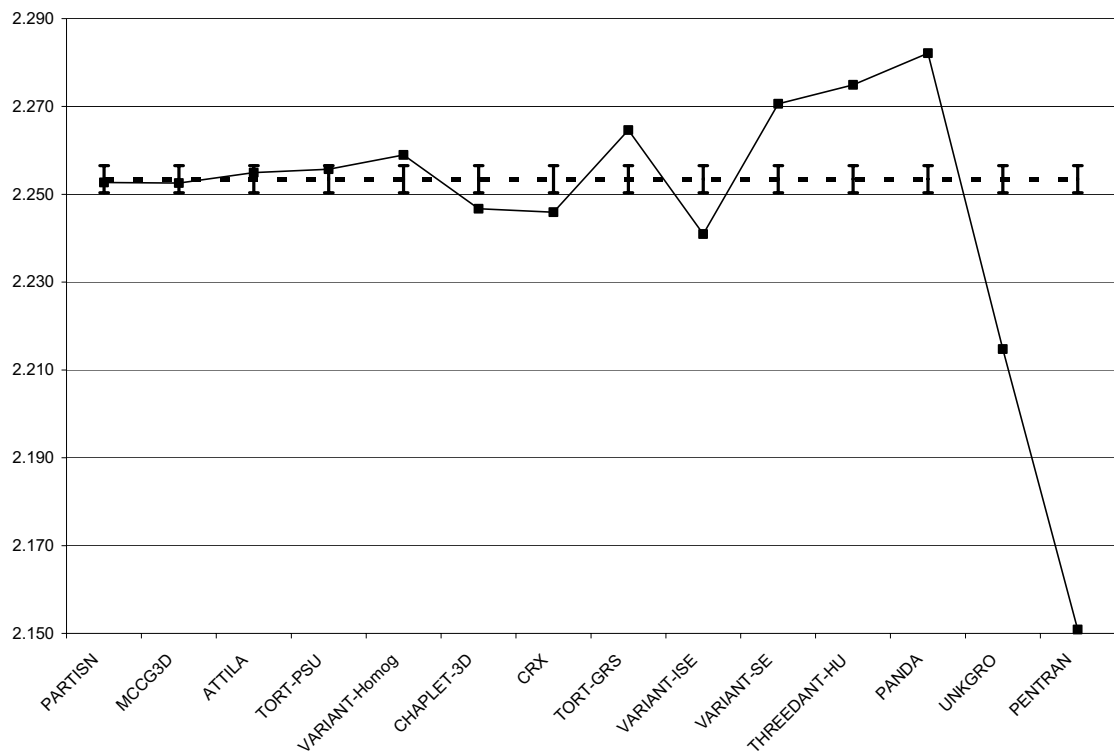


Figure 22. Maximum per cent errors for the *Rodded A* configuration

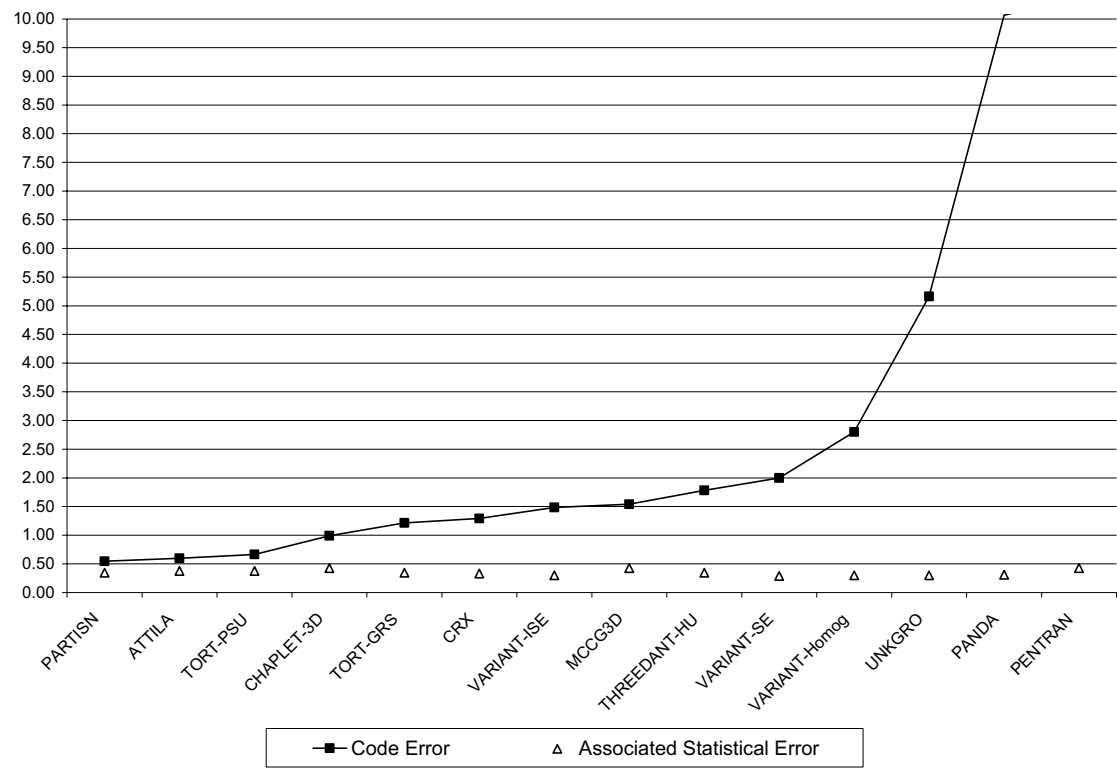


Table 51. Assembly power per cent errors for slice #1 of the *Rodded A* configuration

Code names	Inner UO ₂	Per cent error	MOX	Per cent error	Outer UO ₂	Per cent error
Reference MCNP	237.4	±0.20	104.5	±0.15	69.8	±0.11
ATTILA	237.7	0.13	104.4	-0.12	69.7	-0.09
CHAPLET-3D	236.8	-0.25	104.6	0.16	70.0	0.34
CRX	236.5	-0.39	104.2	-0.24	69.6	-0.35
MCCG3D	237.9	0.19	104.7	0.20	70.0	0.26
PANDA	240.0	1.11	104.1	-0.33	70.0	0.24
PARTISN	238.4	0.42	104.7	0.25	70.0	0.33
PENTRAN	220.3	-7.23	101.8	-2.60	67.2	-3.75
THREEDANT-HU	239.6	0.92	103.8	-0.62	69.9	0.14
TORT-GRS	238.8	0.57	104.2	-0.22	69.8	0.02
TORT-PSU	238.0	0.26	104.4	-0.05	69.8	0.04
UNKGRO	235.1	-0.96	104.5	0.00	70.1	0.39
VARIANT-ISE	236.8	-0.25	104.2	-0.27	70.2	0.56
VARIANT-SE	240.1	1.12	103.4	-1.00	70.3	0.73
VARIANT-Homog	239.0	0.69	104.8	0.35	70.2	0.53

Table 52. Assembly power per cent errors for slice #2 of the *Rodded A* configuration

Code names	Inner UO ₂	Per cent error	MOX	Per cent error	Outer UO ₂	Per cent error
Reference MCNP	167.5	±0.17	78.0	±0.13	53.4	±0.09
ATTILA	167.4	-0.07	77.9	-0.18	53.4	-0.05
CHAPLET-3D	167.3	-0.13	78.1	0.11	53.5	0.25
CRX	167.0	-0.32	78.1	0.09	53.4	0.11
MCCG3D	167.4	-0.08	78.0	-0.04	53.5	0.13
PANDA	168.6	0.65	77.5	-0.69	53.4	-0.01
PARTISN	167.4	-0.05	78.0	-0.07	53.5	0.17
PENTRAN	163.4	-2.43	80.4	3.01	54.1	1.25
THREEDANT-HU	168.7	0.73	77.4	-0.79	53.4	0.09
TORT-GRS	168.0	0.27	77.7	-0.36	53.4	-0.03
TORT-PSU	167.3	-0.13	77.8	-0.23	53.4	-0.04
UNKGRO	166.4	-0.66	78.6	0.78	54.0	1.07
VARIANT-ISE	166.6	-0.55	77.8	-0.22	53.8	0.71
VARIANT-SE	168.0	0.31	77.1	-1.21	53.8	0.75
VARIANT-Homog	167.5	0.01	78.0	-0.04	53.5	0.30

Table 53. Assembly power per cent errors for slice #3 of the *Rodded A* configuration

Code names	Inner UO ₂	Per cent error	MOX	Per cent error	Outer UO ₂	Per cent error
Reference MCNP	56.3	±0.09	39.2	±0.09	28.2	±0.07
ATTILA	56.5	0.44	39.3	0.19	28.3	0.17
CHAPLET-3D	56.3	0.04	39.2	-0.07	28.2	-0.18
CRX	56.8	1.05	39.8	1.37	28.5	1.14
MCCG3D	55.7	-0.94	39.1	-0.42	28.2	-0.19
PANDA	55.5	-1.40	38.7	-1.45	28.0	-0.71
PARTISN	55.3	-1.68	38.9	-0.77	28.1	-0.29
PENTRAN	66.5	18.23	44.8	14.12	30.8	9.15
THREEDANT-HU	56.2	-0.16	38.8	-1.13	28.2	-0.20
TORT-GRS	56.2	-0.10	39.0	-0.66	28.0	-0.68
TORT-PSU	56.4	0.32	39.2	-0.02	28.1	-0.33
UNKGRO	55.9	-0.56	39.8	1.58	28.6	1.36
VARIANT-ISE	56.9	1.17	39.5	0.74	28.6	1.48
VARIANT-SE	56.3	0.16	38.9	-0.75	28.6	1.35
VARIANT-Homog	54.1	-3.84	38.9	-0.72	28.1	-0.43

Table 54. Assembly power per cent errors for the *Rodded A* configuration

Code names	Inner UO ₂	Per cent error	MOX	Per cent error	Outer UO ₂	Per cent error
Reference MCNP	461.2	±0.28	221.7	±0.22	151.4	±0.16
ATTILA	461.6	0.10	221.5	-0.09	151.3	-0.03
CHAPLET-3D	460.4	-0.17	221.9	0.10	151.7	0.21
CRX	460.3	-0.19	222.1	0.16	151.5	0.09
MCCG3D	461.0	-0.05	221.7	0.00	151.6	0.13
PANDA	464.1	0.64	220.3	-0.65	151.4	-0.03
PARTISN	461.1	-0.01	221.6	-0.04	151.6	0.16
PENTRAN	450.2	-2.38	226.9	2.33	152.0	0.42
THREEDANT-HU	464.5	0.72	220.0	-0.77	151.5	0.06
TORT-GRS	462.9	0.38	220.9	-0.35	151.2	-0.13
TORT-PSU	461.7	0.12	221.5	-0.11	151.3	-0.06
UNKGRO	457.5	-0.80	222.9	0.55	152.6	0.81
VARIANT-ISE	460.3	-0.19	221.5	-0.08	152.6	0.78
VARIANT-SE	464.5	0.71	219.4	-1.03	152.7	0.86
VARIANT-Homog	460.7	-0.11	221.8	0.02	151.8	0.27

Figure 23. Inner UO₂ assembly power per cent errors for the *Rodded A* configuration

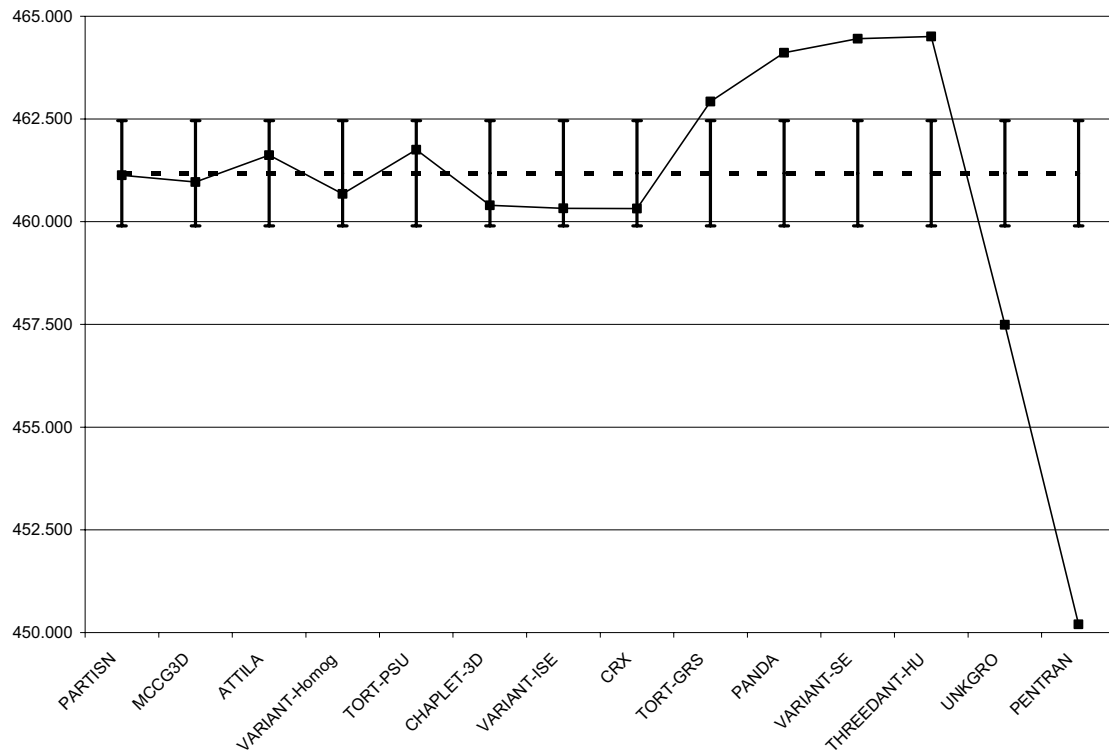


Figure 24. MOX assembly power per cent errors for the *Rodded A* configuration

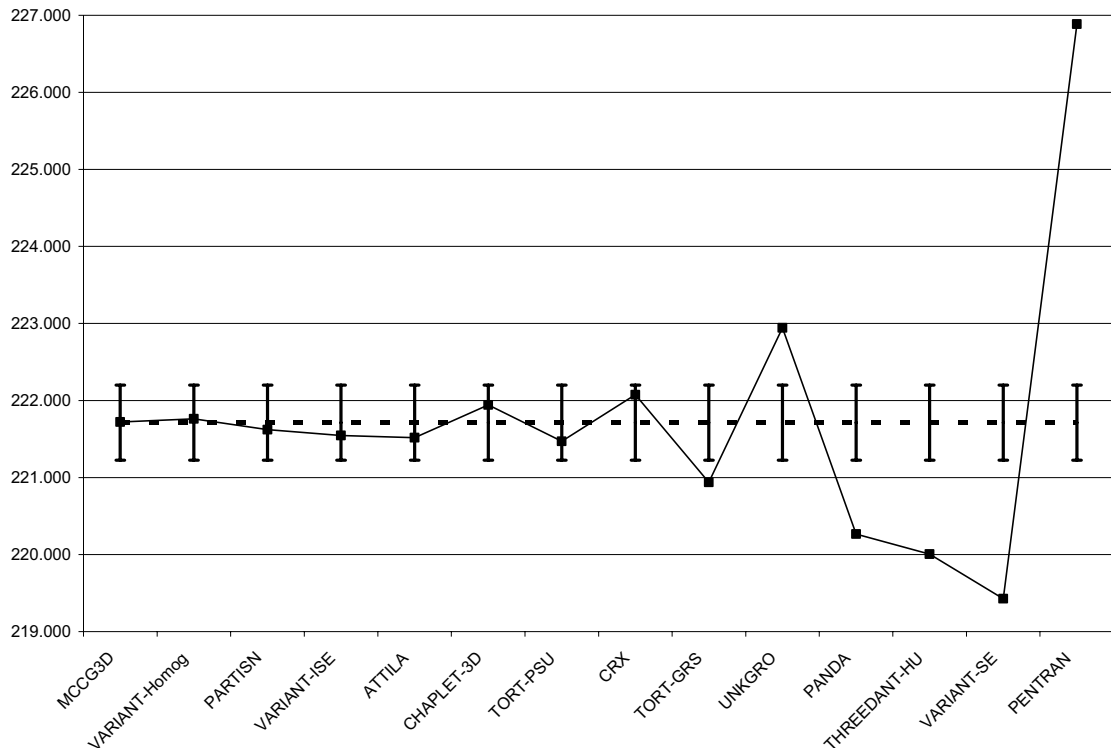


Figure 25. Outer UO₂ assembly power per cent errors for the *Rodded A* configuration

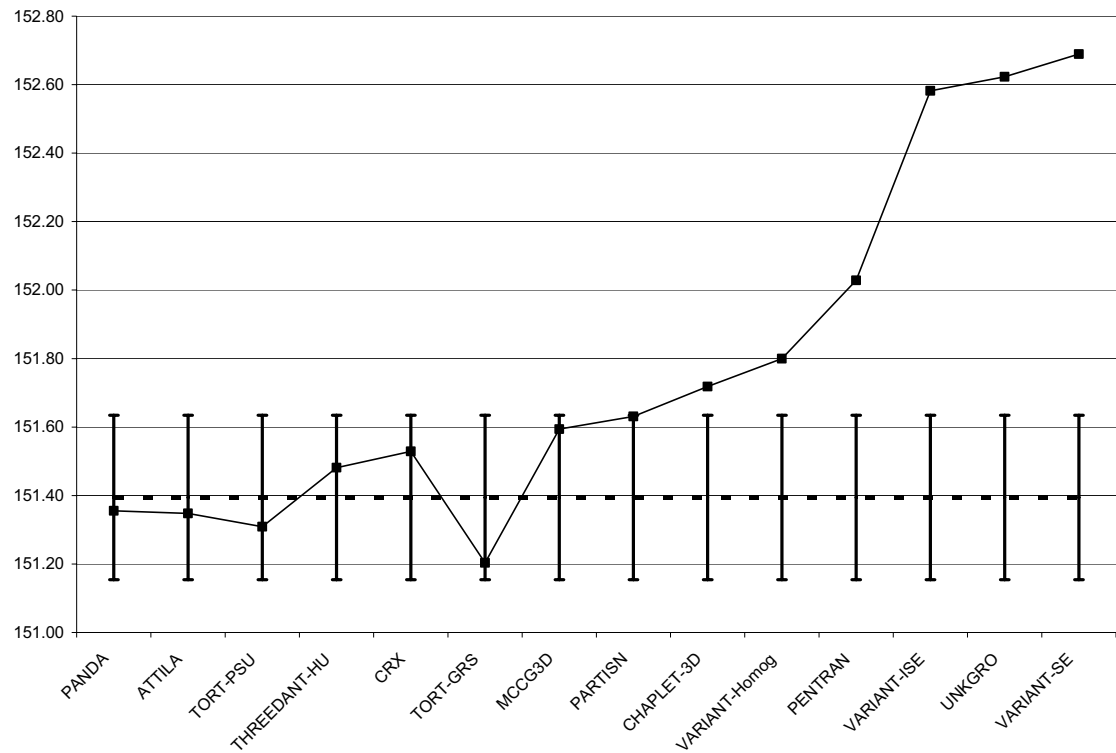


Table 55. Pin power distribution error measures for slice #1 of the *Rodded A* configuration

Code names	AVG	RMS	MRE
Reference MCNP	0.37	0.38	0.15
ATTILA	0.18	0.23	0.08
CHAPLET-3D	0.30	0.38	0.13
CRX	0.37	0.42	0.18
MCCG3D	0.29	0.40	0.12
PANDA	0.64	0.91	0.37
PARTISN	0.31	0.35	0.17
PENTRAN	4.05	4.81	2.39
THREEDANT-HU	0.63	0.75	0.35
TORT-GRS	0.35	0.43	0.20
TORT-PSU	0.19	0.24	0.10
UNKGRO	0.97	1.29	0.45
VARIANT-ISE	0.39	0.47	0.18
VARIANT-SE	1.00	1.10	0.50
VARIANT-Homog	0.68	0.91	0.33

Table 56. Pin power distribution error measures for slice #2 of the *Rodded A* configuration

Code names	AVG	RMS	MRE
Reference MCNP	0.42	0.43	0.13
ATTILA	0.20	0.25	0.06
CHAPLET-3D	0.25	0.34	0.07
CRX	0.32	0.43	0.11
MCCG3D	0.28	0.39	0.08
PANDA	0.68	0.90	0.24
PARTISN	0.18	0.23	0.05
PENTRAN	2.96	3.27	1.03
THREEDANT-HU	0.66	0.78	0.25
TORT-GRS	0.33	0.40	0.11
TORT-PSU	0.22	0.28	0.07
UNKGRO	1.13	1.60	0.32
VARIANT-ISE	0.52	0.61	0.19
VARIANT-SE	0.89	1.08	0.27
VARIANT-Homog	0.59	0.81	0.18

Table 57. Pin power distribution error measures for slice #3 of the *Rodded A* configuration

Code names	AVG	RMS	MRE
Reference MCNP	0.60	0.62	0.09
ATTILA	0.32	0.39	0.05
CHAPLET-3D	0.23	0.30	0.03
CRX	1.26	1.32	0.19
MCCG3D	0.60	0.69	0.10
PANDA	1.32	1.49	0.21
PARTISN	0.87	1.05	0.16
PENTRAN	13.43	14.26	2.27
THREEDANT-HU	0.76	0.92	0.11
TORT-GRS	0.60	0.71	0.08
TORT-PSU	0.31	0.38	0.05
UNKGRO	1.51	1.95	0.20
VARIANT-ISE	1.08	1.20	0.16
VARIANT-SE	0.87	1.05	0.12
VARIANT-Homog	1.65	2.21	0.30

Table 58. Pin power distribution error measures for the *Rodded A* configuration

Code names	AVG	RMS	MRE
Reference MCNP	0.25	0.26	0.22
ATTILA	0.13	0.16	0.12
CHAPLET-3D	0.21	0.28	0.18
CRX	0.25	0.35	0.22
MCCG3D	0.23	0.33	0.18
PANDA	0.64	0.87	0.65
PARTISN	0.12	0.16	0.10
PENTRAN	2.57	2.92	2.55
THREEDANT-HU	0.64	0.75	0.67
TORT-GRS	0.35	0.41	0.35
TORT-PSU	0.14	0.18	0.14
UNKGRO	0.99	1.40	0.84
VARIANT-ISE	0.43	0.53	0.37
VARIANT-SE	0.93	1.04	0.87
VARIANT-Homog	0.56	0.76	0.48

Figure 26. AVG per cent error for the *Rodded A* configuration

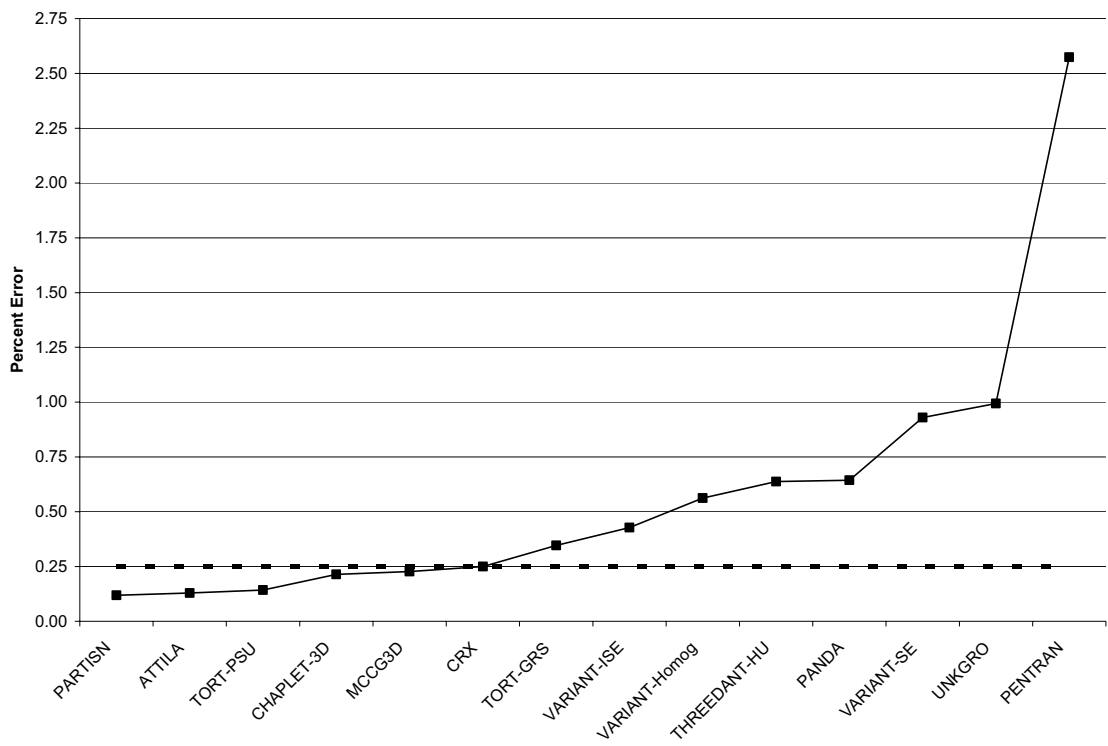


Figure 27. RMS per cent error for the *Rodded A* configuration

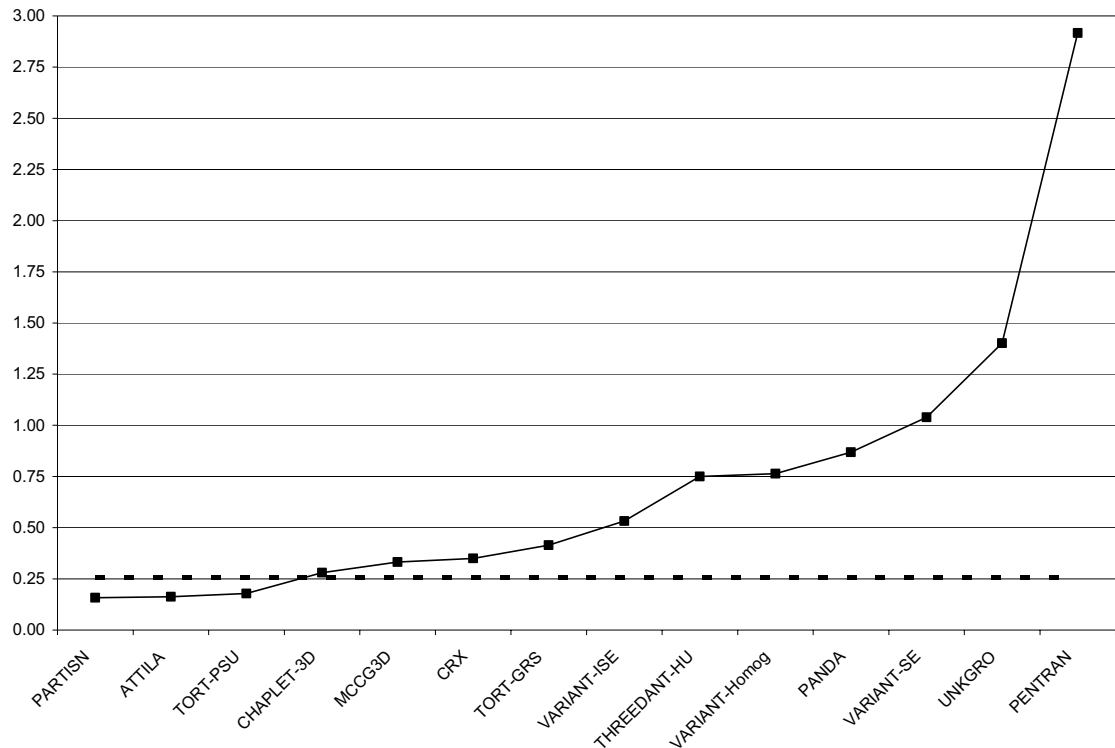


Figure 28. MRE per cent error for the *Rodded A* configuration

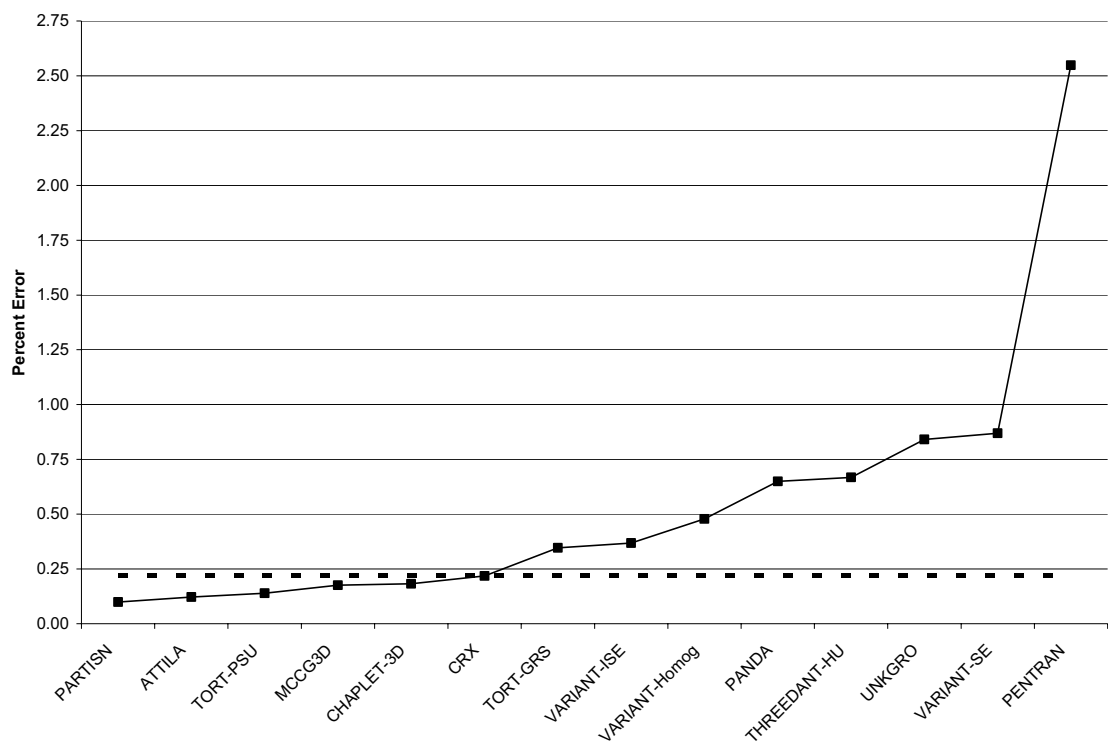


Table 59. Number of fuel pins within the reference confidence intervals for slice #1 of the *Rodded A* configuration

Code names	68%	90%	98%	99.8%
ATTILA	257	430	495	525
CHAPLET-3D	150	300	385	453
CRX	111	217	298	379
MCCG3D	176	331	401	455
PANDA	87	178	234	296
PARTISN	132	258	342	410
PENTRAN	1	4	5	7
THREEDANT-HU	89	160	203	244
TORT-GRS	164	284	344	394
TORT-PSU	269	401	446	486
UNKGRO	65	112	148	183
VARIANT-ISE	126	216	272	346
VARIANT-SE	27	41	65	92
VARIANT-Homog	83	155	197	258

Table 60. Percentage of fuel pins within the reference confidence intervals for slice #1 of the *Rodded A* configuration

Code names	68%	90%	98%	99.8%
ATTILA	47.6	79.6	91.7	97.2
CHAPLET-3D	27.8	55.6	71.3	83.9
CRX	20.6	40.2	55.2	70.2
MCCG3D	32.6	61.3	74.3	84.3
PANDA	16.1	33.0	43.3	54.8
PARTISN	24.4	47.8	63.3	75.9
PENTRAN	0.2	0.7	0.9	1.3
THREEDANT-HU	16.5	29.6	37.6	45.2
TORT-GRS	30.4	52.6	63.7	73.0
TORT-PSU	49.8	74.3	82.6	90.0
UNKGRO	12.0	20.7	27.4	33.9
VARIANT-ISE	23.3	40.0	50.4	64.1
VARIANT-SE	5.0	7.6	12.0	17.0
VARIANT-Homog	15.4	28.7	36.5	47.8

Table 61. Number of fuel pins within the reference confidence intervals for slice #2 of the *Rodded A* configuration

Code names	68%	90%	98%	99.8%
ATTILA	271	465	511	534
CHAPLET-3D	233	414	482	508
CRX	195	334	399	453
MCCG3D	231	391	449	494
PANDA	74	160	198	242
PARTISN	306	481	524	537
PENTRAN	10	17	22	31
THREEDANT-HU	87	151	198	241
TORT-GRS	173	298	385	461
TORT-PSU	237	418	491	526
UNKGRO	55	115	157	191
VARIANT-ISE	99	177	239	300
VARIANT-SE	56	116	155	188
VARIANT-Homog	99	202	249	309

Table 62. Percentage of fuel pins within the reference confidence intervals for slice #2 of the *Rodded A* configuration

Code names	68%	90%	98%	99.8%
ATTILA	50.2	86.1	94.6	98.9
CHAPLET-3D	43.1	76.7	89.3	94.1
CRX	36.1	61.9	73.9	83.9
MCCG3D	42.8	72.4	83.1	91.5
PANDA	13.7	29.6	36.7	44.8
PARTISN	56.7	89.1	97.0	99.4
PENTRAN	1.9	3.1	4.1	5.7
THREEDANT-HU	16.1	28.0	36.7	44.6
TORT-GRS	32.0	55.2	71.3	85.4
TORT-PSU	43.9	77.4	90.9	97.4
UNKGRO	10.2	21.3	29.1	35.4
VARIANT-ISE	18.3	32.8	44.3	55.6
VARIANT-SE	10.4	21.5	28.7	34.8
VARIANT-Homog	18.3	37.4	46.1	57.2

Table 63. Number of fuel pins within the reference confidence intervals for slice #3 of the Rodded A configuration

Code names	68%	90%	98%	99.8%
ATTILA	253	408	464	512
CHAPLET-3D	330	496	528	537
CRX	1	5	24	79
MCCG3D	125	249	316	366
PANDA	38	72	101	125
PARTISN	106	191	244	306
PENTRAN	4	8	10	12
THREEDANT-HU	115	200	243	318
TORT-GRS	91	227	326	445
TORT-PSU	265	424	484	521
UNKGRO	59	101	133	173
VARIANT-ISE	17	83	146	204
VARIANT-SE	89	174	225	282
VARIANT-Homog	65	128	165	209

Table 64. Percentage of fuel pins within the reference confidence intervals for slice #3 of the Rodded A configuration

Code names	68%	90%	98%	99.8%
ATTILA	46.9	75.6	85.9	94.8
CHAPLET-3D	61.1	91.9	97.8	99.4
CRX	0.2	0.9	4.4	14.6
MCCG3D	23.1	46.1	58.5	67.8
PANDA	7.0	13.3	18.7	23.1
PARTISN	19.6	35.4	45.2	56.7
PENTRAN	0.7	1.5	1.9	2.2
THREEDANT-HU	21.3	37.0	45.0	58.9
TORT-GRS	16.9	42.0	60.4	82.4
TORT-PSU	49.1	78.5	89.6	96.5
UNKGRO	10.9	18.7	24.6	32.0
VARIANT-ISE	3.1	15.4	27.0	37.8
VARIANT-SE	16.5	32.2	41.7	52.2
VARIANT-Homog	12.0	23.7	30.6	38.7

Table 65. Number of fuel pins within the reference confidence intervals for the Rodded A configuration

Code names	68%	90%	98%	99.8%
ATTILA	248	435	488	520
CHAPLET-3D	158	297	379	446
CRX	153	291	355	414
MCCG3D	193	323	386	442
PANDA	52	99	129	158
PARTISN	289	458	504	527
PENTRAN	16	28	33	41
THREEDANT-HU	54	109	136	164
TORT-GRS	99	182	232	285
TORT-PSU	233	396	460	506
UNKGRO	40	75	104	127
VARIANT-ISE	75	146	183	243
VARIANT-SE	23	39	46	57
VARIANT-Homog	45	106	145	189

Table 66. Percentage of fuel pins within the reference confidence intervals for the Rodded A configuration

Code names	68%	90%	98%	99.8%
ATTILA	45.9	80.6	90.4	96.3
CHAPLET-3D	29.3	55.0	70.2	82.6
CRX	28.3	53.9	65.7	76.7
MCCG3D	35.7	59.8	71.5	81.9
PANDA	9.6	18.3	23.9	29.3
PARTISN	53.5	84.8	93.3	97.6
PENTRAN	3.0	5.2	6.1	7.6
THREEDANT-HU	10.0	20.2	25.2	30.4
TORT-GRS	18.3	33.7	43.0	52.8
TORT-PSU	43.1	73.3	85.2	93.7
UNKGRO	7.4	13.9	19.3	23.5
VARIANT-ISE	13.9	27.0	33.9	45.0
VARIANT-SE	4.3	7.2	8.5	10.6
VARIANT-Homog	8.3	19.6	26.9	35.0

Figure 29. Percentage of fuel pins within the *Rodded A* configuration confidence intervals

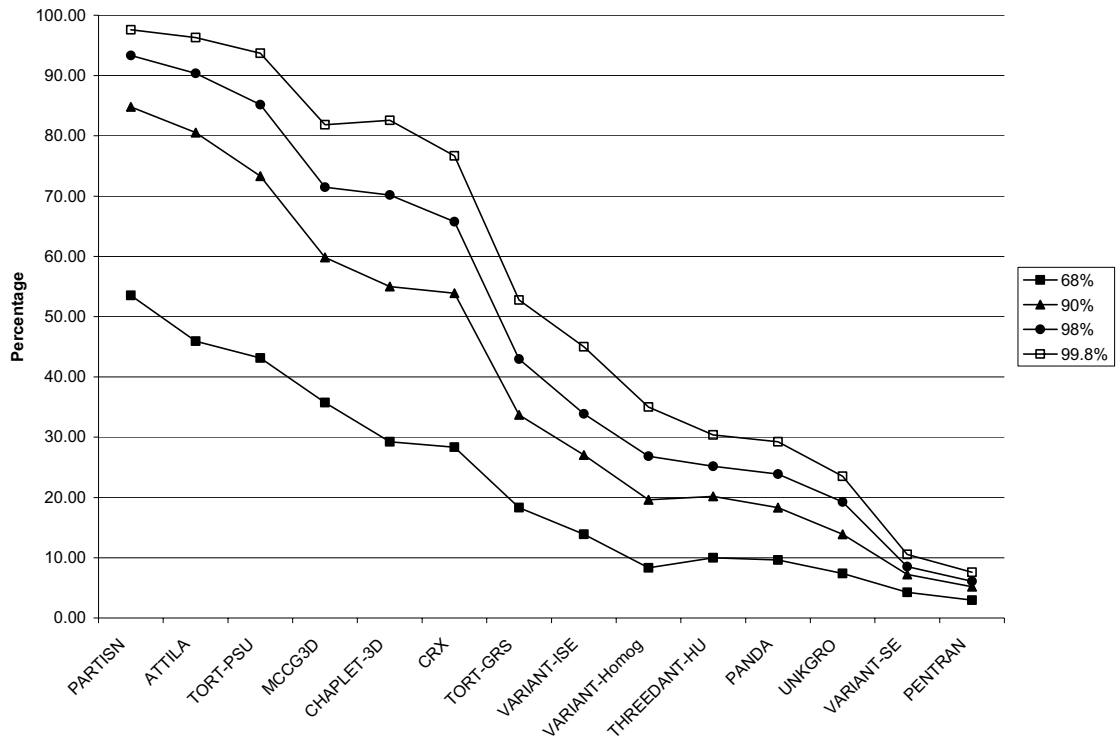


Table 67. Estimated CPU time for the *Rodded A* configuration

Code names	Estimated CPU Time
ATTILA	hours
CHAPLET-3D	days
CRX	Not Given
MCCG3D	weeks
PANDA	hours
PARTISN	hours
PENTRAN	hours
THREEDANT-HU	days
TORT-GRS	days
TORT-PSU	days
UNKGRO	days
VARIANT-ISE	days
VARIANT-SE	days
VARIANT-Homog	minutes

Chapter 8

RODDED B CONFIGURATION BENCHMARK RESULTS

As discussed in Chapter 2, the three-dimensional extension benchmark contains three configurations: *Unrodded*, *Rodded A*, and *Rodded B*. The results for the *Rodded B* configuration will be inspected in this chapter. To minimise the content of this report, plots of the data will only be provided for the core pin power solutions.

Table 68 tabulates the participant eigenvalue solutions and the per cent errors with respect to the reference MCNP solution. Figure 30 displays the eigenvalue solutions ordered with respect to decreasing eigenvalue accuracy where the dashed line represents the reference MCNP solution and the confidence intervals are too small to view. Figure 31 displays the eigenvalue per cent error with respect to decreasing eigenvalue accuracy where the reference MCNP statistical error again is too small to be distinguished on this plot. As can be seen in Figures 30 and 31 and Table 68, a majority of the solutions are reasonably close to the reference MCNP solution. Similar to the *Unrodded* configuration, none of the participants' codes are within the 98% confidence interval of the MCNP eigenvalue. The average error for all the participant solutions has also increased from to 0.19% (up from 0.11% and 0.12%). The number of participants greater than 0.1% or 100 pcm in error from the reference solution has increased to nine.

The specific pin power error measures for each slice are tabulated in Tables 69-71 with the results for the core distribution given in Table 72. Figure 32 displays the maximum pin power results and Figure 33 the maximum per cent errors found in each participant solution. For each participant solution, the pin location of the maximum error was determined and the statistical error associated with that pin obtained. This statistical error has been tabulated for each participant in Tables 69-71 in the column titled "associated reference MCNP statistical error" and included in Figure 33 as "associated statistical error." All of the participant solutions in Figures 32 and 33 are ordered with respect to decreasing solution accuracy.

In slice #1, Table 69, one participant obtained a maximum pin power within the 98% confidence interval with the remainder of participants significantly greater than the 98% confidence interval (in general a factor of two). This pattern is not continued for slices #2 and #3 where six participants succeed in slice #2 and seven succeed in slice #3 as seen in Tables 70 and 71. The core pin power results are different from slices #1-3 in Table 72 with only three participants within the 98% confidence interval.

As was the case with the *Unrodded And Rodded A* configuration, the maximum per cent error results in Tables 69-72 and Figure 33 show that none of the participants' codes succeed in coming within the 98% MCNP confidence intervals. For the core pin power results, only four of the participant codes have maximum errors less than 1% and eleven achieved maximum errors less than 5%.

The assembly power error measures results are tabulated in Tables 73-76. Figure 34 displays the participant results for the inner UO₂ assembly power, Figure 35 the results for the MOX assembly power, and Figure 36 the results of the outer UO₂ assembly power. For the slice #1 inner UO₂ assembly power three participant solutions are within the 98% confidence interval. For slice #2, four are within the 98% confidence intervals and two for slice #3. For the core assembly power distribution, eight participants are within the 98% confidence interval. For the outer UO₂ assembly, only a single solution is within the 98% confidence interval for each slice. For the core pin power results in Table 76, three succeeded in meeting the 98% confidence interval. For the MOX assembly, four meet the 98% interval for slice #1 with only three in slice #2 and none in slice #3. For the core result in Table 76, seven participant solutions are within the 98% confidence interval.

Tables 77-80 give the pin power distribution error measures. Figure 37 displays the AVG error measure results, Figure 38 the RMS error measure results, and Figure 39 the MRE error measure results. Four of the participants are within the 98% confidence interval for the AVG error measure in slices #1-3. For the core wide results, three participants agree with the reference MCNP solution with twelve participants less than 1% in error. For the RMS error measure, three of the participants are within the 98% confidence interval in slice #1 with four in slice #2 and four in slice #3. The core wide results are slightly worse than the AVG results with only two of the participants within the 98% confidence interval and nine less than 1% in error. For the MRE error measure, four of the participants are within the 98% confidence interval for slice #1 with four for slice #2 and five for slice #3. For the core wide results, four participants are within the 98% confidence interval with thirteen less than 1% in error. Compared to the *Unrodded And Rodded A* configuration, the AVG, RMS, and MRE participant error has increased noticeably for the *Rodded B* configuration. As was the case in the *Unrodded* configuration, a majority of the error in the participants results is still small as indicated by the AVG error measure. In the *Unrodded* configuration most of this error appeared to lie in the low power region of the core since the accuracy of the MRE and AVG error measures were similar. In the *Rodded B* configuration the introduction of the control rods introduced a significant flux gradient. This leads to significant inaccuracies in the assembly power results and the planer AVG, RMS, and MRE results (thereby the increased error in the participants results). The radial and axial error, as would be expected, noticeably increased when compared to the *Unrodded And Rodded A* configuration.

Tables 81, 83, 85, and 87 tabulate the number of fuel pins within the various confidence intervals while Tables 82, 84, 86, and 88 tabulate the percentage of fuel pins that are within the confidence intervals. Figure 40 plots the participant results, ordered with respect to the 98% confidence interval results. As can be seen, none of the participants match the 98% confidence interval for any individual slice and relatively few are close. This error measure represents by far the strictest measure of accuracy that can be applied to the pin power distribution; however, it is subject to significant uncertainty from the normalization procedure applied as discussed in the original benchmark. For this reason, this error measure should not be assumed essential to guarantee the accuracy of any given solution.

Overall, the *Rodded B* configuration results are significantly worse than those seen in the *Unrodded* or the *Rodded A* configuration. This is most likely a result of the steeper flux gradients caused by the introduction of control rods into the low power region. Once again, the inaccuracies in this benchmark can be attributed to insufficient space-angle approximations implemented by the participants in their codes. For completeness, an estimate of each participant CPU time is provided in Table 89. The analysis tools used for the *Rodded B* configuration are provided electronically in Appendix F.

Table 68. Eigenvalue solutions for the *Rodded B* configuration

Code names	Eigenvalue	Per cent error
Reference MCNP	1.07777	± 0.006
ATTILA	1.07691	-0.080
CHAPLET-3D	1.07667	-0.102
CRX	1.07707	-0.065
MCCG3D	1.07801	0.022
PANDA	1.07497	-0.260
PARTISN	1.07551	-0.210
PENTRAN	1.07356	-0.391
THREEDANT-HU	1.07667	-0.102
TORT-GRS	1.07327	-0.418
TORT-PSU	1.07606	-0.159
UNKGRO	1.07731	-0.043
VARIANT-ISE	1.07887	0.102
VARIANT-SE	1.07098	-0.630
VARIANT-Homog	1.07865	0.082

Figure 30. Eigenvalue solutions for the *Rodded B* configuration

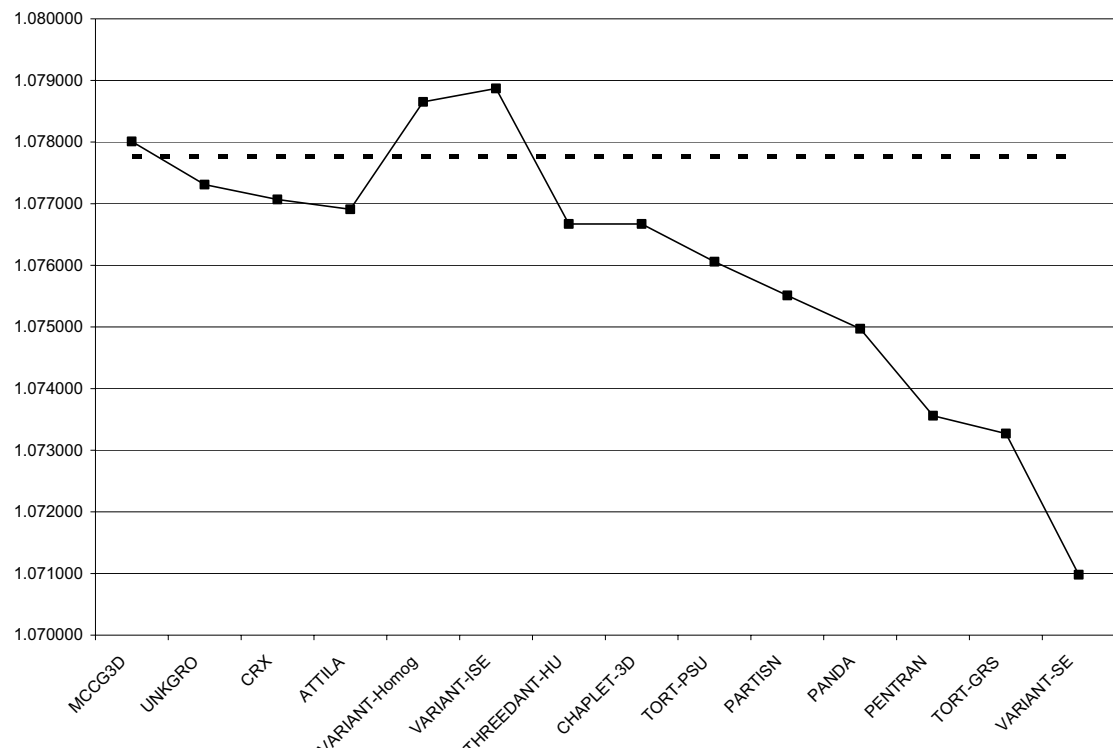


Figure 31. Eigenvalue per cent errors for the *Rodded B* configuration

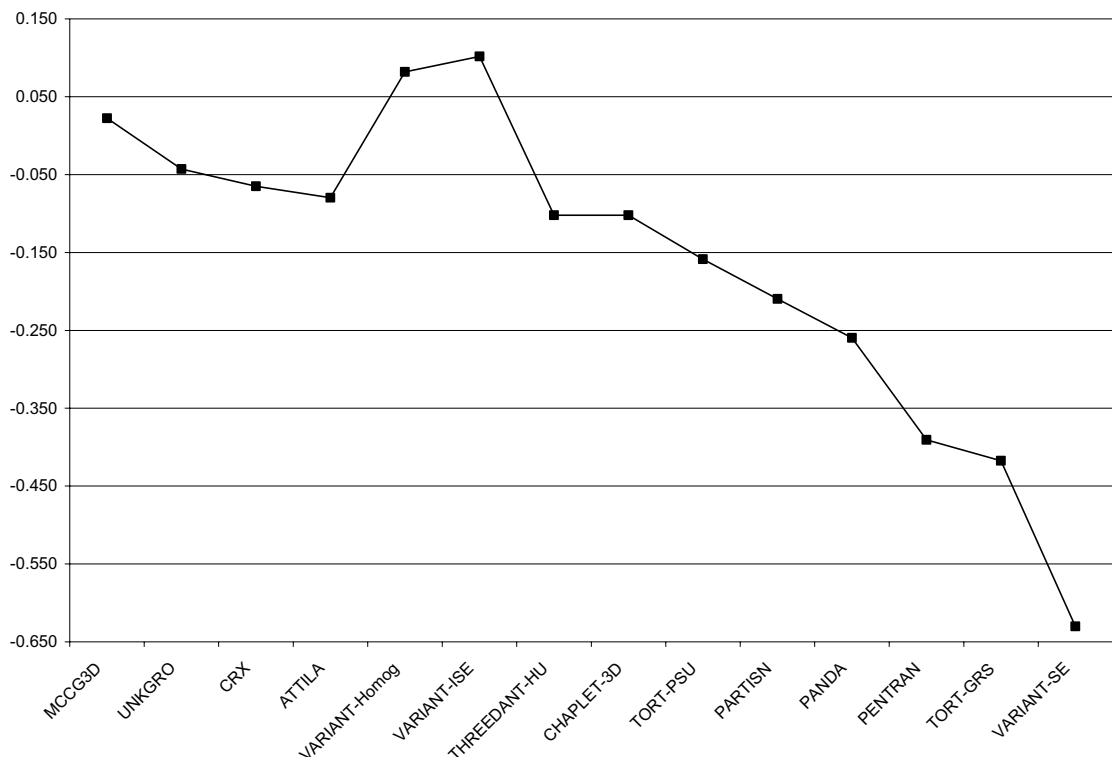


Table 69. Participant results for specific pin powers in slice #1 of the *Rodded B* configuration

Code names	Maximum pin power	Per cent error	Maximum per cent error	Associated reference MCNP statistical error
Reference MCNP	1.200	± 0.21		
ATTILA	1.196	-0.35	0.71	± 0.56
CHAPLET-3D	1.194	-0.49	1.47	± 0.56
CRX	1.182	-1.50	1.64	± 0.23
MCCG3D	1.196	-0.31	1.12	± 0.28
PANDA	1.220	1.67	10.84	± 0.42
PARTISN	1.204	0.32	1.96	± 0.56
PENTRAN	1.108	-7.68	8.98	± 0.56
THREEDANT-HU	1.214	1.19	1.54	± 0.53
TORT-GRS	1.203	0.23	1.00	± 0.49
TORT-PSU	1.197	-0.22	0.98	± 0.53
UNKGRO	1.165	-2.89	5.04	± 0.56
VARIANT-ISE	1.182	-1.50	1.59	± 0.21
VARIANT-SE	1.201	0.11	3.27	± 0.53
VARIANT-Homog	1.213	1.06	4.89	± 0.56

Table 70. Participant results for specific pin powers in slice #2 of the *Rodded B* configuration

Code names	Maximum pin power	Per cent error	Maximum per cent error	Associated reference MCNP statistical error
Reference MCNP	0.554	± 0.35		
ATTILA	0.554	0.10	0.89	± 0.47
CHAPLET-3D	0.552	-0.25	1.04	± 0.47
CRX	0.556	0.37	2.31	± 0.56
MCCG3D	0.559	0.97	1.46	± 0.33
PANDA	0.554	0.04	11.11	± 0.51
PARTISN	0.545	-1.58	2.11	± 0.30
PENTRAN	0.575	3.82	10.56	± 0.63
THREEDANT-HU	0.556	0.36	1.72	± 0.49
TORT-GRS	0.556	0.38	1.05	± 0.49
TORT-PSU	0.554	0.02	0.94	± 0.49
UNKGRO	0.559	0.90	5.98	± 0.56
VARIANT-ISE	0.552	-0.26	1.82	± 0.47
VARIANT-SE	0.554	0.00	3.30	± 0.60
VARIANT-Homog	0.542	-2.17	5.89	± 0.30

Table 71. Participant results for specific pin powers in slice #3 of the *Rodded B* configuration

Code names	Maximum pin power	Per cent error	Maximum per cent error	Associated reference MCNP statistical error
Reference MCNP	0.217	± 0.56		
ATTILA	0.217	-0.07	1.73	± 0.86
CHAPLET-3D	0.217	0.25	1.78	± 0.86
CRX	0.218	0.53	4.43	± 0.88
MCCG3D	0.216	-0.34	2.30	± 0.79
PANDA	0.212	-2.24	8.07	± 0.86
PARTISN	0.208	-3.94	4.29	± 0.53
PENTRAN	0.202	-7.03	26.51	± 0.91
THREEDANT-HU	0.215	-0.63	2.60	± 0.86
TORT-GRS	0.217	0.02	1.15	± 0.86
TORT-PSU	0.216	-0.42	2.11	± 0.86
UNKGRO	0.212	-2.07	7.11	± 0.77
VARIANT-ISE	0.220	1.50	3.28	± 0.86
VARIANT-SE	0.217	0.08	4.39	± 0.88
VARIANT-Homog	0.206	-4.92	8.77	± 0.51

Table 72. Participant results for specific pin powers in the *Rodded B* configuration

Code names	Maximum pin power	Per cent error	Maximum Per cent error	Associated reference MCNP statistical error
Reference MCNP	1.835	± 0.19		
ATTILA	1.835	0.03	0.79	± 0.37
CHAPLET-3D	1.832	-0.15	1.14	± 0.37
CRX	1.825	-0.55	1.95	± 0.37
MCCG3D	1.839	0.25	0.99	± 0.28
PANDA	1.846	0.61	10.64	± 0.30
PARTISN	1.822	-0.67	1.71	± 0.37
PENTRAN	1.778	-3.11	12.61	± 0.38
THREEDANT-HU	1.847	0.68	1.67	± 0.37
TORT-GRS	1.842	0.38	0.90	± 0.35
TORT-PSU	1.836	0.08	0.76	± 0.37
UNKGRO	1.824	-0.58	5.23	± 0.28
VARIANT-ISE	1.826	-0.50	1.52	± 0.28
VARIANT-SE	1.843	0.47	3.47	± 0.37
VARIANT-Homog	1.818	-0.92	4.44	± 0.38

Figure 32. Maximum pin power results for the *Rodded B* configuration

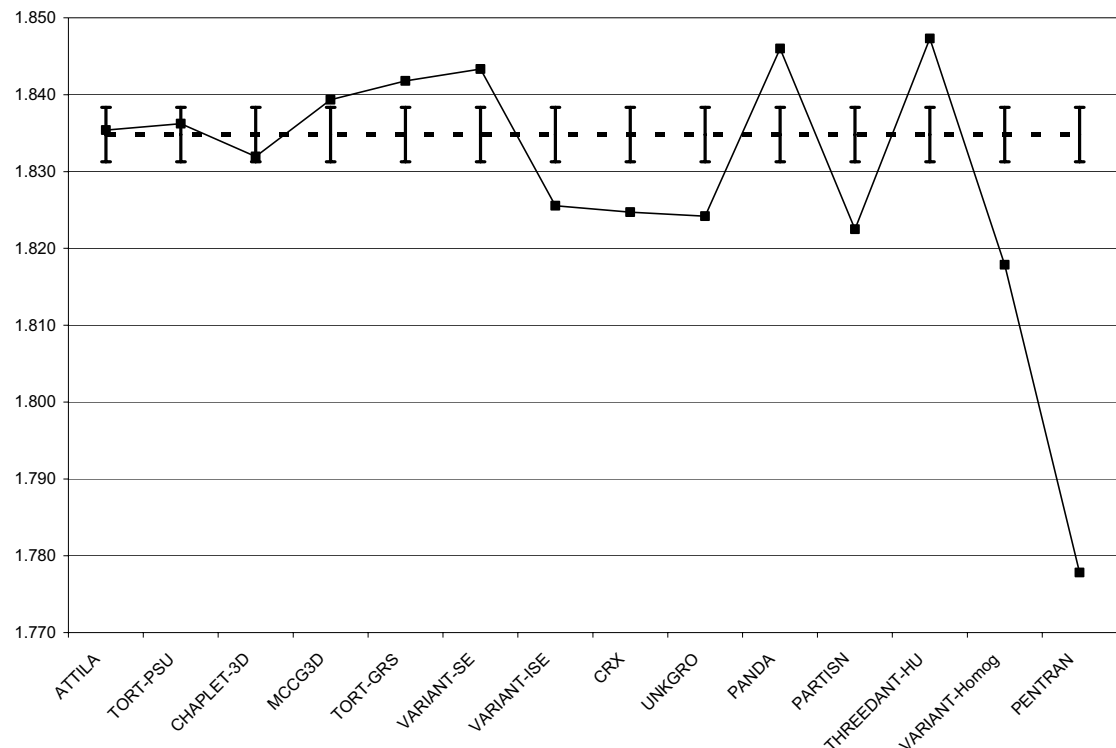


Figure 33. Maximum per cent errors for the *Rodded B* configuration

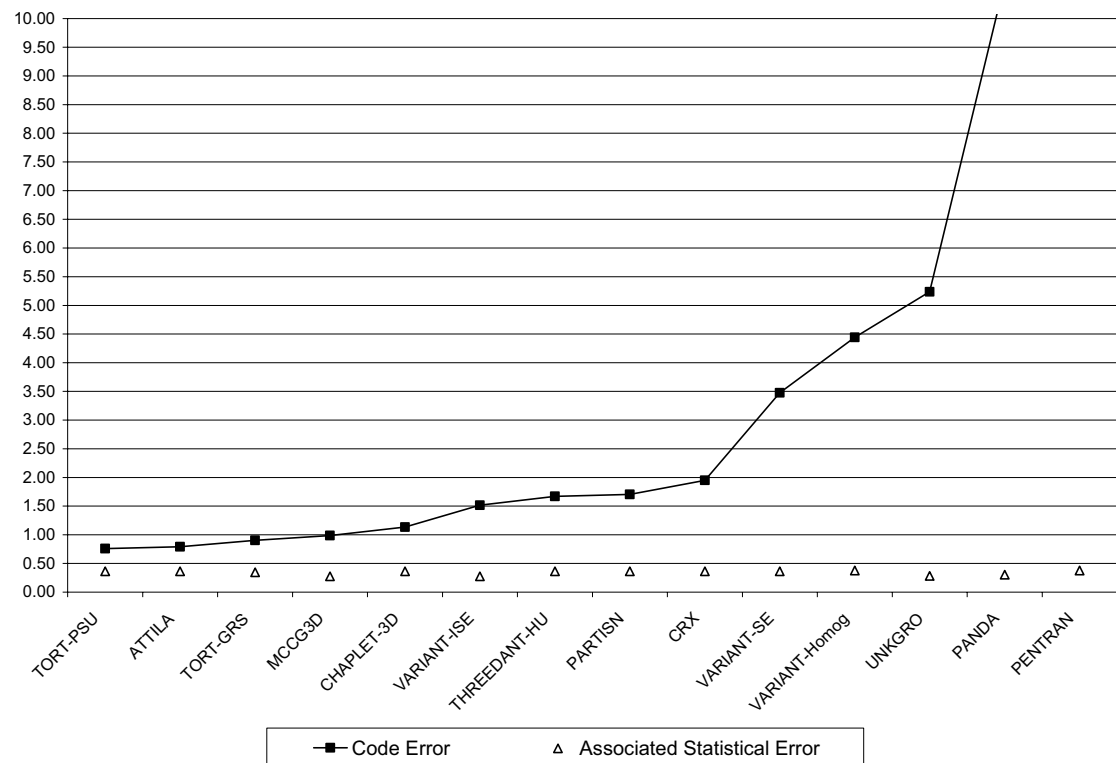


Table 73. Assembly power per cent errors for slice #1 of the *Rodded B* configuration

Code names	Inner UO ₂	Per cent error	MOX	Per cent error	Outer UO ₂	Per cent error
Reference MCNP	247.7	±0.21	125.8	±0.17	91.6	±0.13
ATTILA	247.2	-0.21	125.7	-0.08	91.7	0.10
CHAPLET-3D	247.0	-0.32	125.9	0.09	91.9	0.29
CRX	244.6	-1.28	125.0	-0.60	91.3	-0.34
MCCG3D	247.1	-0.28	125.4	-0.32	91.5	-0.19
PANDA	250.1	0.97	125.8	0.04	92.8	1.28
PARTISN	248.9	0.46	126.7	0.76	92.7	1.19
PENTRAN	235.5	-4.95	128.7	2.32	92.9	1.33
THREEDANT-HU	250.1	0.96	125.2	-0.43	92.2	0.65
TORT-GRS	248.2	0.20	125.6	-0.18	92.0	0.38
TORT-PSU	247.5	-0.08	125.7	-0.05	91.8	0.21
UNKGRO	243.6	-1.66	125.5	-0.25	91.8	0.21
VARIANT-ISE	245.4	-0.96	125.2	-0.48	92.0	0.39
VARIANT-SE	248.5	0.32	125.0	-0.63	93.2	1.74
VARIANT-Homog	249.4	0.69	127.0	0.99	93.1	1.63

Table 74. Assembly power per cent errors for slice #2 of the *Rodded B* configuration

Code names	Inner UO ₂	Per cent error	MOX	Per cent error	Outer UO ₂	Per cent error
Reference MCNP	106.6	±0.13	81.4	±0.14	65.0	±0.11
ATTILA	106.7	0.15	81.3	-0.12	65.2	0.20
CHAPLET-3D	106.5	-0.06	81.3	-0.10	65.1	0.06
CRX	106.9	0.35	82.1	0.83	65.6	0.93
MCCG3D	107.2	0.60	81.6	0.19	65.3	0.36
PANDA	105.5	-1.02	81.0	-0.54	65.6	0.94
PARTISN	105.0	-1.45	81.3	-0.16	65.5	0.71
PENTRAN	113.0	6.08	85.1	4.50	65.7	0.99
THREEDANT-HU	106.6	0.01	80.8	-0.80	65.4	0.58
TORT-GRS	106.6	0.02	81.2	-0.31	65.2	0.34
TORT-PSU	106.8	0.22	81.2	-0.25	65.1	0.16
UNKGRO	106.5	-0.05	82.3	1.13	65.9	1.35
VARIANT-ISE	107.0	0.44	81.3	-0.19	65.5	0.71
VARIANT-SE	106.0	-0.50	80.5	-1.10	66.2	1.78
VARIANT-Homog	103.0	-3.36	81.5	0.09	65.8	1.20

Table 75. Assembly power per cent errors for slice #3 of the *Rodded B* configuration

Code names	Inner UO ₂	Per cent error	MOX	Per cent error	Outer UO ₂	Per cent error
Reference MCNP	41.1	±0.08	29.4	±0.08	30.7	±0.07
ATTILA	41.2	0.16	29.6	0.52	30.8	0.54
CHAPLET-3D	41.3	0.52	29.6	0.48	30.6	-0.12
CRX	41.6	1.14	30.1	2.40	31.5	2.55
MCCG3D	41.0	-0.32	29.6	0.60	30.9	0.88
PANDA	40.0	-2.85	28.8	-2.04	30.7	0.14
PARTISN	39.7	-3.46	28.8	-2.17	30.6	-0.25
PENTRAN	39.1	-5.03	27.9	-5.15	26.5	-13.46
THREEDANT-HU	40.8	-0.71	29.0	-1.40	30.8	0.45
TORT-GRS	41.1	-0.18	29.4	-0.18	30.7	0.12
TORT-PSU	41.1	-0.04	29.5	0.39	30.7	-0.03
UNKGRO	41.1	-0.10	30.1	2.29	31.3	1.93
VARIANT-ISE	42.2	2.54	29.9	1.75	31.2	1.78
VARIANT-SE	41.1	-0.08	29.2	-0.63	31.4	2.47
VARIANT-Homog	38.9	-5.51	29.0	-1.46	30.8	0.26

Table 76. Assembly power per cent errors for the *Rodded B* configuration

Code names	Inner UO ₂	Per cent error	MOX	Per cent error	Outer UO ₂	Per cent error
Reference MCNP	395.4	±0.26	236.6	±0.23	187.3	±0.18
ATTILA	395.1	-0.07	236.6	-0.02	187.7	0.21
CHAPLET-3D	394.8	-0.16	236.8	0.08	187.6	0.14
CRX	393.1	-0.59	237.2	0.26	188.4	0.57
MCCG3D	395.2	-0.05	236.5	-0.03	187.7	0.18
PANDA	395.6	0.04	235.6	-0.42	189.2	0.98
PARTISN	393.6	-0.47	236.8	0.08	188.8	0.79
PENTRAN	387.6	-1.99	241.7	2.14	185.1	-1.21
THREEDANT-HU	397.5	0.53	235.0	-0.68	188.5	0.59
TORT-GRS	395.9	0.11	236.1	-0.22	187.9	0.32
TORT-PSU	395.4	0.00	236.5	-0.06	187.6	0.15
UNKGRO	391.2	-1.06	237.9	0.54	189.0	0.88
VARIANT-ISE	394.6	-0.22	236.4	-0.10	188.7	0.73
VARIANT-SE	395.7	0.06	234.7	-0.79	190.9	1.87
VARIANT-Homog	391.3	-1.05	237.5	0.38	189.7	1.26

Figure 34. Inner UO₂ assembly power per cent errors for the *Rodded B* configuration

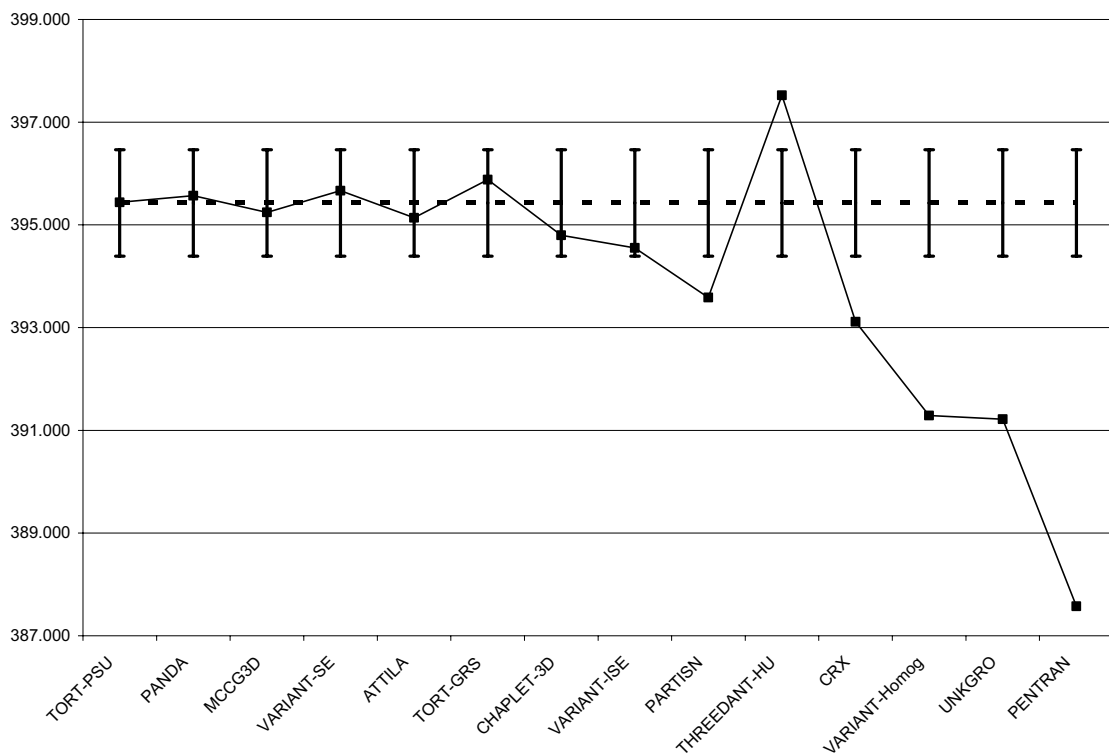


Figure 35. MOX assembly power per cent errors for the *Rodded B* configuration

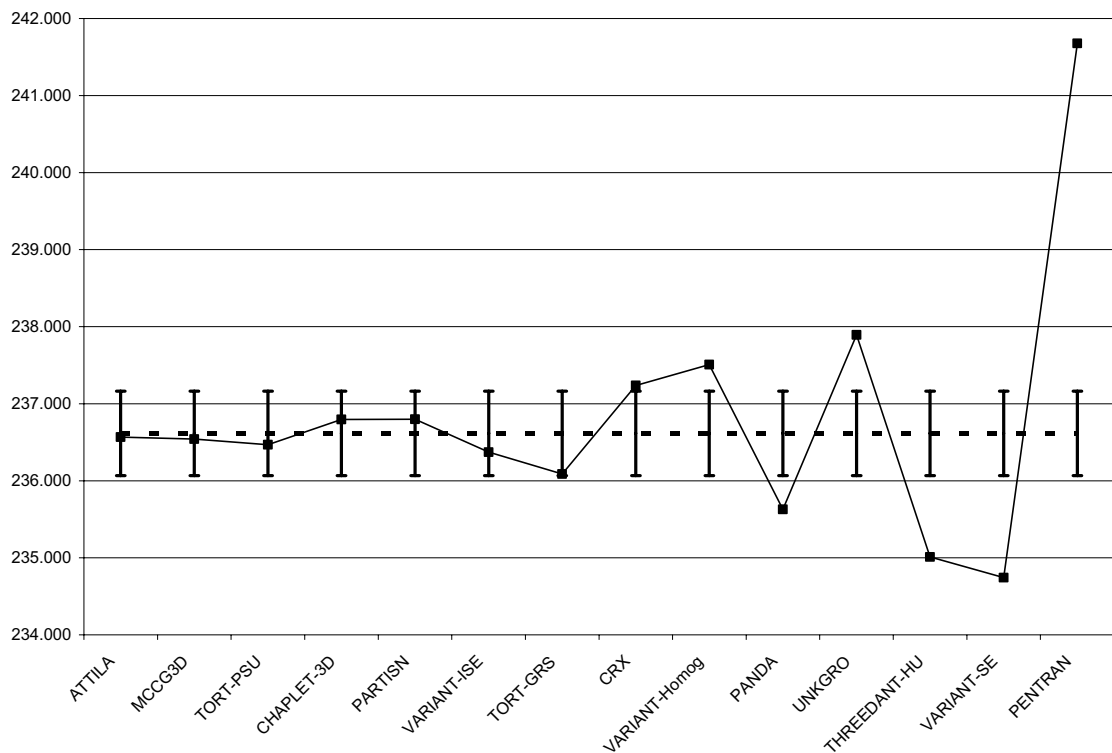


Figure 36. Outer UO₂ assembly power per cent errors for the *Rodded B* configuration

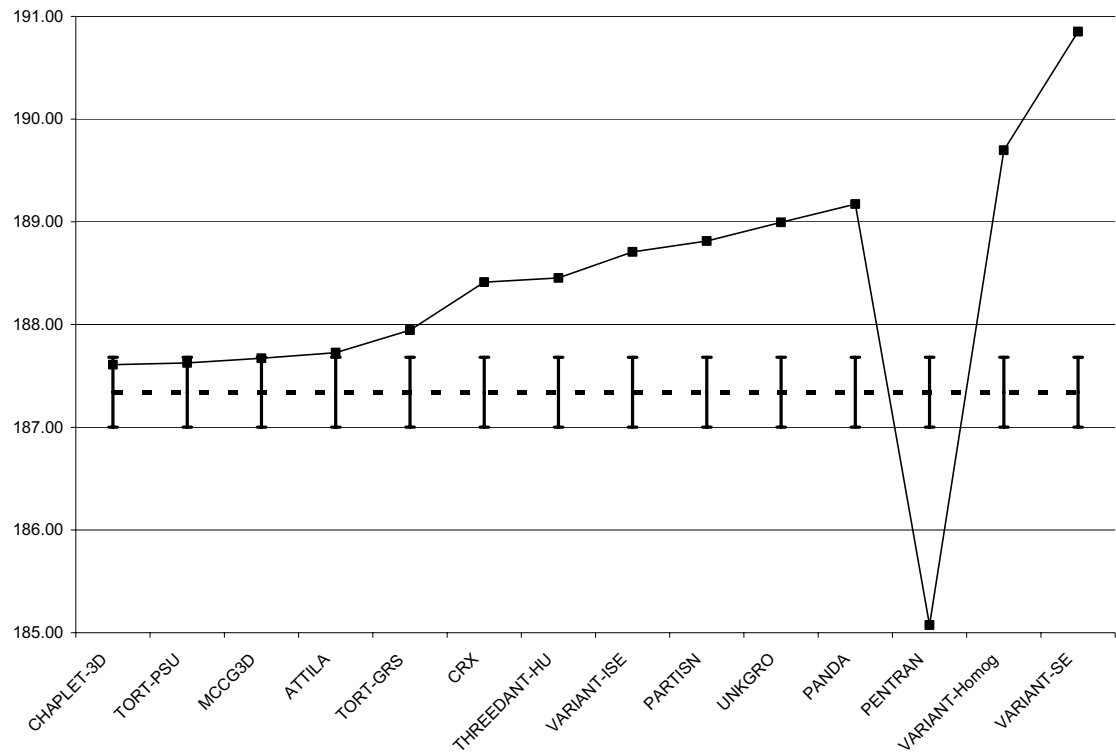


Table 77. Pin power distribution error measures for slice #1 of the *Rodded B* configuration

Code names	AVG	RMS	MRE
Reference MCNP	0.34	0.35	0.17
ATTILA	0.17	0.21	0.10
CHAPLET-3D	0.29	0.38	0.15
CRX	0.74	0.85	0.50
MCCG3D	0.34	0.42	0.19
PANDA	0.79	1.10	0.43
PARTISN	0.82	0.89	0.39
PENTRAN	3.23	3.68	2.02
THREEDANT-HU	0.66	0.75	0.40
TORT-GRS	0.29	0.35	0.14
TORT-PSU	0.17	0.22	0.08
UNKGRO	1.20	1.49	0.71
VARIANT-ISE	0.58	0.69	0.40
VARIANT-SE	0.93	1.17	0.41
VARIANT-Homog	1.11	1.42	0.54

Table 78. Pin power distribution error measures for slice #2 of the *Rodded B* configuration

Code names	AVG	RMS	MRE
Reference MCNP	0.42	0.43	0.13
ATTILA	0.20	0.25	0.06
CHAPLET-3D	0.21	0.27	0.06
CRX	0.77	0.89	0.22
MCCG3D	0.43	0.53	0.14
PANDA	0.87	1.12	0.27
PARTISN	0.72	0.90	0.25
PENTRAN	4.57	4.91	1.53
THREEDANT-HU	0.63	0.75	0.18
TORT-GRS	0.31	0.39	0.09
TORT-PSU	0.26	0.32	0.08
UNKGRO	1.20	1.74	0.32
VARIANT-ISE	0.48	0.56	0.15
VARIANT-SE	1.17	1.37	0.34
VARIANT-Homog	1.51	2.07	0.52

Table 79. Pin power distribution error measures for slice #3 of the *Rodded B* configuration

Code names	AVG	RMS	MRE
Reference MCNP	0.66	0.67	0.08
ATTILA	0.47	0.57	0.05
CHAPLET-3D	0.45	0.53	0.06
CRX	2.19	2.35	0.25
MCCG3D	0.71	0.87	0.08
PANDA	1.93	2.21	0.25
PARTISN	2.04	2.36	0.27
PENTRAN	7.41	9.00	0.87
THREEDANT-HU	1.05	1.22	0.12
TORT-GRS	0.31	0.38	0.04
TORT-PSU	0.35	0.45	0.04
UNKGRO	1.91	2.43	0.21
VARIANT-ISE	1.98	2.04	0.25
VARIANT-SE	1.21	1.56	0.14
VARIANT-Homog	2.40	3.17	0.33

Table 80. Pin power distribution error measures for the *Rodded B* configuration

Code names	AVG	RMS	MRE
Reference MCNP	0.24	0.25	0.23
ATTILA	0.14	0.18	0.12
CHAPLET-3D	0.19	0.25	0.17
CRX	0.50	0.64	0.48
MCCG3D	0.28	0.34	0.26
PANDA	0.63	0.93	0.52
PARTISN	0.45	0.55	0.42
PENTRAN	2.51	3.00	2.39
THREEDANT-HU	0.65	0.72	0.61
TORT-GRS	0.26	0.31	0.23
TORT-PSU	0.13	0.17	0.11
UNKGRO	1.09	1.50	0.98
VARIANT-ISE	0.43	0.52	0.41
VARIANT-SE	0.99	1.26	0.81
VARIANT-Homog	0.92	1.21	0.90

Figure 37. AVG per cent error for the *Rodded B* configuration

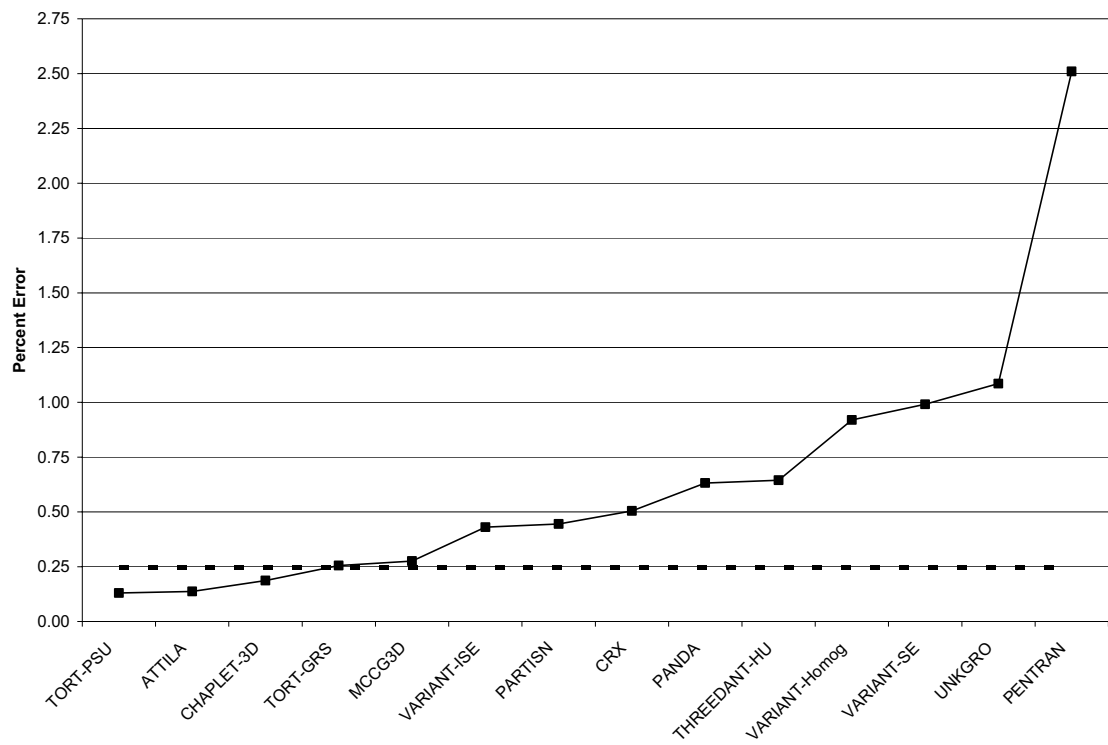


Figure 38. RMS per cent error for the *Rodded B* configuration

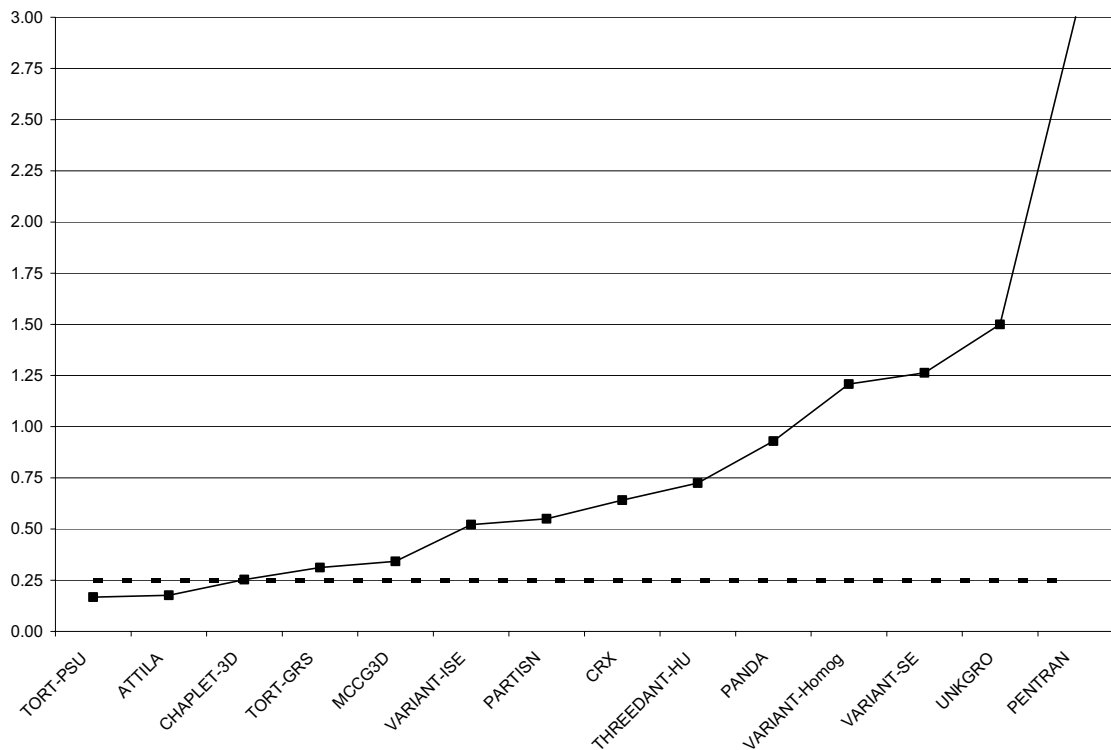


Figure 39. MRE per cent error for the *Rodded B* configuration

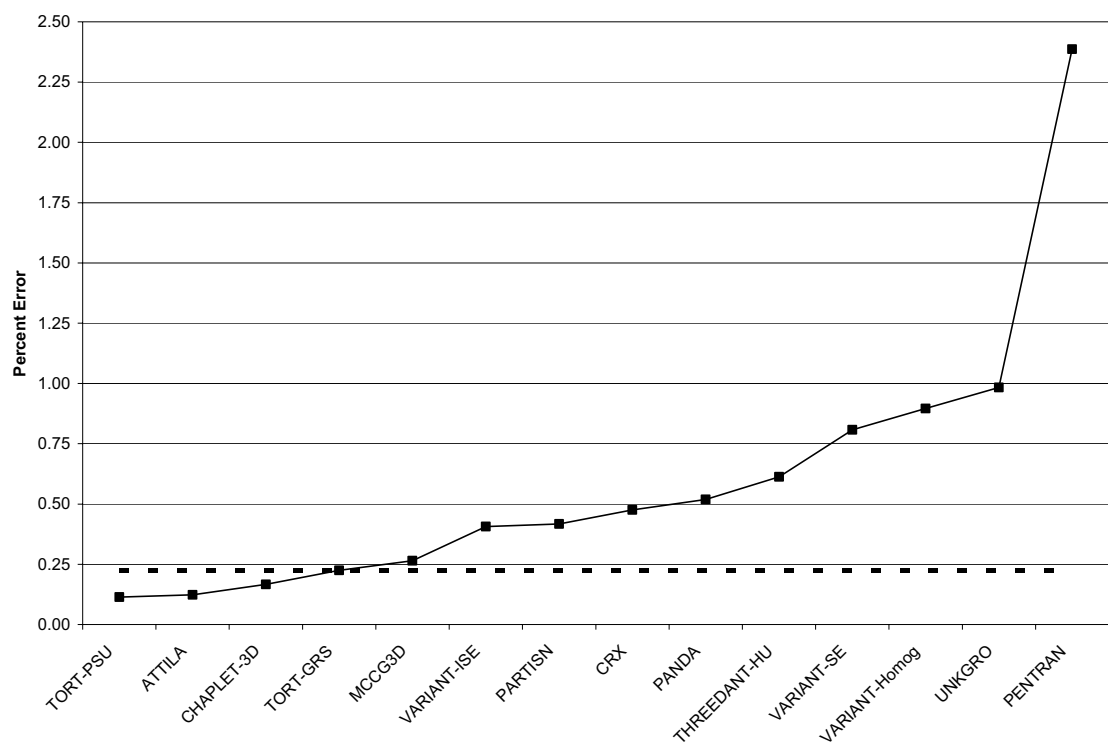


Table 81. Number of fuel pins within the reference confidence intervals for slice #1 of the *Rodded B* configuration

Code names	68%	90%	98%	99.8%
ATTILA	265	426	476	503
CHAPLET-3D	173	299	367	419
CRX	47	96	138	180
MCCG3D	134	269	331	382
PANDA	83	139	187	231
PARTISN	0	3	11	40
PENTRAN	6	15	19	23
THREEDANT-HU	49	95	128	172
TORT-GRS	141	274	373	458
TORT-PSU	272	434	506	528
UNKGRO	38	85	108	133
VARIANT-ISE	75	156	202	261
VARIANT-SE	36	79	114	153
VARIANT-Homog	38	71	95	121

Table 82. Percentage of fuel pins within the reference confidence intervals for slice #1 of the *Rodded B* configuration

Code names	68%	90%	98%	99.8%
ATTILA	49.1	78.9	88.1	93.1
CHAPLET-3D	32.0	55.4	68.0	77.6
CRX	8.7	17.8	25.6	33.3
MCCG3D	24.8	49.8	61.3	70.7
PANDA	15.4	25.7	34.6	42.8
PARTISN	0.0	0.6	2.0	7.4
PENTRAN	1.1	2.8	3.5	4.3
THREEDANT-HU	9.1	17.6	23.7	31.9
TORT-GRS	26.1	50.7	69.1	84.8
TORT-PSU	50.4	80.4	93.7	97.8
UNKGRO	7.0	15.7	20.0	24.6
VARIANT-ISE	13.9	28.9	37.4	48.3
VARIANT-SE	6.7	14.6	21.1	28.3
VARIANT-Homog	7.0	13.1	17.6	22.4

Table 83. Number of fuel pins within the reference confidence intervals for slice #2 of the *Rodded B* configuration

Code names	68%	90%	98%	99.8%
ATTILA	272	441	506	534
CHAPLET-3D	276	451	499	530
CRX	15	63	113	200
MCCG3D	147	248	311	376
PANDA	60	103	133	189
PARTISN	106	183	216	268
PENTRAN	7	12	15	22
THREEDANT-HU	76	157	207	261
TORT-GRS	182	328	424	491
TORT-PSU	211	377	457	512
UNKGRO	58	121	153	204
VARIANT-ISE	106	206	259	331
VARIANT-SE	36	73	94	120
VARIANT-Homog	61	118	164	199

Table 84. Percentage of fuel pins within the reference confidence intervals for slice #2 of the *Rodded B* configuration

Code names	68%	90%	98%	99.8%
ATTILA	50.4	81.7	93.7	98.9
CHAPLET-3D	51.1	83.5	92.4	98.1
CRX	2.8	11.7	20.9	37.0
MCCG3D	27.2	45.9	57.6	69.6
PANDA	11.1	19.1	24.6	35.0
PARTISN	19.6	33.9	40.0	49.6
PENTRAN	1.3	2.2	2.8	4.1
THREEDANT-HU	14.1	29.1	38.3	48.3
TORT-GRS	33.7	60.7	78.5	90.9
TORT-PSU	39.1	69.8	84.6	94.8
UNKGRO	10.7	22.4	28.3	37.8
VARIANT-ISE	19.6	38.1	48.0	61.3
VARIANT-SE	6.7	13.5	17.4	22.2
VARIANT-Homog	11.3	21.9	30.4	36.9

Table 85. Number of fuel pins within the reference confidence intervals for slice #3 of the *Rodded B* configuration

Code names	68%	90%	98%	99.8%
ATTILA	167	340	446	507
CHAPLET-3D	180	349	423	502
CRX	0	1	8	16
MCCG3D	127	235	306	389
PANDA	40	90	115	142
PARTISN	53	96	118	138
PENTRAN	0	3	4	5
THREEDANT-HU	56	129	176	245
TORT-GRS	288	468	515	534
TORT-PSU	262	443	503	529
UNKGRO	51	87	123	160
VARIANT-ISE	0	0	3	10
VARIANT-SE	94	168	219	266
VARIANT-Homog	57	106	130	168

Table 86. Percentage of fuel pins within the reference confidence intervals for slice #3 of the *Rodded B* configuration

Code names	68%	90%	98%	99.8%
ATTILA	30.9	63.0	82.6	93.9
CHAPLET-3D	33.3	64.6	78.3	93.0
CRX	0.0	0.2	1.5	3.0
MCCG3D	23.5	43.5	56.7	72.0
PANDA	7.4	16.7	21.3	26.3
PARTISN	9.8	17.8	21.9	25.6
PENTRAN	0.0	0.6	0.7	0.9
THREEDANT-HU	10.4	23.9	32.6	45.4
TORT-GRS	53.3	86.7	95.4	98.9
TORT-PSU	48.5	82.0	93.1	98.0
UNKGRO	9.4	16.1	22.8	29.6
VARIANT-ISE	0.0	0.0	0.6	1.9
VARIANT-SE	17.4	31.1	40.6	49.3
VARIANT-Homog	10.6	19.6	24.1	31.1

Table 87. Number of fuel pins within the reference confidence intervals for the *Rodded B* Configuration

Code names	68%	90%	98%	99.8%
ATTILA	252	421	481	516
CHAPLET-3D	207	343	410	458
CRX	73	135	180	217
MCCG3D	124	230	291	360
PANDA	65	121	156	188
PARTISN	77	150	189	232
PENTRAN	10	21	34	40
THREEDANT-HU	24	64	79	106
TORT-GRS	121	229	304	387
TORT-PSU	262	426	497	528
UNKGRO	30	64	95	124
VARIANT-ISE	65	146	184	229
VARIANT-SE	41	85	127	147
VARIANT-Homog	39	72	102	127

Table 88. Percentage of fuel pins within the reference confidence intervals for the *Rodded B* Configuration

Code names	68%	90%	98%	99.8%
ATTILA	46.7	78.0	89.1	95.6
CHAPLET-3D	38.3	63.5	75.9	84.8
CRX	13.5	25.0	33.3	40.2
MCCG3D	23.0	42.6	53.9	66.7
PANDA	12.0	22.4	28.9	34.8
PARTISN	14.3	27.8	35.0	43.0
PENTRAN	1.9	3.9	6.3	7.4
THREEDANT-HU	4.4	11.9	14.6	19.6
TORT-GRS	22.4	42.4	56.3	71.7
TORT-PSU	48.5	78.9	92.0	97.8
UNKGRO	5.6	11.9	17.6	23.0
VARIANT-ISE	12.0	27.0	34.1	42.4
VARIANT-SE	7.6	15.7	23.5	27.2
VARIANT-Homog	7.2	13.3	18.9	23.5

Figure 40. Percentage of fuel pins within the *Rodded B* configuration confidence intervals

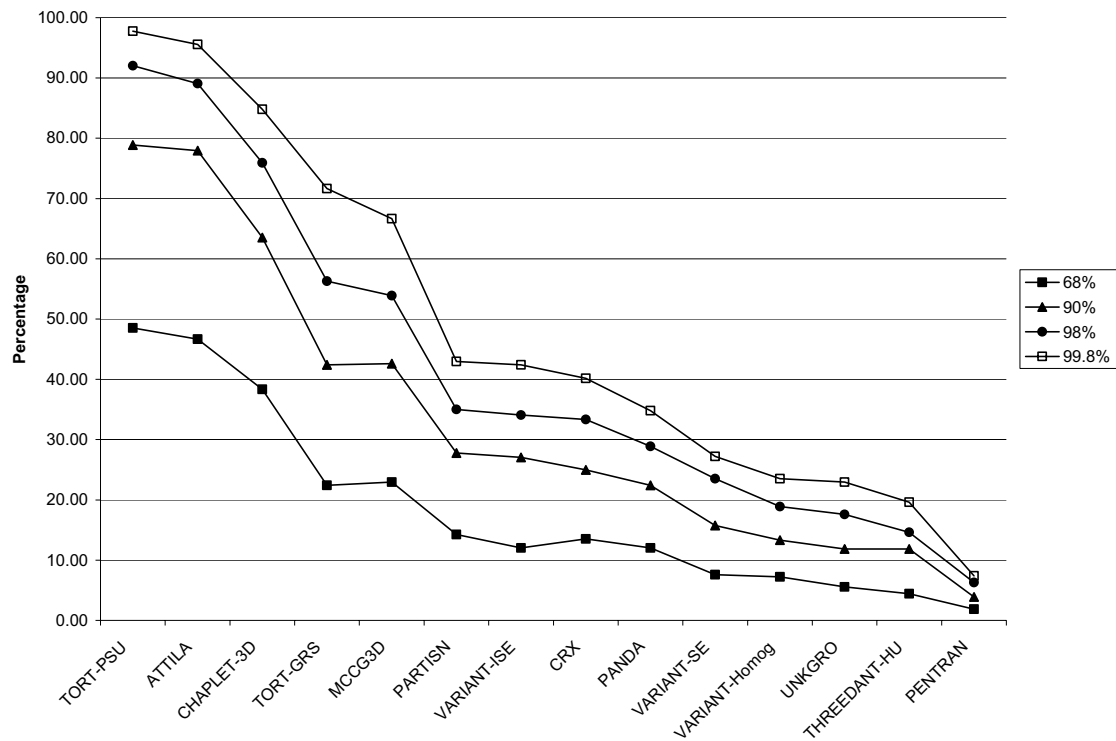


Table 89. Estimated CPU time for the *Rodded B* configuration

Code names	Estimated CPU time
ATTILA	hours
CHAPLET-3D	days
CRX	Not Given
MCCG3D	weeks
PANDA	hours
PARTISN	hours
PENTRAN	hours
THREEDANT-HU	days
TORT-GRS	days
TORT-PSU	days
UNKGRO	days
VARIANT-ISE	days
VARIANT-SE	days
VARIANT-Homog	minutes

Chapter 9
CONCLUSIONS

To test the ability of current deterministic transport codes treating reactor core problems without spatial homogenisation, an OECD/NEA international benchmark problem was undertaken. Compared to the previous benchmark, this 3-D extension case was designed to simulate the three core configurations with the different levels of axial heterogeneity utilising control rods.

A total of twenty participants attempted the benchmark with only twelve completing and submitting a total of thirteen results. A fourteenth result utilising a homogenisation approach to the benchmark was performed by the authors of this benchmark and was included for comparison purposes. All of the participant solutions were compared to a reference Monte Carlo solution. Overall all the results submitted by the participants agree very well with the reference solutions. A majority of the participants obtained solutions that were more than acceptable for typical reactor calculations, showing that modern deterministic transport codes and methods can calculate the flux distribution reasonably well without relying upon spatial homogenisation techniques. As was the case with the original benchmark, the remaining errors in the participant solutions can be attributed to the high order space-angle approximation necessary to solve these particular benchmark problems, which may not be indicative of all heterogeneous problems.

References

1. Lewis, E.E., M.A. Smith, N. Tsoulfanidis, G. Palmiotti, T.A. Taiwo and R.N. Blomquist (2001), “Benchmark for Deterministic 2-D/3-D MOX Fuel Assembly Transport Calculations Without Spatial Homogenization (C5G7MOX)”, NEA/NSC/DOC (2003) 17, September 2001.
2. M.A. Smith, E.E. Lewis and B.C. Na, *Benchmark on Deterministic Transport Calculations Without Spatial Homogenisation – A2-D/3-D Mox Fuel Assembly Benchmark (C5G7 MOX Benchmark)*, OECD/NEA report, NEA/NSC/DOC(2003)16, March 2003.
3. E.E. Lewis, M.A. Smith, and B.C. Na, Guest Editors, Progress in Nuclear Energy, “OECD/NEA Benchmark on (MOX-fuelled Core) Transport Calculations without Spatial Homogenisation,” Volume 45, Issues 2-4, 2004.
4. M.A. Smith, G. Palmiotti, et al., “Benchmark Specification for Deterministic MOX Fuel Assembly Transport Calculations Without Spatial Homogenization (3-D extension C5G7 MOX),” OECD/NEA document, NEA/NSC/DOC(2003)6, April 30, 2003.
5. Kobayashi, K., Sugimura, N., and Nagaya, Y., *3-D Radiation Transport Benchmarks for Simple Geometries with Void Regions*, OECD/NEA report, ISBN 92-64-18274-8, November 2000.
6. Kobayashi, K. and Sartori, E., Guest Editors, Progress in Nuclear Energy, “3-D Radiation Transport Benchmarks for Simple Geometries with Void Regions,” Volume 39, Number 2, 2001.
7. Cavarec, C., et al., “The OECD/NEA Benchmark Calculations of Power Distributions within Assemblies,” Electricity de France, Sept. 1994.
8. Cathalau, J.C. Lefebvre, J.P. West, “Proposal for a Second Stage of the Benchmark on Power Distributions within Assemblies,” An earlier version of the published OECD/NEA Benchmark, April 1996.
9. G. Marleau, A. Hébert, R. Roy, “A User’s Guide for DRAGON”, École Polytechnique de Montréal, December 1997.
10. Briesmeister, J.F., XTM, MCNP™-A General Monte Carlo N-Particle Transport code. LOS ALAMOS National Laboratory LA-12625-M, March 1997.

APPENDIX A

**Benchmark Specification for
Deterministic MOX Fuel Assembly
Transport Calculations
Without Spatial Homogenisation
(3-D Extension C5G7 MOX)**

E.E. Lewis
Northwestern University
Department of Mechanical Engineering
Evanston, Illinois 60208

N. Tsoulfanidis
University of Missouri, Rolla
Department of Nuclear Engineering
Rolla, Missouri 65409

M.A. Smith, G. Palmiotti, & T.A. Taiwo
Argonne National Laboratory
9700 South Cass Avenue
Argonne, Illinois 60439

Outline

- Benchmark specification
- Appendix 1: Description of computational model used to obtain benchmark solutions
- Appendix 2: Results to be reported

Problem Specification

We hereby propose the following extension of the three-dimensional calculations of reference 1. This modification of the geometry is to provide a more challenging test of present day three-dimensional methods' abilities to handle spatial heterogeneities while still allowing participants to investigate sensitivities to spatial and angular approximations implemented in their codes. There are three significant changes that have been made to the three-dimensional geometry. First, the height of the geometry is reduced to 64.26 cm from 192.78 cm to allow participants to put the entire problem domain into memory and reduce computational times without trivialising the problem. Second, the control rod guide tubes and fission chamber are defined in the upper axial reflector. Third, a control rod macroscopic cross-section definition is introduced and is used to replace the control rod guide composition, in certain parts of the reactor. Figure 1 gives the new dimensions of the three-dimensional geometry where the pin-cell (Figure 2) and assembly layout (Figure 3) of reference 1 have been maintained. In Figure 2, the side length of the fuel-pin cell is 1.26 cm and the radius of the cylinder is 0.54 cm. It is important to note that in Figure 1 the fuel assemblies have been split into three axial zones. The intent is to allow each participant to provide fission rates for each pin-cell in each zone and from these the fission rate for each fuel pin is obtained.

We have chosen to define three calculational problems named *Unrodded*, *Rodded A*, and *Rodded B*. We begin by defining the *Unrodded* configuration detailed by Figure 4. In this configuration control rod clusters (one cluster for each assembly) are inserted into the upper axial water reflector as indicated by the shading in Figure 4. Figure 5 shows a slice in the radial direction through the upper axial reflector and should more clearly show the layout of the control rod clusters and fission chamber in the axial reflector region. It is important to note that the fission chambers and control rods are present in the axial reflector region and thus should be modelled.

The second configuration, *Rodded A*, takes the *Unrodded* configuration as its starting position. In this configuration a control rod cluster is inserted 1/3 of the way into the inner UO₂ assembly as indicated by the shading in Figure 6. Similarly, the *Rodded B* configuration also takes the *Unrodded* configuration as its starting point. In this configuration, however, control rod clusters are inserted 2/3 of the way into the inner UO₂ assembly and 1/3 of the way into both MOX assemblies as indicated by the shading in Figure 6.

Table 1 provides the new seven group, transport corrected, isotropic scattering cross-sections for the control rod composition. Similar to the previous approach, these seven-group cross-sections were obtained using the UO₂ pin cell spectrum. Tables 2a to 2g provide seven group, transport corrected, isotropic scattering cross-sections for UO₂, the three enrichments of MOX, the guide tubes and fission chamber, and the moderator described in the problem specification.

Problem Objectives

are to calculate:

- (a) The eigenvalue
- (b) The fission rates in each pin over each axial slice (34 x 34 x 3 total numbers)

Reference Seven-group Monte Carlo Eigenvalue Answers

Approximate eigenvalue for the *Unrodded* configuration: 1.14

Approximate eigenvalue for the *Rodded A* configuration: 1.13

Approximate eigenvalue for the *Rodded B* configuration: 1.08

Comments

We are well aware that the homogenisation and group collapse introduced some error into the cross-sections. Our object, however, is not to examine the validity of the group collapse, or fuel-cladding homogenisation, instead, it is to provide a reasonable set of multigroup cross-sections in which there is no fuel-coolant homogenisation. Moreover, for brevity in data input we utilize a single set of water cross-section in both the UO₂ and MOX assemblies and in the reflector. The geometry specification combined with these transport-corrected, isotropic scattering, seven-group cross-sections provides a basis for comparing the accuracy of deterministic transport codes with reference seven-group Monte Carlo solutions. Each reference solution required approximately one week of CPU time on a Sun 60. These solutions may also serve to test the validity of spatial fuel-coolant homogenisation procedures at the fuel-pin cell and/or at the fuel assembly level.

References

1. E.E. Lewis, G. Palmiotti, T.A. Taiwo, M.A. Smith, and N. Tsoufianidis, Benchmark Specification for Deterministic 2-D/3-D MOX Fuel Assembly Transport Calculations without Spatial Homogenisation (C5G7 MOX), NEA/NSC/DOC(2001)4, March 28, 2001.
2. Cavarec, C., et al., “The OECD/NEA Benchmark Calculations of Power Distributions within Assemblies,” Electricity de France, Sept. 1994.
3. S. Cathalau, J.C. Lefebvre, J.P. West, “Proposal for a Second Stage of the Benchmark on Power Distributions within Assemblies,” An earlier version of the published OECD/NEA Benchmark, April 1996.
4. G. Marleau, A. Hébert, R. Roy, “A User’s Guide for DRAGON”, École Polytechnique de Montréal, December 1997

Figure 1. Modified three-dimensional configuration for the benchmark problem

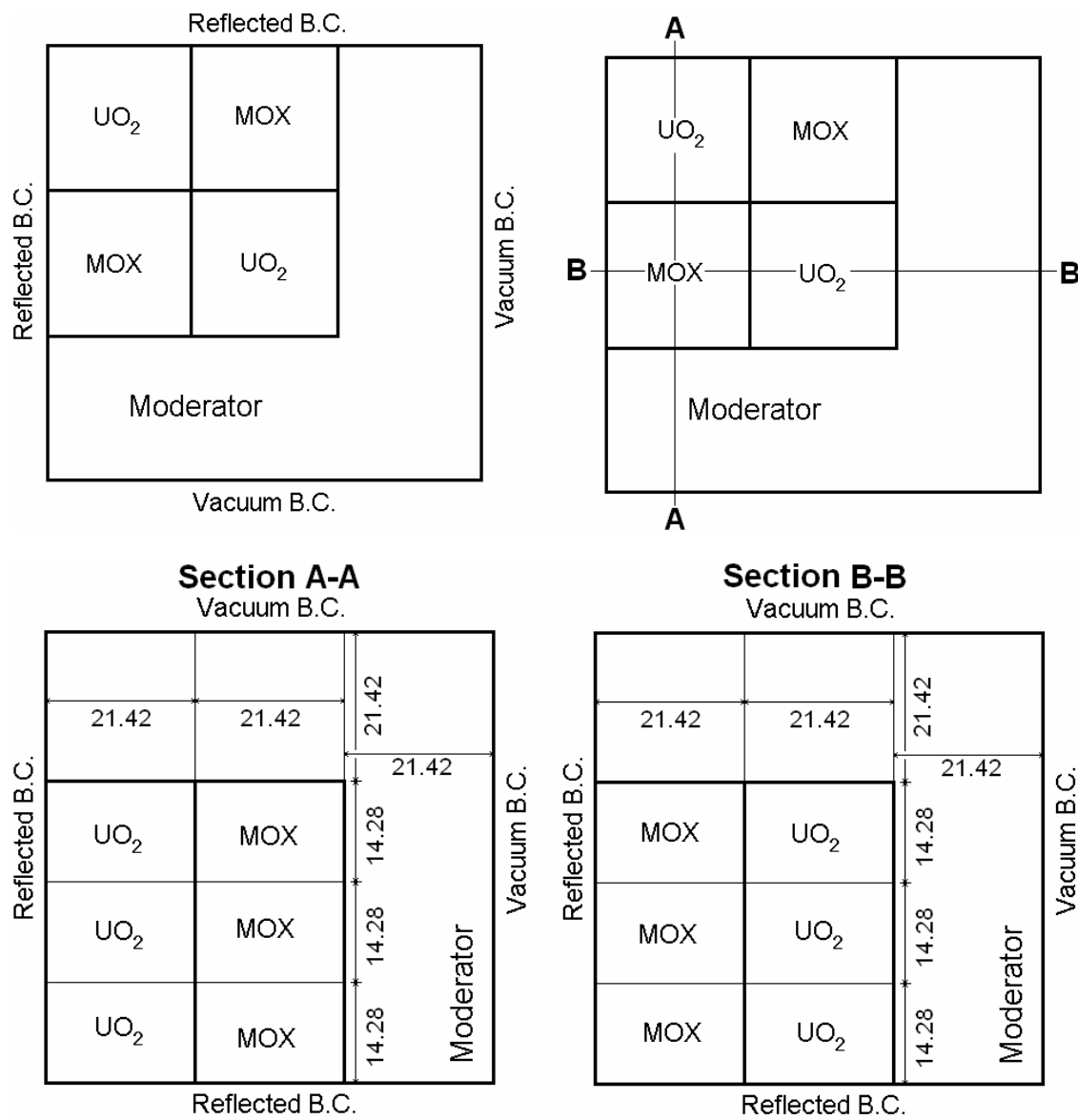


Figure 2. Fuel pin layout

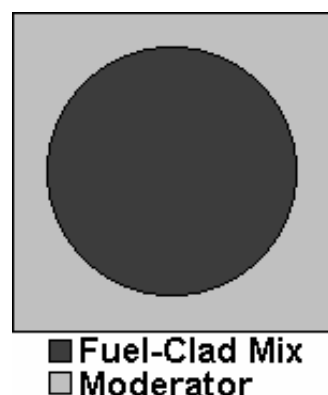


Figure 3. Benchmark fuel pin compositions and numbering scheme

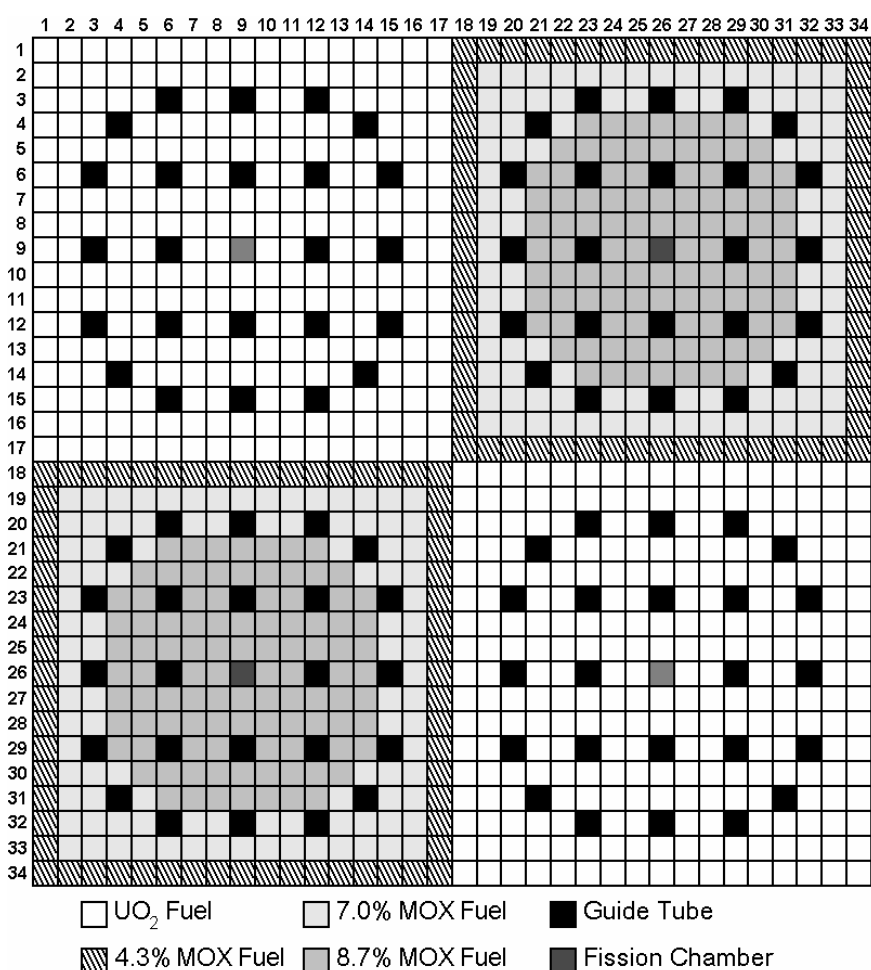


Figure 4. Three-dimensional geometry for the *Unrodded* configuration

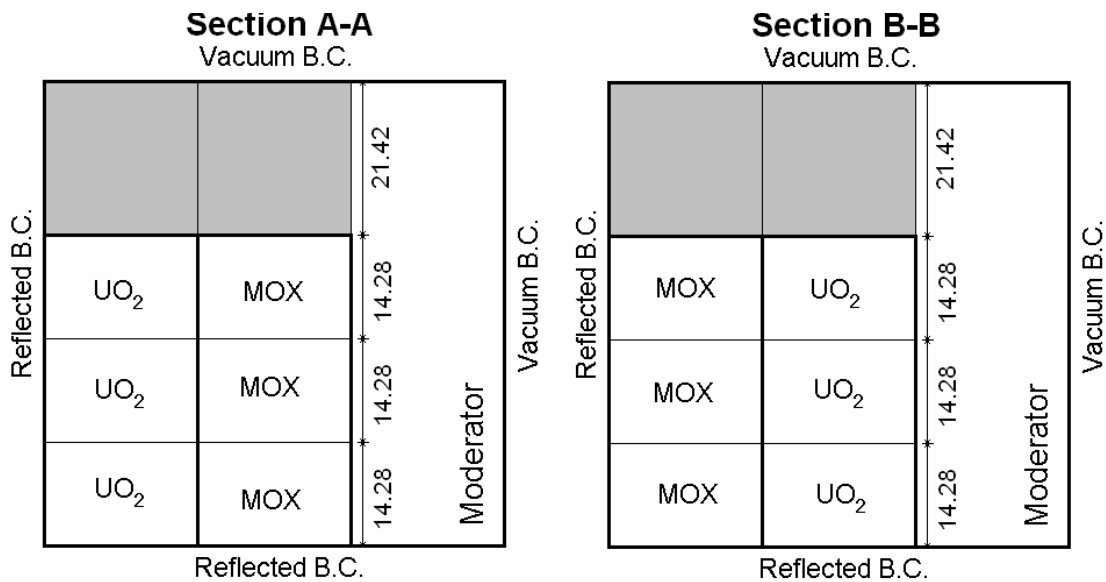


Figure 5. Geometry configuration for the upper axial water reflector

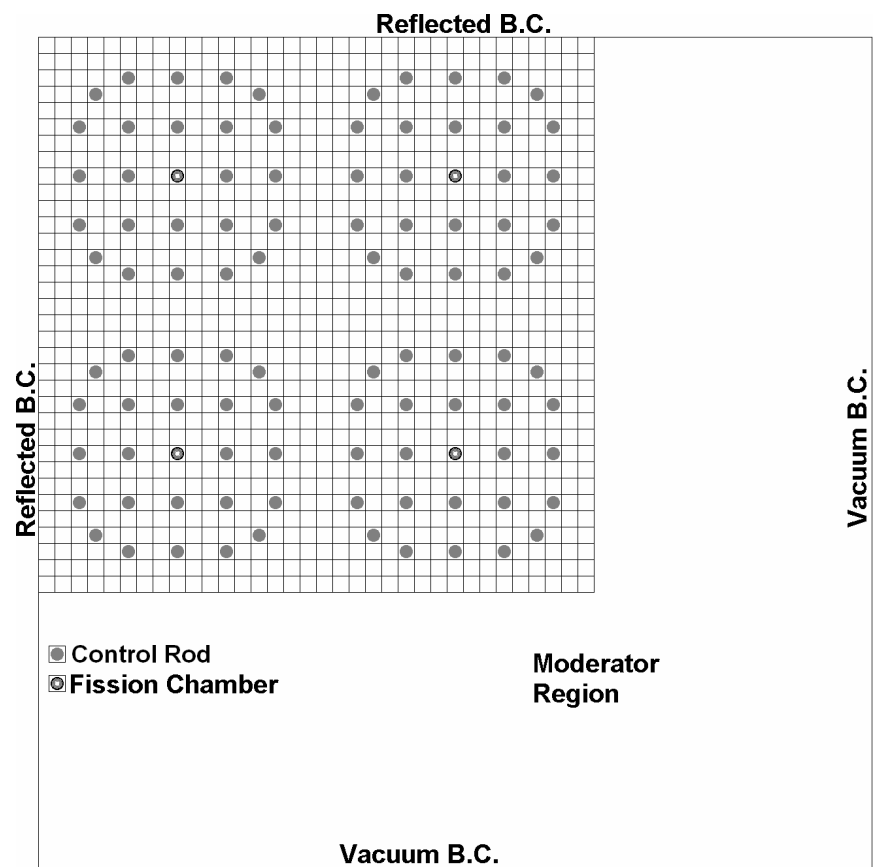


Figure 6. Three-dimensional geometry for the *Rodded A* configuration

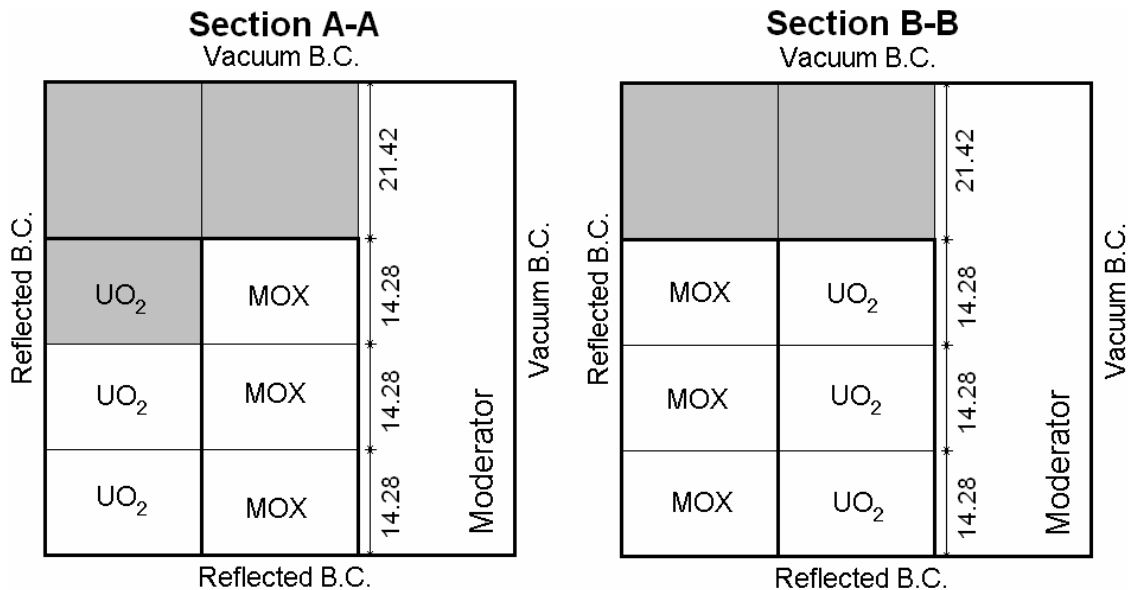


Figure 7. Three-dimensional geometry for the *Rodded B* configuration

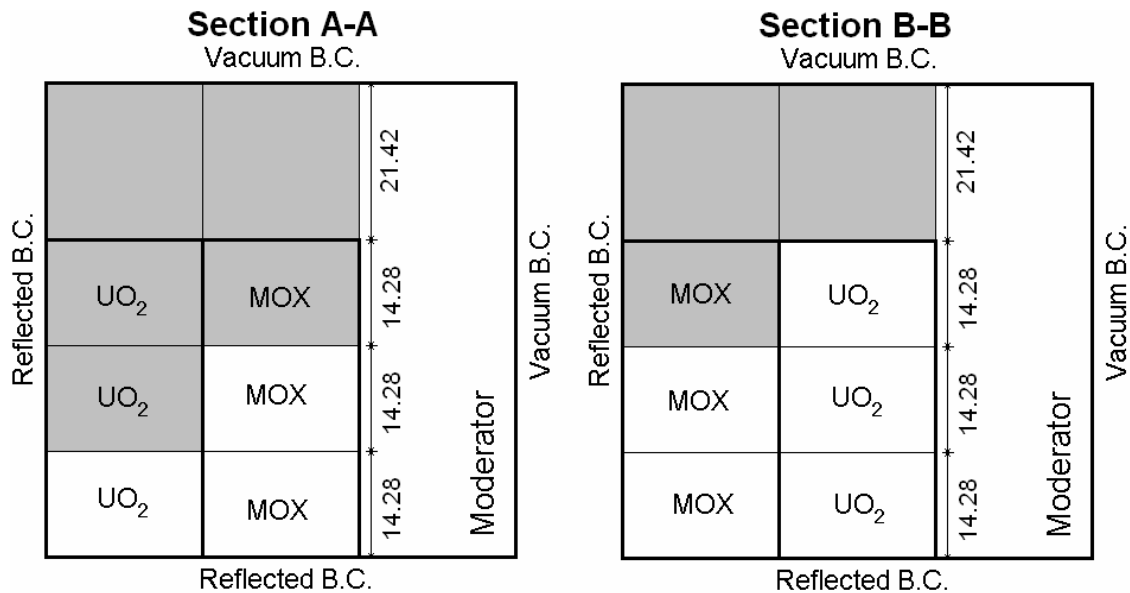


Table 1. Control rod macroscopic cross-sections

	Transport Cross-section	Absorption Cross-section	Capture Cross-section
Group 1	2.16768E-01	1.70490E-03	1.70490E-03
Group 2	4.80098E-01	8.36224E-03	8.36224E-03
Group 3	8.86369E-01	8.37901E-02	8.37901E-02
Group 4	9.70009E-01	3.97797E-01	3.97797E-01
Group 5	9.10482E-01	6.98763E-01	6.98763E-01
Group 6	1.13775E+00	9.29508E-01	9.29508E-01
Group 7	1.84048E+00	1.17836E+00	1.17836E+00

Scattering block

Group 1	1.70563E-01	4.44012E-02	9.83670E-05	1.27786E-07	0.00000E+00	0.00000E+00	0.00000E+00
Group 2	0.00000E+00	4.71050E-01	6.85480E-04	3.91395E-10	0.00000E+00	0.00000E+00	0.00000E+00
Group 3	0.00000E+00	0.00000E+00	8.01859E-01	7.20132E-04	0.00000E+00	0.00000E+00	0.00000E+00
Group 4	0.00000E+00	0.00000E+00	0.00000E+00	5.70752E-01	1.46015E-03	0.00000E+00	0.00000E+00
Group 5	0.00000E+00	0.00000E+00	0.00000E+00	6.55562E-05	2.07838E-01	3.81486E-03	3.69760E-09
Group 6	0.00000E+00	0.00000E+00	0.00000E+00	0.00000E+00	1.02427E-03	2.02465E-01	4.75290E-03
Group 7	0.00000E+00	0.00000E+00	0.00000E+00	0.00000E+00	0.00000E+00	3.53043E-03	6.58597E-01

Table 2a. UO₂ fuel-clad macroscopic cross-sections

	Transport Cross-section	Absorption Cross-section	Capture Cross-section	Fission Cross-section	Nu	Chi
Group 1	1.77949E-01	8.02480E-03	8.12740E-04	7.21206E-03	2.78145E+00	5.87910E-01
Group 2	3.29805E-01	3.71740E-03	2.89810E-03	8.19301E-04	2.47443E+00	4.11760E-01
Group 3	4.80388E-01	2.67690E-02	2.03158E-02	6.45320E-03	2.43383E+00	3.39060E-04
Group 4	5.54367E-01	9.62360E-02	7.76712E-02	1.85648E-02	2.43380E+00	1.17610E-07
Group 5	3.11801E-01	3.00200E-02	1.22116E-02	1.78084E-02	2.43380E+00	0.00000E+00
Group 6	3.95168E-01	1.11260E-01	2.82252E-02	8.30348E-02	2.43380E+00	0.00000E+00
Group 7	5.64406E-01	2.82780E-01	6.67760E-02	2.16004E-01	2.43380E+00	0.00000E+00

Scattering block

	to Group 1	to Group 2	to Group 3	to Group 4	to Group 5	to Group 6	to Group 7
Group 1	1.27537E-01	4.23780E-02	9.43740E-06	5.51630E-09	0.00000E+00	0.00000E+00	0.00000E+00
Group 2	0.00000E+00	3.24456E-01	1.63140E-03	3.14270E-09	0.00000E+00	0.00000E+00	0.00000E+00
Group 3	0.00000E+00	0.00000E+00	4.50940E-01	2.67920E-03	0.00000E+00	0.00000E+00	0.00000E+00
Group 4	0.00000E+00	0.00000E+00	0.00000E+00	4.52565E-01	5.56640E-03	0.00000E+00	0.00000E+00
Group 5	0.00000E+00	0.00000E+00	0.00000E+00	1.25250E-04	2.71401E-01	1.02550E-02	1.00210E-08
Group 6	0.00000E+00	0.00000E+00	0.00000E+00	0.00000E+00	1.29680E-03	2.65802E-01	1.68090E-02
Group 7	0.00000E+00	0.00000E+00	0.00000E+00	0.00000E+00	0.00000E+00	8.54580E-03	2.73080E-01

Table 2b. 4.3% MOX fuel-clad macroscopic cross-sections

	Transport Cross-section	Absorption Cross-section	Capture Cross-section	Fission Cross-section	Nu	Chi
Group 1	1.78731E-01	8.43390E-03	8.06860E-04	7.62704E-03	2.85209E+00	5.87910E-01
Group 2	3.30849E-01	3.75770E-03	2.88080E-03	8.76898E-04	2.89099E+00	4.11760E-01
Group 3	4.83772E-01	2.79700E-02	2.22717E-02	5.69835E-03	2.85486E+00	3.39060E-04
Group 4	5.66922E-01	1.04210E-01	8.13228E-02	2.28872E-02	2.86073E+00	1.17610E-07
Group 5	4.26227E-01	1.39940E-01	1.29177E-01	1.07635E-02	2.85447E+00	0.00000E+00
Group 6	6.78997E-01	4.09180E-01	1.76423E-01	2.32757E-01	2.86415E+00	0.00000E+00
Group 7	6.82852E-01	4.09350E-01	1.60382E-01	2.48968E-01	2.86780E+00	0.00000E+00

Scattering block

	to Group 1	to Group 2	to Group 3	to Group 4	to Group 5	to Group 6	to Group 7
Group 1	1.28876E-01	4.14130E-02	8.22900E-06	5.04050E-09	0.00000E+00	0.00000E+00	0.00000E+00
Group 2	0.00000E+00	3.25452E-01	1.63950E-03	1.59820E-09	0.00000E+00	0.00000E+00	0.00000E+00
Group 3	0.00000E+00	0.00000E+00	4.53188E-01	2.61420E-03	0.00000E+00	0.00000E+00	0.00000E+00
Group 4	0.00000E+00	0.00000E+00	0.00000E+00	4.57173E-01	5.53940E-03	0.00000E+00	0.00000E+00
Group 5	0.00000E+00	0.00000E+00	0.00000E+00	1.60460E-04	2.76814E-01	9.31270E-03	9.16560E-09
Group 6	0.00000E+00	0.00000E+00	0.00000E+00	0.00000E+00	2.00510E-03	2.52962E-01	1.48500E-02
Group 7	0.00000E+00	0.00000E+00	0.00000E+00	0.00000E+00	0.00000E+00	8.49480E-03	2.65007E-01

Table 2c. 7.0% MOX fuel-clad macroscopic cross-sections

	Transport Cross-section	Absorption Cross-section	Capture Cross-section	Fission Cross-section	Nu	Chi
Group 1	1.81323E-01	9.06570E-03	8.11240E-04	8.25446E-03	2.88498E+00	5.87910E-01
Group 2	3.34368E-01	4.29670E-03	2.97105E-03	1.32565E-03	2.91079E+00	4.11760E-01
Group 3	4.93785E-01	3.28810E-02	2.44594E-02	8.42156E-03	2.86574E+00	3.39060E-04
Group 4	5.91216E-01	1.22030E-01	8.91570E-02	3.28730E-02	2.87063E+00	1.17610E-07
Group 5	4.74198E-01	1.82980E-01	1.67016E-01	1.59636E-02	2.86714E+00	0.00000E+00
Group 6	8.33601E-01	5.68460E-01	2.44666E-01	3.23794E-01	2.86658E+00	0.00000E+00
Group 7	8.53603E-01	5.85210E-01	2.22407E-01	3.62803E-01	2.87539E+00	0.00000E+00

Scattering block

	to Group 1	to Group 2	to Group 3	to Group 4	to Group 5	to Group 6	to Group 7
Group 1	1.30457E-01	4.17920E-02	8.51050E-06	5.13290E-09	0.00000E+00	0.00000E+00	0.00000E+00
Group 2	0.00000E+00	3.28428E-01	1.64360E-03	2.20170E-09	0.00000E+00	0.00000E+00	0.00000E+00
Group 3	0.00000E+00	0.00000E+00	4.58371E-01	2.53310E-03	0.00000E+00	0.00000E+00	0.00000E+00
Group 4	0.00000E+00	0.00000E+00	0.00000E+00	4.63709E-01	5.47660E-03	0.00000E+00	0.00000E+00
Group 5	0.00000E+00	0.00000E+00	0.00000E+00	1.76190E-04	2.82313E-01	8.72890E-03	9.00160E-09
Group 6	0.00000E+00	0.00000E+00	0.00000E+00	0.00000E+00	2.27600E-03	2.49751E-01	1.31140E-02
Group 7	0.00000E+00	0.00000E+00	0.00000E+00	0.00000E+00	0.00000E+00	8.86450E-03	2.59529E-01

Table 2d. 8.7% MOX fuel-clad macroscopic cross-sections

	Transport Cross-section	Absorption Cross-section	Capture Cross-section	Fission Cross-section	Nu	Chi
Group 1	1.83045E-01	9.48620E-03	8.14110E-04	8.67209E-03	2.90426E+00	5.87910E-01
Group 2	3.36705E-01	4.65560E-03	3.03134E-03	1.62426E-03	2.91795E+00	4.11760E-01
Group 3	5.00507E-01	3.62400E-02	2.59684E-02	1.02716E-02	2.86986E+00	3.39060E-04
Group 4	6.06174E-01	1.32720E-01	9.36753E-02	3.90447E-02	2.87491E+00	1.17610E-07
Group 5	5.02754E-01	2.08400E-01	1.89142E-01	1.92576E-02	2.87175E+00	0.00000E+00
Group 6	9.21028E-01	6.58700E-01	2.83812E-01	3.74888E-01	2.86752E+00	0.00000E+00
Group 7	9.55231E-01	6.90170E-01	2.59571E-01	4.30599E-01	2.87808E+00	0.00000E+00

Scattering block

	to Group 1	to Group 2	to Group 3	to Group 4	to Group 5	to Group 6	to Group 7
Group 1	1.31504E-01	4.20460E-02	8.69720E-06	5.19380E-09	0.00000E+00	0.00000E+00	0.00000E+00
Group 2	0.00000E+00	3.30403E-01	1.64630E-03	2.60060E-09	0.00000E+00	0.00000E+00	0.00000E+00
Group 3	0.00000E+00	0.00000E+00	4.61792E-01	2.47490E-03	0.00000E+00	0.00000E+00	0.00000E+00
Group 4	0.00000E+00	0.00000E+00	0.00000E+00	4.68021E-01	5.43300E-03	0.00000E+00	0.00000E+00
Group 5	0.00000E+00	0.00000E+00	0.00000E+00	1.85970E-04	2.85771E-01	8.39730E-03	8.92800E-09
Group 6	0.00000E+00	0.00000E+00	0.00000E+00	0.00000E+00	2.39160E-03	2.47614E-01	1.23220E-02
Group 7	0.00000E+00	0.00000E+00	0.00000E+00	0.00000E+00	0.00000E+00	8.96810E-03	2.56093E-01

Table 2e. Fission chamber macroscopic cross-sections

	Transport Cross-section	Absorption Cross-section	Capture Cross-section	Fission Cross-section	Nu	Chi
Group 1	1.26032E-01	5.11320E-04	5.11315E-04	4.79002E-09	2.76283E+00	5.87910E-01
Group 2	2.93160E-01	7.58130E-05	7.58072E-05	5.82564E-09	2.46239E+00	4.11760E-01
Group 3	2.84250E-01	3.16430E-04	3.15966E-04	4.63719E-07	2.43380E+00	3.39060E-04
Group 4	2.81020E-01	1.16750E-03	1.16226E-03	5.24406E-06	2.43380E+00	1.17610E-07
Group 5	3.34460E-01	3.39770E-03	3.39755E-03	1.45390E-07	2.43380E+00	0.00000E+00
Group 6	5.65640E-01	9.18860E-03	9.18789E-03	7.14972E-07	2.43380E+00	0.00000E+00
Group 7	1.17214E+00	2.32440E-02	2.32419E-02	2.08041E-06	2.43380E+00	0.00000E+00

Scattering block

	to Group 1	to Group 2	to Group 3	to Group 4	to Group 5	to Group 6	to Group 7
Group 1	6.61659E-02	5.90700E-02	2.83340E-04	1.46220E-06	2.06420E-08	0.00000E+00	0.00000E+00
Group 2	0.00000E+00	2.40377E-01	5.24350E-02	2.49900E-04	1.92390E-05	2.98750E-06	4.21400E-07
Group 3	0.00000E+00	0.00000E+00	1.83425E-01	9.22880E-02	6.93650E-03	1.07900E-03	2.05430E-04
Group 4	0.00000E+00	0.00000E+00	0.00000E+00	7.90769E-02	1.69990E-01	2.58600E-02	4.92560E-03
Group 5	0.00000E+00	0.00000E+00	0.00000E+00	3.73400E-05	9.97570E-02	2.06790E-01	2.44780E-02
Group 6	0.00000E+00	0.00000E+00	0.00000E+00	0.00000E+00	9.17420E-04	3.16774E-01	2.38760E-01
Group 7	0.00000E+00	0.00000E+00	0.00000E+00	0.00000E+00	0.00000E+00	4.97930E-02	1.09910E+00

Table 2f. Guide tube macroscopic cross-sections

	Transport Cross-section	Absorption Cross-section	Capture Cross-section
Group 1	1.26032E-01	5.11320E-04	5.11320E-04
Group 2	2.93160E-01	7.58010E-05	7.58010E-05
Group 3	2.84240E-01	3.15720E-04	3.15720E-04
Group 4	2.80960E-01	1.15820E-03	1.15820E-03
Group 5	3.34440E-01	3.39750E-03	3.39750E-03
Group 6	5.65640E-01	9.18780E-03	9.18780E-03
Group 7	1.17215E+00	2.32420E-02	2.32420E-02

Scattering block

	to Group 1	to Group 2	to Group 3	to Group 4	to Group 5	to Group 6	to Group 7
Group 1	6.61659E-02	5.90700E-02	2.83340E-04	1.46220E-06	2.06420E-08	0.00000E+00	0.00000E+00
Group 2	0.00000E+00	2.40377E-01	5.24350E-02	2.49900E-04	1.92390E-05	2.98750E-06	4.21400E-07
Group 3	0.00000E+00	0.00000E+00	1.83297E-01	9.23970E-02	6.94460E-03	1.08030E-03	2.05670E-04
Group 4	0.00000E+00	0.00000E+00	0.00000E+00	7.88511E-02	1.70140E-01	2.58810E-02	4.92970E-03
Group 5	0.00000E+00	0.00000E+00	0.00000E+00	3.73330E-05	9.97372E-02	2.06790E-01	2.44780E-02
Group 6	0.00000E+00	0.00000E+00	0.00000E+00	0.00000E+00	9.17260E-04	3.16765E-01	2.38770E-01
Group 7	0.00000E+00	0.00000E+00	0.00000E+00	0.00000E+00	0.00000E+00	4.97920E-02	1.09912E+00

Table 2g. Moderator macroscopic cross-sections

	Transport Cross-section	Absorption Cross-section	Capture Cross-section
Group 1	1.59206E-01	6.01050E-04	6.01050E-04
Group 2	4.12970E-01	1.57930E-05	1.57930E-05
Group 3	5.90310E-01	3.37160E-04	3.37160E-04
Group 4	5.84350E-01	1.94060E-03	1.94060E-03
Group 5	7.18000E-01	5.74160E-03	5.74160E-03
Group 6	1.25445E+00	1.50010E-02	1.50010E-02
Group 7	2.65038E+00	3.72390E-02	3.72390E-02

Scattering block

	to Group 1	to Group 2	to Group 3	to Group 4	to Group 5	to Group 6	to Group 7
Group 1	4.44777E-02	1.13400E-01	7.23470E-04	3.74990E-06	5.31840E-08	0.00000E+00	0.00000E+00
Group 2	0.00000E+00	2.82334E-01	1.29940E-01	6.23400E-04	4.80020E-05	7.44860E-06	1.04550E-06
Group 3	0.00000E+00	0.00000E+00	3.45256E-01	2.24570E-01	1.69990E-02	2.64430E-03	5.03440E-04
Group 4	0.00000E+00	0.00000E+00	0.00000E+00	9.10284E-02	4.15510E-01	6.37320E-02	1.21390E-02
Group 5	0.00000E+00	0.00000E+00	0.00000E+00	7.14370E-05	1.39138E-01	5.11820E-01	6.12290E-02
Group 6	0.00000E+00	0.00000E+00	0.00000E+00	0.00000E+00	2.21570E-03	6.99913E-01	5.37320E-01
Group 7	0.00000E+00	0.00000E+00	0.00000E+00	0.00000E+00	0.00000E+00	1.32440E-01	2.48070E+00

Appendix A.1

DESCRIPTION OF COMPUTATIONAL MODEL USED TO OBTAIN BENCHMARK SOLUTIONS (preferred format is WORD)

We would like to have as detailed a description as you are able to provide on your treatment of the space-angle variables and the procedures by which you carried out the calculations, (but limited to 5 pages). Please include the following:

1. Name of participant(s)
2. Establishment(s)
3. Name of code system(s) used
4. Computational method used (e.g. S_N , P_N , collision probability, characteristic, etc.)
5. Type and level of angular approximation (e.g. S_8 , P_7 , number of characteristic angles, etc.)
6. Type and level of spatial discretisation (e.g. linear-triangular finite elements, flat source region collision probabilities, etc.). Provide number of mesh points, source regions, tracking pitch etc. per lattice cell. If possible include a drawing or diagram of the spatial mesh for one lattice cell
7. Convergence
 - a. eigenvalue (at least 10 E-5)
 - b. pointwise (e.g. flux, fission source, etc.)
8. Machine on which the calculations were performed and (if possible) CPU time
9. Other assumptions and characteristics, comments useful for interpreting correctly the results

APPENDIX B

Calculation Details Provided by the Participants

1. Gesellschaft fuer Anlagen- und Reaktorsicherheit (GRS) mbH, Germany

Participants: A. Seubert, S. Langenbuch and W. Zwermann

Code used: TORT (S_N)

Name of participants

A. Seubert, S. Langenbuch and W. Zwermann

Establishment

Gesellschaft für Anlagen- und Reaktorsicherheit (GRS) mbH, Forschungsinstitute, D-85748 Garching, Germany

Name of code system used

TORT 3.2 from the DOORS package distributed by NEA data bank.

Computational method used

Discrete ordinates S_N transport method using cartesian finite differences and level symmetric quadratures.

Type and level of angular approximation

S_{16} , resulting in 320 discrete angular directions in three spatial dimensions. For comparison, calculations using the lower-order directional quadrature sets S_8 and S_4 , comprising 96 and 32 discrete directions, respectively, have also been performed.

Type and level of spatial discretisation

For the spatial discretisation of the problem region, a regular spatial mesh is used as described below.

Discretisation within the x-y plane:

The circular cross-section of the fuel clad mix is approximated by a 5x5 step function, resulting in a 7x7 cartesian nodalisation of each fuel pin cell as shown in Figure 1 (a). Two constraints are imposed on the shape of this step function: First, the circular cross-section area must be preserved. Second, the step function has to be chosen such that the sum of the areas above and below the circle is minimised. This approximation is also used for the control rod and guide tube pin cells. For the moderator region, a coarser mesh grid is applied with its width equal to the fuel pitch of 1.26 cm. Special attention is paid to the interface between the fuel region and the surrounding reflector region where the mesh size is gradually increased in the direction towards boundary. Guided by the regular spatial mesh, in x-direction this is done by constructing the following mesh grid: 5x7, 3x7 and 1x7. In y-direction, it is just the other way round. This is illustrated in Figure 1 (b).

Discretisation in z-direction:

Generally, a mesh size of 3.570 cm is used. For an accurate modelling of interfaces between adjacent axial slices, if different material compositions are facing each other there, the outermost mesh of both slices is halvened to 1.785 cm as indicated in Figure 2. For the *Unrodded* configuration there is only one interface, whereas for the *Rodded A* and the *Rodded B* configurations there are two and three interfaces, respectively (cf. Figure 2). As shown in Figure 2, close to the interface two nodes of the fine mesh size (1.785 cm) are used to take account of the different material compositions of the two adjacent axial slices.

Using the spatial discretisation described above, the overall number of mesh points for the three control rod configurations are as follows:

$261 \cdot 261 \cdot 20 = 1\ 362\ 420$ nodes for the *Unrodded* configuration, $261 \cdot 261 \cdot 22 = 1\ 498\ 662$ nodes for the *Rodded A* case and $261 \cdot 261 \cdot 24 = 1\ 634\ 904$ nodes for the *Rodded B* configuration.

Convergence

The convergence criterions used are:

Eigenvalue: $1.0 \cdot 10^{-5}$

Fission source: $5.0 \cdot 10^{-6}$

Pointwise fluxes: $1.0 \cdot 10^{-6}$

Machines on which the calculations were performed

Compaq XP 1000 Professional Workstation 500 MHz (*Rodded B* calculation) and Intel Pentium 4 based Personal Computer 2.4 GHz (*UnRodded And Rodded A* calculation).

Fig 1. Schematic drawing of (a) the 7x7 pin cell nodalisation and (b) the mesh grid of the moderator region (denoted by a light-gray shading) close to the reactor core

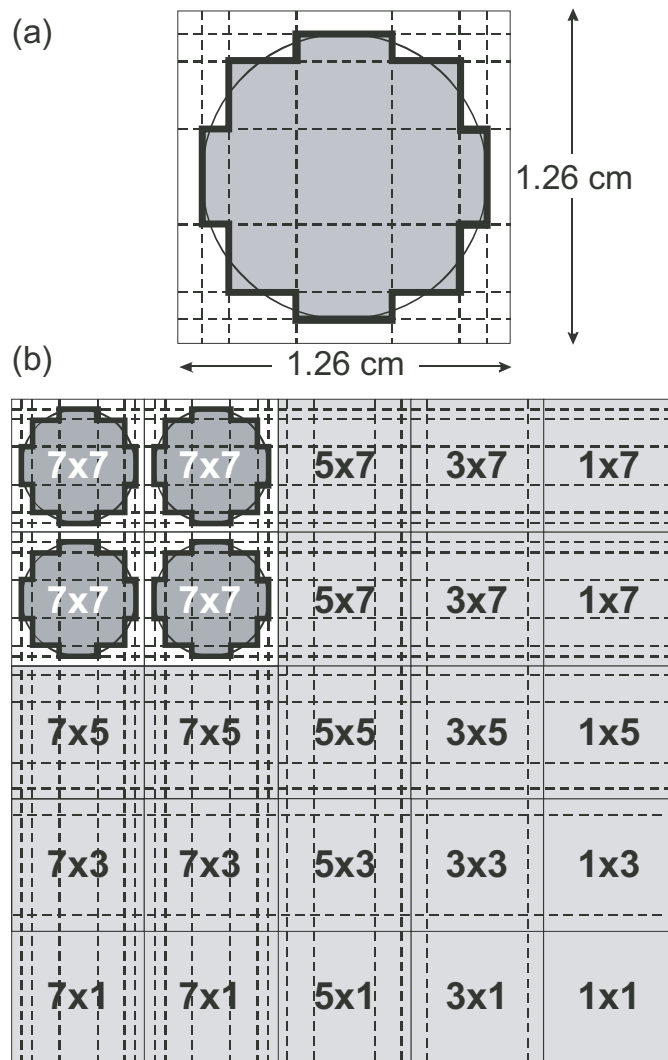
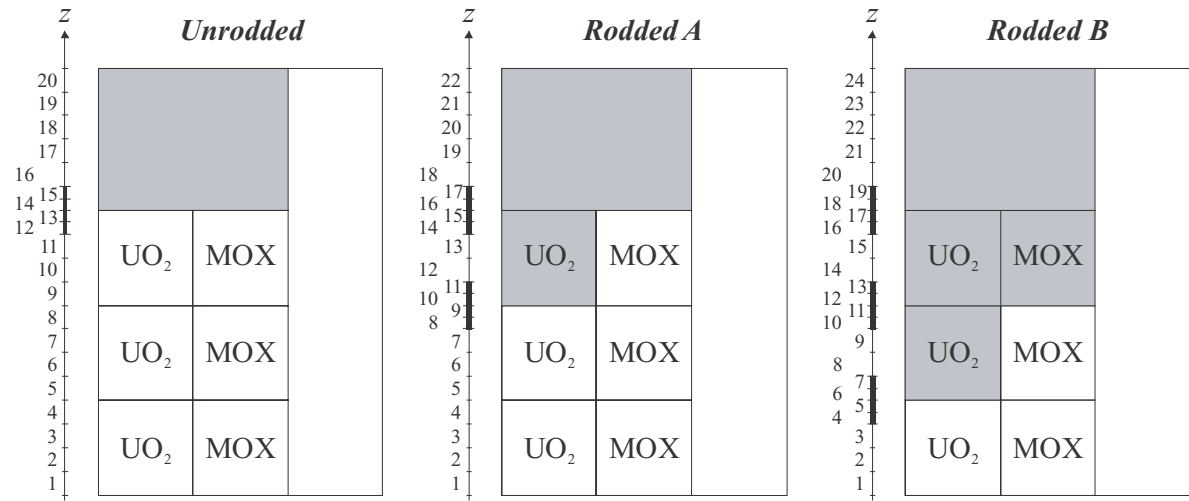


Fig 2. Details of the spatial discretisation in z-direction. The number of *interfaces* (indicated by thick line segments along z-axis) depends on the control rod configuration. Since close to the interface the fine 1.785 cm mesh size is used, the number of z-meshes varies with the three control rod configurations, ranging from 20 for *Unrodded* up to 24 for *Rodded B*.



2. Hanyang University (HU), Korea

Participants: Hong-Chul KIM, Chi Young HAN and Jong Kyung KIM

Code used: THREEDANT (S_N)

Name of participant(s)

Hong-Chul KIM, Chi Young HAN, and Jong Kyung KIM

Establishment(s)

Department of Nuclear Engineering, Hanyang University, Seoul, Korea

Name of code system(s) used

THREEDANT within DANTSYS 3.0 code system

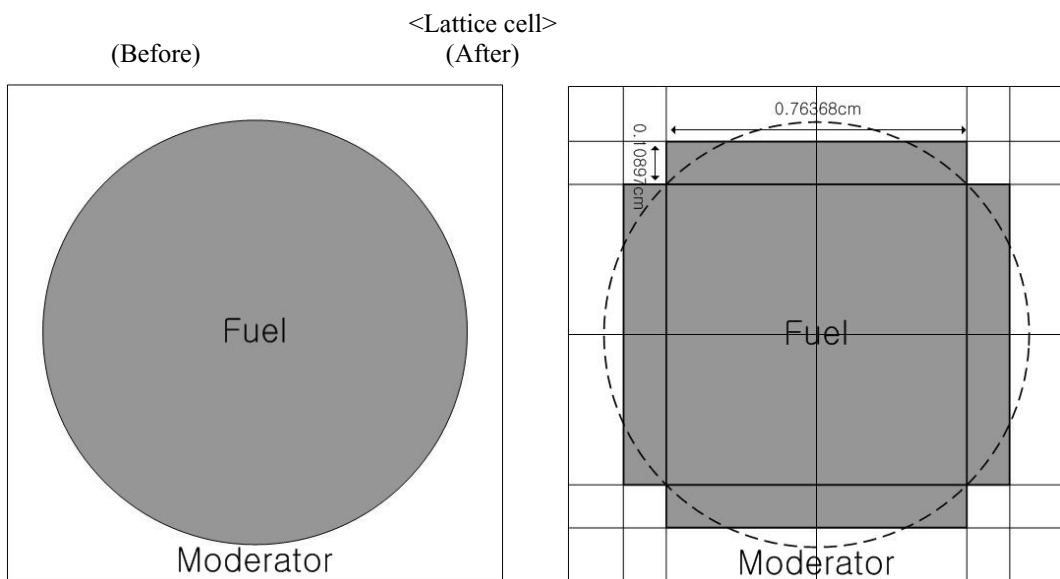
Computational method used

Discrete Ordinates method (S_N method)

Type and level of angular approximation

S_8P_0

Type and level of spatial discretisation



- The circular fuel pin was modeled on an equivalent-area cross pin and the number of fine mesh per lattice pin cell is 6x6 as the above drawing.
- The each fuel pin cell was divided into 30 fine meshes in axial direction.

Convergence

- a. eigenvalue : 1.0E-5
- b. pointwise : 1.0E-5

Machine on which the calculations were performed and (if possible) CPU time

HP-UX 9000/785 (HP Workstation C3700), CPU time of 2.3 days.

3. Korea Advanced Institute of Science and Technology (KAIST), Korea

Participants: N. Z. Cho and G. S. Lee

Code used: CRX (method of characteristics 2-D/ S_N 1-D)

Name of participant(s)

Nam Zin Cho, Gil Soo Lee

Establishment(s)

Korea Advanced Institute of Science and Technology (KAIST)

Name of code system(s) used

CRX code

Computational method used (e.g. S_N , P_N , collision probability, characteristic, etc. and describe briefly the method used)

Fusion method (2D method of characteristics + 1D S_N)

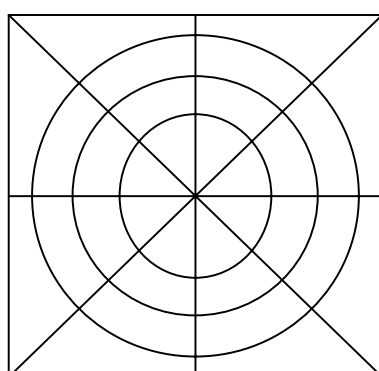
Type and level of angular approximation (e.g. S_8 , P_7 , number of characteristic angles, etc.)

8 azimuthal/ 2 polar angles per octant

Type and level of spatial discretisation (e.g. linear-triangular finite elements, flat source region collision probabilities, etc.). Provide number of mesh points, source regions, tracking pitch etc. per lattice cell. If possible include a drawing or diagram of the spatial mesh for one lattice cell.

32 flat source regions/ cell (1,498,176 regions total)

50 rays per cell/direction



$$R1=0.4\text{cm}$$

$$R2=0.54\text{cm}$$

$$R3=0.6\text{cm}$$

Convergence

- a. eigenvalue (at least 10 E-5)
1.e-6
- b. pointwise (e.g. flux, fission source, etc.)
1.e-4 fission source

Machine on which the calculations were performed and (if possible) CPU time

KAIST*GALAXY cluster system (using 24 CPUs of 64 Intel PentiumIV machines)

Other assumptions and characteristics, comments useful for interpreting correctly the results, including discussion on what, if any, difficulties encountered when solving the benchmark problem

Sensitivity test of Rodded B configuration (mesh size)

(axial meshes, radial meshes per cell)		(18,32)	(8,32)	(8,16)	(8,40)
k_{eff} (% difference from reference)		1.07707 (-0.06)	1.07634 (-0.13)	1.07622 (-0.14)	1.07634 (-0.13)
Max. pinpower in each slice	1	1.182	1.175	1.167	1.175
	2	0.556	0.565	0.560	0.566
	3	0.218	0.212	0.210	0.212
RMS error in each slice	1	0.847	1.169	1.548	1.160
	2	0.894	1.786	2.229	1.771
	3	2.347	1.770	2.323	1.746
RMS error (axial averaged)		0.641	0.721	1.497	0.684

It seems that calculation with more refined computational mesh is required.

4. Institute of Physics and Power Engineering (IPPE), Russian Federation

Participants: I.R. Suslov

Code used: MCCG3-D (method of characteristics)

Name of participant(s)

Igor Suslov

Establishment(s)

IPPE (Russia)

Name of code system(s) used

MCCG3-D

Computational method used (e.g. S_N , P_N , collision probability, characteristic, etc. and describe briefly the method used)

Extrapolation of characteristic solutions

Type and level of angular approximation (e.g. S_8 , P_7 , number of characteristic angles, etc.)

Extrapolation

Three sets of angular approximation parameters have been used in MCCG3-D calculations:

1. A_Base: S4 for polar angle, 2 characteristic angles in 45-grad symmetry sector;
2. A_mu: S16 for polar angle, 2 characteristic angles in 45-grad symmetry sector;
3. A_theta: S4 for polar angle, 12 characteristic angles in 45-grad symmetry sector;

The extrapolated angular approximation for calculated values F (eigenvalues or power distribution) has been constructed as:

$$F(A_{\text{ext}}) = F(A_{\text{Base}}) + \text{del}_\mu + \text{del}_\theta$$

where

$$\text{Del}_\mu = [F(A_\mu) - F(A_{\text{Base}})]$$

$$\text{Del}_\theta = [F(A_\theta) - F(A_{\text{Base}})]$$

Type and level of spatial discretisation (e.g. linear-triangular finite elements, flat source region collision probabilities, etc.). Provide number of mesh points, source regions, tracking pitch etc. per lattice cell. If possible include a drawing or diagram of the spatial mesh for one lattice cell.

Extrapolation of MCCG3-D QSD-DD Plane Tracing scheme solutions

Three spatial discretisations have been used:

S_base (m13z40): with 13 meshes per lattice cell (5 in pin and 8 in moderator) and 40 Z-intervals with tracking pitch 0.1 cm

S_r (m41z40): with 41 meshes per lattice cell (9 in pin and 32 in moderator) and 40 Z-intervals with tracking pitch 0.05 cm

S_z (m13z80): with 13 meshes per lattice cell (5 in pin and 8 in moderator) and 80 Z-intervals with tracking pitch 0.1 cm.

The extrapolated space approximation for calculated values F (eigenvalues or power distribution) has been constructed as

$$F(A_{\text{ext}}) = F(S_{\text{Base}}) + \Delta_r + \Delta_z$$

where

$$\Delta_r = 4/3 [F(S_r) - F(S_{\text{Base}})]$$

$$\Delta_z = 4/3 [F(S_z) - F(S_{\text{Base}})]$$

Convergence

- a. eigenvalue - 10 E-5
- b. fission source – 10 E-3

Machine on which the calculations were performed and (if possible) CPU time

RoverBook (P-IV, 2.79 Gh, 225 Mb). Approximately 1-2 weeks per case.

Other assumptions and characteristics, comments useful for interpreting correctly the results, including discussion on what, if any, difficulties encountered when solving the benchmark problem

Angular corrections Δ_{μ} and Δ_{θ} have been calculated for S_base mesh grid.
Calculations have been performed with no acceleration due to insufficient computer memory.

5. Russian Research Center Kurchatov Institute (RRC KI), Russian Federation

Participants: V.D. Davidenko and V.F. Tsibulsky

Code used: UNKGRO (method of characteristics with stochastic rays)

Name of participant(s)

Vladimir D. Davidenko

Viktor Phi. Tsibulsky

Establishment(s)

Russian Research Centre “Kurchatov Institute”

Name of code system(s) used

UNKGRO

Computational method used

Method of characteristics with stochastic rays and nonlinear correction of scattering cross-section

General provisions

Series of rays along which the modification of a neutrons flux calculates is selected, at the given source in region. The neutron source is neutrons from external source, neutrons of intragroup scattering or neutrons of fission. After calculation along all rays the average value of neutron flux to registration zones calculates.

Equation along ray is:

$$\frac{d\varphi(x, \Omega)}{dx} + \Sigma_{tot}\varphi(x, \Omega) = \frac{1}{4\pi} \int_{4\pi} \Sigma_s \varphi(x, \Omega') d\Omega' + Q(x, \Omega) , \quad (1)$$

(Here standard labels are used).

Boundary conditions for $\varphi(x, W)$ ($x \in \Gamma = J$, if $(\Omega, n^+) < 0$
 $(n^- -$ external normal line to boundary of region).

The calculated scheme realised in UNKGRO code

The region is divided into registration zones in which scalar function of neutron flux is considered to be a stationary value. In this case the average value of a densities of neutron flux for a zone j is defined as an average value of a flux along all rays intersecting a zone:

$$\Phi(\vec{r}_j) = \frac{\sum_m \int \omega_i \varphi_{ji}(x) dx}{\sum_m \omega_i l_{ji}} , \quad (2)$$

Here summing will be carried out on all rays $i \in (1, \dots, m)$, intersecting a zone j ,

l_j - length of a side of intersection, (m_j - complete number of rays intersecting a zone j),

ω - weight coefficient describing the contribution of each direction to the aggregate flux.

Given scheme completely satisfies to balancing relation.

Integrating equation (1) and summing on all rays intersecting a zone, for any of zones and all calculated volume, we obtain:

$$\sum_m (\varphi_j^+ - \varphi_j^-) \omega_i + \Sigma_a \Phi_j \sum_m \omega_i l_{ij} = Q \sum_m \omega_i l_{ij}. \quad (3)$$

The first item in this equation corresponds to leakage of neutrons; the second there is absorption. The collision integral in a right part of equation (1) precisely corresponds to a similar integral of scattering on the left of equation.

The most essential approximation of this scheme is considering that a scalar flux inside registration zone is constant. To obtain precise result by this algorithm calculations should be fulfilled with sizes of registration zones much more smaller than path lengths of neutrons.

Influence of a size of a registration zones size on a solution

The solution of equation (1) along a ray inside registration zone has an analytical solution:

$$\varphi(x) = \varphi_0 e^{-\Sigma_t x} + \frac{\Sigma_s \Phi + Q}{\Sigma_t} (1 - e^{-\Sigma_t x}), \quad (4)$$

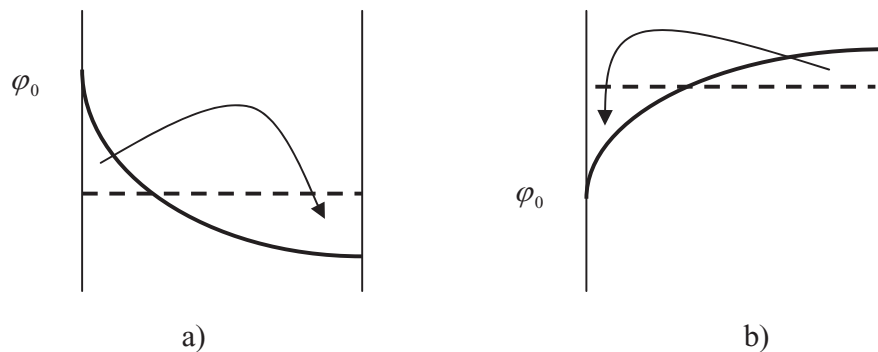
here Φ - scalar neutron flux (constant inside registration zone), Q -external neutrons source.

This first stage of calculation does not bring in any errors to a solution. The following procedure – an average through the volume of a registration zone with the purpose to calculate a collision integral. The procedure of an average formally implies from a requirement of balance for the equation (1). But we will try to understand, what means this average from the point of view of transport neutrons.

Depending on a relation between values φ_0 and $\frac{\Sigma_s \Phi + Q}{\Sigma_t}$ a solution (4) will have the following aspect (fig. 1) (a continuous fat line).

Fig 1. Solution along a ray and an average value

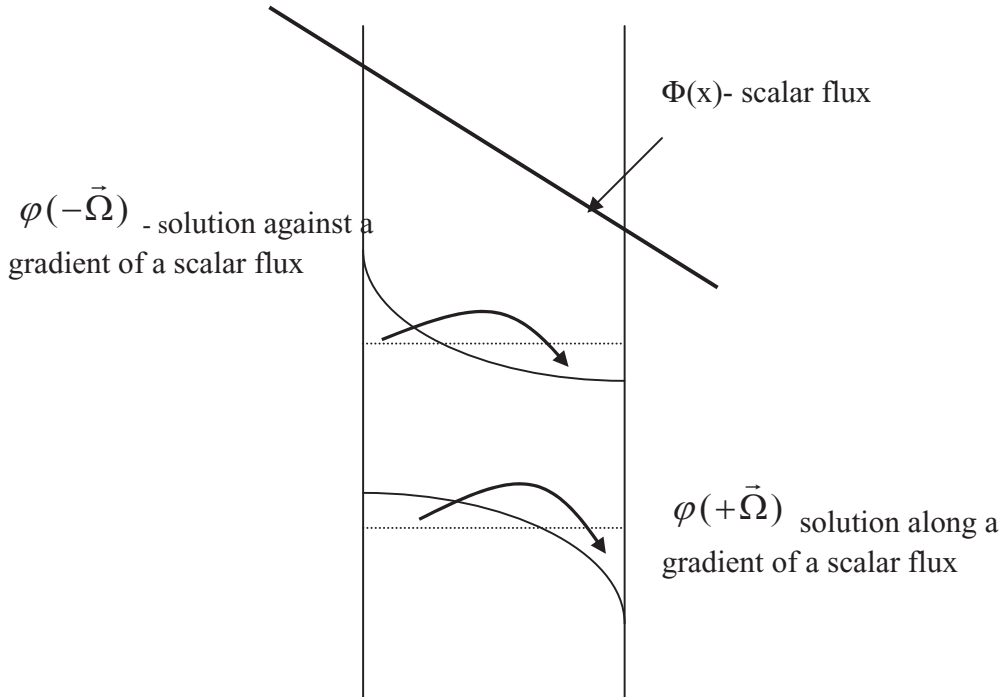
$$\varphi_0 > \frac{\Sigma_s \Phi + Q}{\Sigma_t} \quad \varphi_0 < \frac{\Sigma_s \Phi + Q}{\Sigma_t}$$



During an average we substitute this function by its average value (dashed line). Thus, both in a case a) and b) additional neutrons transport indicated on figure is carried out an arrow. And, it is important, that both in a case a), and in a case b) this additional transport causes the procedure of an average, there is in a direction opposite to a common gradient of scalar neutrons flux (Figure 2).

In Figure 2 the aspect of function from an analytical solution and by arrows neutrons transport is indicated during an average.

Fig 2. Additional neutron transport depending on a gradient of scalar function



Apparently both in the first and in the second cases additional neutrons transport during an average happens in a direction opposite to a gradient of a scalar flux. In practical calculations it causes the increasing leakage of neutrons from reactor and eigenvalue is decreases.

To make calculations more precise it is necessary to create computing algorithms in which spatial association of a scalar neutron flux on spatial coordinates is taken into account. In other words not to use an approximation of a flat flux inside registration zone. However, strict algorithms of such scheme, with security of a requirement of conservatism are complicated enough for the arbitrary aspect of geometry.

Nonlinear correction of scattering cross-section

Below the algorithm for different from approximating schemes is offered. The description of a modification of neutron transport submitted above, due to an approximation of a flat flux in registration zones, allows to offer an obvious enough method of correction of a solution. It will consist in the following.

At a solution of the equation along a ray when it intersects a registration zone, it is necessary to pick such scattering cross-section which would allow, in a view of the subsequent passage to a flat flux (procedure of an average), to maintain significant for a functionals of neutrons transport.

As such functional it is natural to consider average quadrate of a free length of neutrons in a registration zone, magnitude significant for neutrons migration. Thus in the common calculation scheme, it is necessary to maintain relations of balance with using of actual cross-sections that will provide correct calculation of reactions rates.

The average quadrate of a path length of neutrons along a ray of terminating length (a ray intersecting a registration zone) will consist of two parts: the first for neutrons flying from the outside and the second for neutrons given born inside the volume.

$$1) \int l^2 \varphi dx = \frac{\int_0^h \varphi_0 x^2 dx}{\int_0^h Q^* dx} = Ch^2 e^{-\Sigma_t h} + (1 - e^{-\Sigma_t h}) \frac{\int_0^h x^2 e^{-\Sigma_t x} dx}{\int_0^h e^{-\Sigma_t x} dx} = C \frac{1}{\Sigma_t^2} (1 - (1 + \Sigma_t h)^* e^{-\Sigma_t h}) \quad (5)$$

$$2) \int l^2 \varrho dx = \frac{\int_0^h Q^* \int_x^h x'^2 dx' dx}{\int_0^h Q^* dx} = \int_0^h (h-x)^2 e^{-\Sigma_t (h-x)} + (1 - e^{-\Sigma_t (h-x)}) \frac{\int_x^h (x'-x)^2 e^{-\Sigma_t (x'-x)} dx'}{\int_x^h e^{-\Sigma_t (x'-x)} dx'} =$$

$$\frac{1}{\Sigma_t^2} (2\Sigma_t h - 4 + 2(2 + \Sigma_t h) e^{-\Sigma_t h}) \quad (6)$$

here $Q^* = \Sigma_s \Phi + Q$.

And now we will calculate, what a correction is given in addition to average quadrate of a path length with procedure of an averaging. As a result of procedure of an averaging the average quadrate of a path length of neutrons will vary through the following value:

$$3) \int l^2 \bar{\Phi} = \frac{\sum_s \int_0^{\bar{x}} (\varphi(x) - \bar{\varphi}) \left(\int_{\bar{x}}^h (x'-x)^2 (\varphi(x') - \bar{\varphi}) dx' \right) dx}{\sum_t \int_{\bar{x}}^h (\varphi(x') - \bar{\varphi}) dx'} = \frac{1}{\int_0^h \varphi(x) dx} =$$

$$\frac{\sum_s \int_0^{\bar{q}} (x^2 (\varphi(x) - \bar{\varphi}) dx - \int_{\bar{x}}^h x'^2 (\varphi(x') - \bar{\varphi}) dx' - 2 \int_0^{\bar{x}} x (\varphi(x) - \bar{\varphi}) dx \int_{\bar{x}}^h x' (\varphi(x') - \bar{\varphi}) dx')}{\sum_t \int_{\bar{x}}^h (\varphi(x') - \bar{\varphi}) dx'} = \frac{1}{\int_0^h \varphi(x) dx} \quad (7)$$

Here the following labels are used:

$$C = \frac{\varphi_0}{Q/\Sigma_t}, \quad \bar{x} = -\frac{1}{\Sigma} \ln((1 - e^{-\Sigma h})/\Sigma h), \quad \bar{\varphi} = \frac{1}{h} \int_0^h \varphi(x) dx, \quad h - \text{zone size.}$$

If to select cross-section ($\Sigma = \Sigma^*$) such as that the average quadrate of a path length coincided with similar value calculated with actual cross-section it is possible to state, that in the modified and initial problem average quadrate of neutrons path will be equal. For this purpose it is necessary to solve the equation

$$L^2_{1,2}(\Sigma) = L^2_{1,2,3}(\Sigma^*) \quad (8)$$

$L^2_{1,2,3}(\Sigma^*)$ – is equal sum $l_\varphi^2 + l_Q^2 + l_\Phi^2$

Found value Σ^* also should be used for calculation of neutron transport inside the registration zone.

Further, from the equation of balance it is necessary to receive a average value of flux along a ray:

$$\bar{\varphi} = ((Q + \Sigma_s \Phi) - (\varphi(0) - \varphi(h))) / \Sigma_t h \quad (9)$$

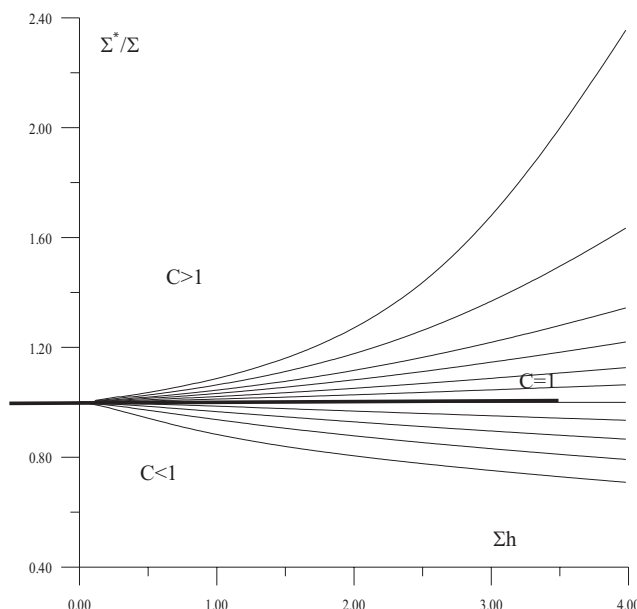
Where values of function $\varphi(h)$ is obtained at the rate of the corrected cross-section.

It is easy to see, that this procedure of correction is conservative, and it only redistributes neutrons between flying off a zone and neutrons collided in it. Thus both the amount of flying neutrons, and a volumetric neutrons source do not vary.

Unfortunately, equation (8) has no analytical solution, but it is easy to solve numeric. A solution of a transcendental equation (8) is the corrected cross-section as a function off scattering cross-section, the total cross-section, an optical zone size and C- the ration a in-flying neutrons and an asymptotic neutrons flux inside registration zone.

On Figure 3 corrected cross-section via an optical zone size for different values $C = \frac{\varphi_0}{Q/\Sigma_t}$ is submitted

Fig 3. The corrected cross-section via an optical zone size for different relations of in flying neutrons and an asymptotic flux.



It is easy to see, that for $C > 1$, the number of taking off neutrons will be less, than flying in (Figure 3), and the corrected cross-section will be more than actual. It will reduce the amount of taking off neutrons will be underestimated, but it means, that in further, procedure of an average, it will be compensated. For $C < 1$ situation inverse, the corrected cross-section less actual, the number of taking off neutrons will increase, but the further procedure of an averaging of it will be reduced. And only for case $C=1$ the corrected cross-section coincides with actual.

From Figure 3 it is easy to see, that at a diminution of an optical distance of a zone the corrected cross-section aspires to actual. It means, that the given procedure cross-section correction is bound exclusively to zone sizes and at a diminution of their optical distances, solutions and with actual will coincide with the corrected cross-section.

From formulas of corrected cross-section calculation (5,7) it is easy to see, that for the volume without scattering (only absorption), no correction should be used.

The submitted logic of calculation reduces in necessity of a nonlinear problem solution along each ray.

Calculations of corrected cross-section:

$$\Sigma^* = f(C, \Sigma_t h, \frac{\Sigma_s}{\Sigma_t}) \quad (10)$$

from calculation a transcendental equation (8)

Calculation of number of taking off neutrons:

$$\varphi(h) = \varphi_0 e^{-\Sigma^* h} + \frac{\Sigma_s \Phi + Q}{\Sigma_t^*} (1 - e^{-\Sigma^* h}) \quad (11)$$

Calculation of integrated neutron flux densetis along a ray:

$$\int_0^h \varphi(x) dx = ((Q + \Sigma_s \Phi) - (\varphi(0) - \varphi(h))) / \Sigma_t \quad (12)$$

Calculation of a medial scalar flux in a zone:

$$\Phi(\vec{r}_j) = \frac{\sum_m \int \omega_i \varphi_{ji}(x) dx}{\sum_m \omega_i l_{ji}} \quad (13)$$

It is clearly, that direct using of this correction, with a solution of a transcendental equation for each side of intersection, demands the considerable computing time. In this connection is useful to approximate association of a solution (submitted on figure 3). As approximating function appeared convenient to pick function of the following aspect:

$$\frac{\Sigma^*}{\Sigma} = a2 + \frac{1-a2}{1 + (\Sigma h / \tau0)^p} \quad (14)$$

In this formula coefficients $a2$, $\tau0$ and p are functions depending from two parameters – ration an absorption cross-section to the total cross-section, and from value C . This approximating formula in a range of zone optical distance from 0 up to 3 path lengths given an error of calculation of the corrected cross-section less than 1 %.

Direct calculations of several test problems with using of approximation (14) and an immediate solution of a transcendental equation showed practically the complete concurrence of outcomes.

For example calculations results of previous C5G7 benchmarks are resented in Table 1 and 2 with addition of results based on cross-section correction.

Table 1. Eigenvalue solutions and estimated number of histories for C5G7 first stage

Code name	Eigenvalue	Per cent error	Zone size, cm
MCNP	1.18655	Reference	
UNKGRO	1.18523	-0.11	0.2
UNKGRO (Corr.L ²)	1.18623	-0.03	0.315
UNKGRO (Corr.L ²)	1.18669	+0.01	0.63
UNKGRO (Corr.L ²)	1.18811	+0.13	1.26

Table 2. Per cent error results for specific pin powers for C5G7 the first stage

Code Name	Maximum per cent error	Per cent error	Minimum per cent error	Per cent error	Maximum per cent error	Zone size, cm
MCNP(ref)	2.498	±0.16	0.232	±0.58		
UNKGRO	2.503	+0.19	0.236	+1.72	4.21	0.2
UNKGRO (Kop.L ²)	2.499	+0.04	0.235	+1.57	2.07	0.315
UNKGRO (Kop.L ²)	2.500	+0.10	0.237	+2.16	3.14	0.63
UNKGRO (Kop.L ²)	2.484	+0.53	0.246	+6.26	6.67	1.26

3-D-Extension C5G7 MOX Calculation Results

In the Table 3 eigenvalue solutions of all three problems 3-D-Extension C5G7 MOX are reduced.

All three calculations were carried on the same structure of registration zones. 11766 zones are in the plan and 92 layers on height. Full number of zones equally 1.08 million. Number of rays is 250000.

Table 3. Eigenvalue solutions for C5G7 the second stage

Task name	Eigenvalue
Unrodded	1.143165
Rods A	1.128014
Rods B	1.077308

Machine on which the calculations were performed and (if possible) CPU time

Machine: Pentium-IV, 2.4 GHz

CPU Time: Approximately 30 hours

Literature

- 1.Benchmark on Deterministic Transport Calculations Without Spatial Homogenization.
A 2-D/3-D MOX Fuel Assembly Benchmark. NEA/NSC/DO(2003)16, OECD 2003.

6. Argonne National Laboratory (ANL), USA

Participants: M.A. Smith, N. Tsoulfanidis, E.E. Lewis, G. Palmiotti, T. Taiwo and R. Blomquist

Code used: VARIANT-ISE (nodal spherical harmonics with integral transport),

VARIANT-SE (nodal spherical harmonics), and

VARIANT-Homog (nodal P_N with homogenised cross-sections)

We would like to have as detailed a description as you are able to provide on your treatment of the space-angle variables and the procedures by which you carried out the calculations, (but limited to 5 pages). Please include the following:

Name of participant(s)

Micheal A. Smith¹, Giuseppe Palmiotti¹, Temitope Taiwo¹, Roger Blomquist¹,
Elmer E. Lewis², Nicholas Tsoulfanidis³

Establishment(s)

¹Argonne National Laboratory

²Northwestern University

³University of Missouri-Rolla

Name of code system(s) used

VARIANT-SE, VARIANT-ISE: Prototypic versions of the VARIANT code

Computational method used (e.g. S_N , P_N , collision probability, characteristic, etc.)

Response matrix form of the variational nodal method. The nodal flux is solved with an integral transport treatment coupled to interface spherical harmonics. These interface nodal spherical harmonics are then coupled together via red-black partial current iterations.

Type and level of angular approximation (e.g. S_8 , P_7 , number of characteristic angles, etc.)

P_5 in 3-D, Square Legendre-Chebychev S_{16} for integral method

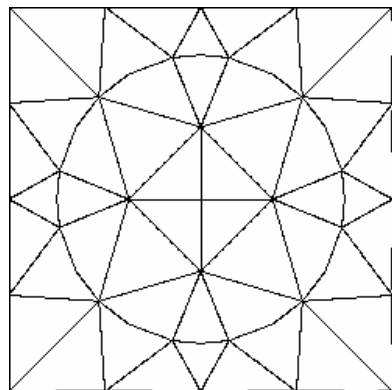
Type and level of spatial discretisation (e.g. linear-triangular finite elements, flat source region collision probabilities, etc.). Provide number of mesh points, source regions, tracking pitch etc. per lattice cell. If possible include a drawing or diagram of the spatial mesh for one lattice cell.

A variational nodal method utilising finite element sub-elements within each node.

A cubic Lagrange multiplier nodal interface approximation (spatial).

A consistent source approximation of the finite element mesh.

A triangular finite element mesh with quadratic basis functions.



Convergence

- a. eigenvalue (at least 10 E-5)

Eigenvalue = 10E-6

- b. pointwise (e.g. flux, fission source, etc.)

Pointwise Fission Source = 10E-5

Average Fission Source = 10E-5

Machine on which the calculations were performed and (if possible) CPU time

Other assumptions and characteristics, comments useful for interpreting correctly the results

The three different methods are shown. For the homogenisation approach, pin-cell homogenisation with P5 transport proved to provide the best solution when compared to the Monte Carlo result. The steep global flux gradient (2.5:0.3) made the flux homogenisation very difficult.

7. Los Alamos National Laboratory (LANL), USA

Participants: J.A. Dahl

Code used: PARTISN (S_N)

Release number: LA-UR-04-8067

Name of participant(s)

Jon A. Dahl

Establishment(s)

CCS-4, Transport Methods Group

Los Alamos National Laboratory

Los Alamos, NM 87545

USA

Name of code system(s) used

PARTISN – (Parallel Time dependent S_N), LA-CC-04-013, Los Alamos National Laboratory, 2004.

Release Number: LA-UR-04-8067

FRAC-IN-THE-BOX – mesh generation code (D.G. Collins and J. T. West, “FRAC-IN-THE-BOX, Utilization – Revision 1”, LA-11606-MS, Los Alamos National Laboratory, Los Alamos, NM, April 1990)

Computational method used (e.g. S_N , P_N , collision probability, characteristic, etc.)

PARTISN uses standard discrete ordinates (S_N) with diamond difference spatial differencing. Diffusion synthetic acceleration is used to accelerate both the inner(source) and outer(multigroup) iterations. The diffusion equation is solved via a parallel multigrid method.

Type and level of angular approximation (e.g. S_8 , P_7 , number of characteristic angles, etc.)

The quadrature used consisted of S_{32} triangular Legendre-Tchebyschev, 1 680 angles (Legendre in polar angle, Tchebyschev azimuthally).

Type and level of spatial discretisation (e.g. linear-triangular finite elements, flat source region collision probabilities, etc.). Provide number of mesh points, source regions, tracking pitch etc. per lattice cell. If possible include a drawing or diagram of the spatial mesh for one lattice cell.

This calculation employed diamond difference (linear continuous) spatial differencing. The mesh was created using the code FRAC-IN-THE_BOX, which calculates the fractions of rectangular parallelepiped mesh cell volumes that are intersected by combinatorial geometry. Each pin cell consisted of a 14x14 mesh where FRAC-IN-THE-BOX calculated the proper volume fraction of material for those cells which contained both moderator and pin material. Each level of the reactor core was meshed with 90 cells in the axial direction. The top of the reactor reflector was meshed similarly with a 14x14 mesh in locations corresponding to pin locations and 90 mesh cells in the axial direction. The water reflector surrounding the reactor was 30 cells thick in the direction moving away from the reactor, and the same number of cells was used for the interior of the reactor when moving along the core. The total mesh was 506x506x360 or 92,172,960,000 mesh cells.

Convergence

- a. eigenvalue (at least 10 E-5)
- b. pointwise (e.g. flux, fission source, etc.)

Both the eigenvalue and the pointwise flux was converged to 10 E-5.

Machine on which the calculations were performed and (if possible) CPU time

Calculations were performed on machine Q at Los Alamos National Laboratory using 500 processors. Calculation time was approximately 10 hours.

Other assumptions and characteristics, comments useful for interpreting correctly the results

Mesh cells which contain material interfaces were volume fractioned into their two constituents. We surmise that this has a negative impact on pin cells containing control rod material, resulting in an artificially increased amount of absorption. We plan to test our hypothesis of this effect and shall report on it at a later date.

8. Radion Technologies, USA

Participants: T. Wareing

Code used: ATTILA (3-D) (S_N)

Name of participant(s)

Todd A. Wareing

Establishment(s)

Radion Technologies

Name of code system(s) used

Attila Version 4.0.0

Computational method used (e.g. S_N , P_N , collision probability, characteristic, etc. and describe briefly the method used)

S_N using Linear Discontinuous Finite-Element spatial differencing on unstructured tetrahedral grids.

Type and level of angular approximation (e.g. S_8 , P_7 , number of characteristic angles, etc.)

S_{16} Square Tchebyschev Double Legendre

Type and level of spatial discretisation (e.g. linear-triangular finite elements, flat source region collision probabilities, etc.). Provide number of mesh points, source regions, tracking pitch etc. per lattice cell. If possible include a drawing or diagram of the spatial mesh for one lattice cell.

Linear Discontinuous Finite Element spatial differencing on tetrahedral elements. The mesh consisted of 945, 326 completely unstructured elements generated by Radion Technologies grid generator.

Convergence

- a. eigenvalue: 1.0e-5
- b. pointwise: 1.0e-4

Machine on which the calculations were performed and (if possible) CPU time

2.5 GHz Intel Xeon processor running Redhat Linux 9. CPU times are on the order of “hours”.

Other assumptions and characteristics, comments useful for interpreting correctly the results, including discussion on what, if any, difficulties encountered when solving the benchmark problem.

none

9. Penn State University (PSU), USA

Participants: J. Klingensmith, Y. Azmy, J. Gehin and R. Orsi (ENEA-Italy)

Code used: TORT (S_N)

Name of participant(s)

Jesse J Klingensmith¹, Yousry Y. Azmy², Jess C. Gehin³, Roberto Orsi⁴

Establishment(s)

1. Pennsylvania State University, 138 Reber Building, University Park, PA 16802
2. Pennsylvania State University, 229 Reber Building, University Park, PA 16802
3. Oak Ridge National Laboratory, P.O. Box 2008, MS 6363, Oak Ridge, TN 37831
4. ENEA FIS-NUC, Via Martiri di Monte Sole, 4, 40129 Bologna, Italy

Name of code system(s) used

TORT (Three-Dimensional Oak Ridge Discrete Ordinates Neutron/Photon Transport Code) – solve multigroup, discrete ordinates, criticality, transport problem in three-dimensional geometry. TORT is part of the DOORS code system developed at Oak Ridge National Laboratory.

BOT3P – mesh generation and geometry input and output visualisation

Computational method used (e.g. S_N , P_N , collision probability, characteristic, etc. and describe briefly the method used)

Directional variables are determined using discrete ordinates and the spatial approximation is based on an optimised x-y-z nodal method.

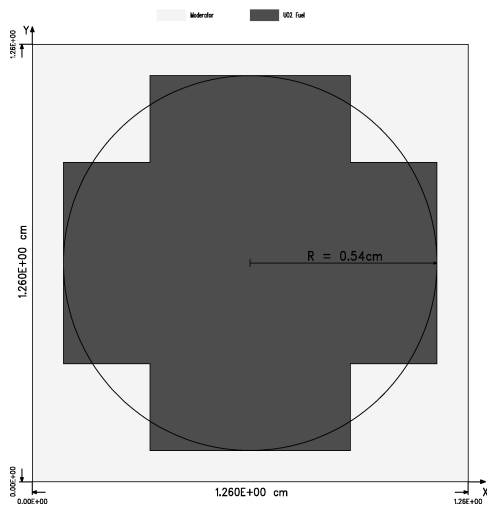
Type and level of angular approximation (e.g. S_8 , P_7 , number of characteristic angles, etc.)

Both fully-symmetric, S_n , and Square Legendre-Chebychev, Q_n . As the results obtained by both sets proved to be similar and the Q_n quadrature sets have shown better convergence in the two dimensional problem, the Q_8 set will be reported.

Type and level of spatial discretisation (e.g. linear-triangular finite elements, flat source region collision probabilities, etc.). Provide number of mesh points, source regions, tracking pitch etc. per lattice cell. If possible include a drawing or diagram of the spatial mesh for one lattice cell.

The cruciform control rod approximation shown below is identified by the BOT3P input of kdiv = 1. Increasing kdiv gives a more accurate staircase approximation, but this was not shown to significantly improve the results, so the case shown below will be submitted.

Lewis MOX Fuel Assembly Benchmark (kdiv=1)
Meshes: 5X, 5Y, 14Z Section at Z = 14.00 cm



Convergence

- a. eigenvalue (at least 10 E-5)
- b. pointwise (e.g. flux, fission source, etc.)

eigenvalue = 10^{-5}

pointwise flux = 10^{-7}

fission source = 10^{-4}

Machine on which the calculations were performed and (if possible) CPU time

Calculations were performed on Oak Ridge National Laboratory's CPILE. CPILE consists of dual processor (2 GHz each) LINUX machines with 512 MB of RAM.

CPU time for the submitted cases was around 22 hours.

Other assumptions and characteristics, comments useful for interpreting correctly the results, including discussion on what, if any, difficulties encountered when solving the benchmark problem.

10. TEPCO Systems Corporation (TEPSYS), Japan

Participants: S. Kosaka

Code used: CHAPLET (method of characteristics)

Name of participant(s)

Shinya Kosaka

Establishment(s)

TEPCO Systems Corporation. (abbr. TEPSYS)

Name of code system(s) used

CHAPLET-3-D

Computational method used (e.g. S_N , P_N , collision probability, characteristic, etc. and describe briefly the method used)

3-D FDM calculation with the corrections of internal 1D/2-D-MOC solutions.

CHAPLET-3-D code employs the non-linear iteration technique, which is widely used in advanced nodal expansion method (NEM) codes, to combine two different type calculations(2-D-MOC/1-D-MOC) for the analysis of 3-D heterogeneous core problems. In the finite difference form NEM calculation by the non-linear iteration technique, replacing radial non-linear terms from the usual \tilde{D}^{NEM} s to \tilde{D}^{MOC} s, 3-D core calculation with the corrections of radial 2-D-MOC solutions can be realized.

$$\bar{\Phi} = \frac{\bar{QV} + \sum_{i=1,4} (D_i^{FDM} - \tilde{D}_i^{MOC}) S_i \bar{\Phi}_I + \sum_{i=5,6} (D_i^{FDM} - \tilde{D}_i^{NEM}) S_i \bar{\Phi}_I}{\sum_{i=1,4} (D_i^{FDM} + \tilde{D}_i^{MOC}) S_i + \sum_{i=5,6} (D_i^{FDM} + \tilde{D}_i^{NEM}) S_i + \Sigma_r V}, \quad (1)$$

$$\tilde{D}^{MOC} = \left\{ -\tilde{J}_i^{MOC} - D_i^{FDM} (\bar{\Phi} - \bar{\Phi}_I) \right\} / (\bar{\Phi} + \bar{\Phi}_I), \quad (2)$$

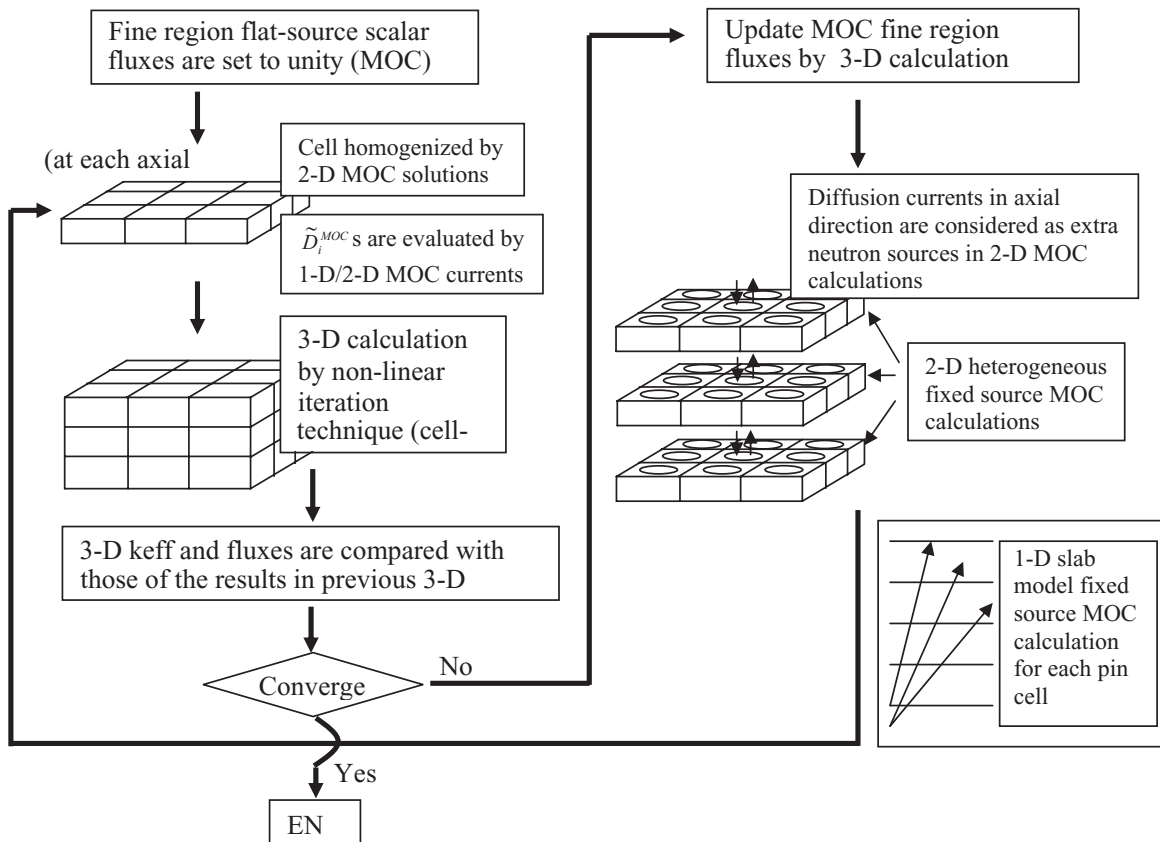
i=1-4 (x-y plane), 5,6(z-direction)

Similarly, as for the axial direction, 1-D-MOC can be applied to take transport effect into account.

$$\tilde{D}^{1D-MOC} = \left\{ -\tilde{J}_i^{1D-MOC} - D_i^{FDM} (\bar{\Phi} - \bar{\Phi}_I) \right\} / (\bar{\Phi} + \bar{\Phi}_I), \quad (3)$$

Then, the equation (1) is now described as bellows,

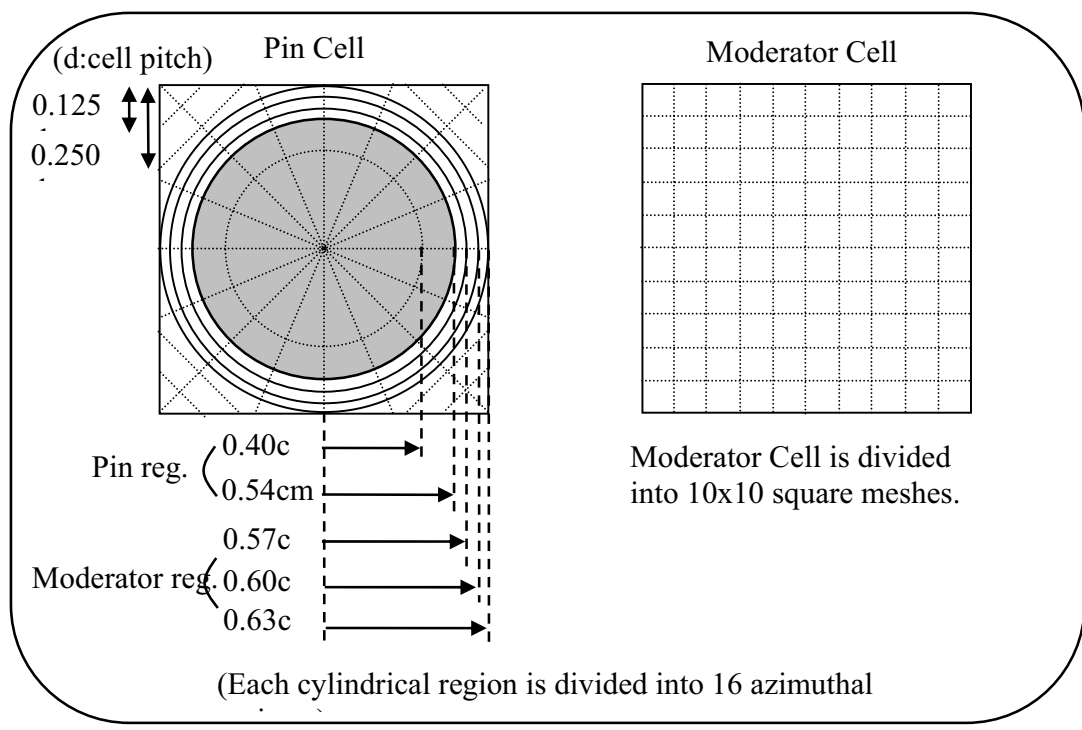
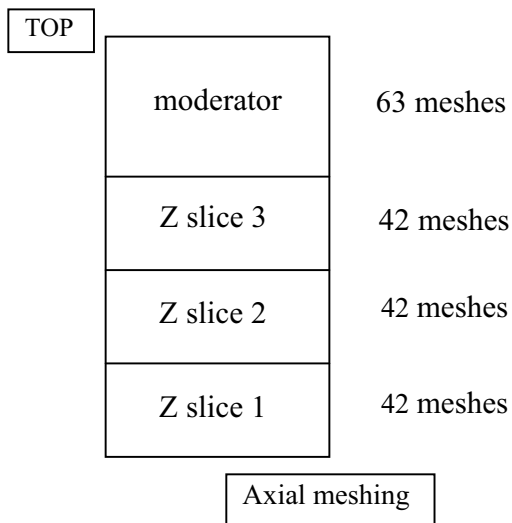
$$\bar{\Phi} = \frac{\bar{QV} + \sum_{i=1,4} (D_i^{FDM} - \tilde{D}_i^{MOC}) S_i \bar{\Phi}_I + \sum_{i=5,6} (D_i^{FDM} - \tilde{D}_i^{1D-MOC}) S_i \bar{\Phi}_I}{\sum_{i=1,4} (D_i^{FDM} + \tilde{D}_i^{MOC}) S_i + \sum_{i=5,6} (D_i^{FDM} + \tilde{D}_i^{1D-MOC}) S_i + \Sigma_r V}. \quad (4)$$



Type and level of angular approximation (e.g. S_8 , P_7 , number of characteristic angles, etc.)

- Radial 2-D MOC calculation
Sixteen azimuthal x eight polar angles/octant.
Width of path interval: 1mm.
- Axial 1-D MOC calculation
Ten(10) polar angles/hemisphere

Type and level of spatial discretisation (e.g. linear-triangular finite elements, flat source region collision probabilities, etc.). Provide number of mesh points, source regions, tracking pitch etc. per lattice cell. If possible include a drawing or diagram of the spatial mesh for one lattice cell.



Convergence

a. eigenvalue (at least 10 E-5)

1.0E-6

b. pointwise (flux)

5.0E-6

Machine on which the calculations were performed and (if possible) CPU time

DELL - Precision 530 (Intel Xenon 2.0GHz)

CPU time ~ 120,000 seconds

Other assumptions and characteristics, comments useful for interpreting correctly the results, including discussion on what, if any, difficulties encountered when solving the benchmark problem.

The accuracy of this combinational method mainly depends on 1-D axial solver. In order to take transport effect into account, 1-D-MOC model has been applied. Consequently, the resultant power distribution becomes better than that of 1-D-NEM model, but the eigenvalue is not so changed, so far.

11. Commissariat à l'Energie Atomique (CEA), France

Participants: P. Humbert

Code used: PANDA (S_N)

Name of participant

Philippe Humbert

Establishment

Commissariat à l'Énergie Atomique
CEA/DIF
BP12 - 91680 Bruyères-le-Châtel, FRANCE

Name of code System used

PANDA

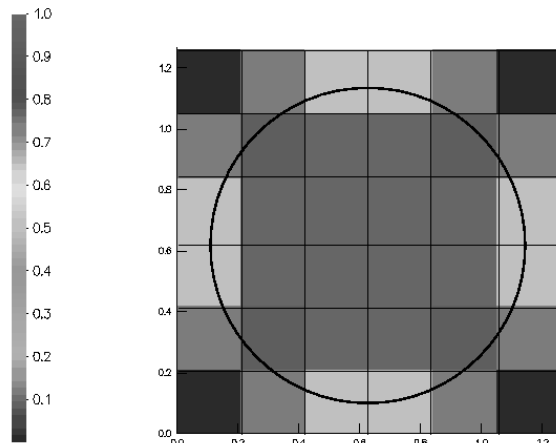
Computational Method used

Discrete ordinates (S_N).

Type and level of angular approximation

- S_N equi-weight quadrature.
- S_{14} (224 directions).

Type and level of spatial discretisation



One lattice mesh. Pure fuel (Magenta), pure moderator (dark blue), other meshes are mixed material cells.

- Diamond difference spatial differencing.
- Uniform cartesian mesh with mixed cells at the material interface (volume fraction).
- Global mesh size: $306 \times 306 \times 27 = 2\ 528\ 172$ cells .
- **One lattice mesh size: $6 \times 6 \times 27 = 2187$ cells (cf. figure).**

Convergence

The eigenvalue calculation is converged when for two successive iterations, the global fission rate relative variation is Less than 10^{-6} .

Machine on which the calculations were performes and CPU time

The three problems were run on the CEA Tera system (HP alphaserver SC).
On 7 processors (DEC alpha EV68 1Ghz) the CPU times were:

- *Unrodded*: 35469 seconds (9h 51mn 9s)
- *Rodded A*: 31883 seconds (8h 51mn 23s)
- *Rodded B*: 31398 seconds (8h 51mn 23s)

Comments

These preliminary results should be improved by spatial and angular mesh size convergence analysis.

12. University of Florida (UF), USA

Participants: Alireza Haghishat, Ce Yi, Glenn E. Sjoden, and G. Longoni
Code used: PENTRAN- SS_N (S_N)

Participants: Alireza Haghishat, Ce Yi, Glenn E. Sjoden, G. Longoni
University of Florida Transport Theory Group (UFTTG)
Nuclear and Radiological Engineering (NRE) Department
University of Florida
202 Nuclear Sciences Building
Gainesville, FL 32611-8300

Code description

PENTRAN-SS_N (Parallel Environment Neutral-Particle TRANsport – preconditioned with even-parity Simplified S_N) is used for this simulation. PENTRAN is a parallel 3-D Discrete Ordinates (Sn) Code developed by G.E. Sjoden and A. Haghishat (Refs. 1 and 2). It can solve eigenvalue and fixed-source problems in a Cartesian geometry. Because of its memory partitioning, domain decomposition algorithms, and other unique numerical features, PENTRAN-SS_N uses PENSS_N (A parallel 3-D code based on the Even-Parity Simplified S_N formulation) as acceleration method (Ref. 3).

Calculation parameters

The full PENTRAN-SS_N model has the following characteristics:

Sn order:	6 (level symmetry quadrature)
No. of fine meshes:	946080
No. of energy groups:	7
Parallel Decomposition:	Space (8) – Angle (2)
No. of Processors:	16
Differencing Scheme:	Directional Theta Weighted (DTW)
Preconditioning Method:	PENSS _N (A parallel 3-D even-parity Simplified S _N code)
Convergence:	1E-5(keff); 1E-3(flux)

Execution Time*

Case	Wall-clock time (hrs)
Unrodded	15.2
Rodded-A	15.9
Rodded-B	17.7

* PCPENII PC Cluster with 16 processors (2 GB RAM per processor, Dual Intel Xenon processors at 2,4 GHz, 1 Gbit full duplex network), Particle Transport & Distributed Computing (PTDC) laboratory, UFTTG, NRE.

References

1. Sjoden G.E. and A. Haghishat, “PENTRAN – A 3-D Cartesian Parallel Sn Code with Angular, Energy, and Spatial Decomposition,” Proceedings of the Joint International Conference on Mathematical Methods and Supercomputing in Nuclear Applications, Vol. II, 1267-1276, Saratoga Springs, NY (1997).
2. Sjoden, G., “PENTRAN: A Parallel 3-D SN Transport Code with Complete Phase Space Decomposition. Adaptive Differencing, and Iterative Solution Methods”, Ph.D. Thesis in Nuclear Engineering, the Pennsylvania State University (1997).
3. Longoni, G. and A. Haghishat, “The Even-Parity Simplified SN Equations Applied to a MOX Fuel Assembly Benchmark Problem on Distributed Memory Environments,” PHYSOR 2004 – The Physics of Fuel Cycles and Advanced Nuclear Systems: Global Developments, Chicago, Illinois, April 25-29, 2004, on CD-ROM, American Nuclear Society, Lagrange Park, IL. (2004).

APPENDIX C

Clarification of the AVG, RMS, and MRE Error Measures

To clarify the three distribution error measures we provide the following brief instructional example. Consider a problem in which there are ten pin powers to be calculated and an “exact” reference solution is available. As a hypothetical, consider the three solutions in Tables 1, 2, and 3 meant to represent solutions contributed by three participants.

As can be seen in Table 1, the participant obtained a solution for which most of the pin powers were calculated correctly (power distribution is the reference solution). The participants lowest pin power had the greatest amount of error: 0.3%. The RMS error is significantly larger than the AVG error measure, indicating that there are a few pins that have substantial error (if all of the per cent errors are roughly the same, then the RMS error will equal the AVG error). The MRE error measure is much smaller than the AVG error measure since a majority of the error resides in the low pin powers.

In Table 2 the participant’s largest error is now on the maximum pin power while the smallest error is on the lowest pin power. As can be seen, the AVG and RMS error do not change from Table 1 to Table 2, but the MRE error changes almost by a factor of two. In terms of the accuracy, this participant’s solution has significantly more error in the pin power distribution, which can only be captured by the MRE error measure.

In Table 3, the participant exactly calculates several of the fuel pins, but four fuel pins have much significantly larger amounts of error compared to Table 1 and Table 2. Overall, the magnitude of the error has not changed as indicated by both the AVG and MRE error measures. The distribution of those errors has changed quite significantly though, which is only captured by the RMS error measure.

In conclusion, the AVG error provides a point of reference for the RMS and MRE error measures. The RMS error measure gives an estimate of the severity of the per cent error distribution and the MRE error measure gives an estimate of the severity of the magnitude of error on the pin power distribution.

Table 1. Hypothetical result #1

Reference power	User per cent error
1.82	0.01
1.64	0.02
1.45	0.03
1.27	0.04
1.09	0.05
0.91	0.06
0.73	0.07
0.55	0.08
0.36	0.09
0.18	0.30
AVG	0.075
RMS	0.109
MRE	0.044

Table 2. Hypothetical result #2

Reference power	User per cent error
1.82	0.30
1.64	0.02
1.45	0.03
1.27	0.04
1.09	0.05
0.91	0.06
0.73	0.07
0.55	0.08
0.36	0.09
0.18	0.01
AVG	0.075
RMS	0.109
MRE	0.091

Table 3. Hypothetical result #3

Reference power	User per cent error
1.82	0.13
1.64	0.00
1.45	0.00
1.27	0.00
1.09	0.00
0.91	0.00
0.73	0.00
0.55	0.12
0.36	0.25
0.18	0.25
AVG	0.075
RMS	0.125
MRE	0.044

APPENDIX D
Reference Multigroup Monte Carlo Solution
(see CD-ROM)

APPENDIX E
All Contributed Results and Descriptions
(see CD-ROM)

APPENDIX F
Benchmark Result Analysis
(see CD-ROM)

APPENDIX G
Additional Continuous Energy Monte Carlo Solutions
(see CD-ROM)

LIST OF CONTRIBUTORS

Authors

Micheal A. Smith (ANL, USA), Elmer E. Lewis (Northwestern University, USA) and Byung-Chan Na (OECD/NEA)

Problem specification

E.E. Lewis (Northwestern University, USA), M.A. Smith (ANL, USA), N. Tsoulfanidis (University of Missouri, Rolla, USA), G. Palmiotti (ANL, USA), T.A. Taiwo (ANL, USA), R.N. Blomquist (ANL, USA)

Reference solutions

MCNP and VIM: M.A. Smith (ANL, USA), N. Tsoulfanidis (University of Missouri, Rolla, USA), R.N. Blomquist (ANL, USA) and E.E. Lewis (Northwestern University, USA)

UNKMK: V.D. Davidenko and V.F. Tsibulsky (RRC KI, Russia)

Benchmark participants

Shinya Kosaka (TEPSYS, Japan)
Nam Zin Cho (KAIST, Korea)
Gil Soo Lee (KAIST, Korea)
Igor R. Suslov (IPPE, Russia)
Philippe Humbert (CEA, France)
Jon A. Dahl (LANL, United States)
Raymond E. Alcouffe (LANL, USA)
Randal S. Baker (LANL, USA)
Todd A. Wareing (RADION, USA)
Hong-Chul Kim (HU-Korea, Korea)
Chi Young Han (HU-Korea, Korea)
Jong Kyung Kim (HU-Korea, Korea)
Armin Seubert (GRS, Germany)
Winfried Zwermann (GRS, Germany)

Siegfried Langenbuch (GRS, Germany)
J. Klingensmith (PSU-USA, USA)
Y. Azmy (PSU-USA, USA)
J. Gehin (PSU-USA, USA)
R. Orsi (ENEA, Italy)
Vladimir D. Davidenko (RRC KI, Russia)
Viktor F. Tsibulsky (RRC KI, Russia)
Alireza Haghigat (Univ. of Florida, USA)
Micheal Smith (ANL, United States)
N. Tsoulfanidis (Univ. of Missouri, Rolla, USA)
E.E. Lewis (Northwestern University, USA)
G. Palmiotti (ANL, USA)
T.A. Taiwo (ANL, USA)
R.N. Blomquist (ANL, USA)

OECD PUBLICATIONS, 2 rue André-Pascal, 75775 PARIS CEDEX 16
Printed in France.